Motor Adaptation under Visual Feedback Uncertainty

Dissertation for the award of the degree

"Doctor rerum naturalium"

of the Georg-August-Universität Göttingen

within the doctoral program *Systems Neuroscience*

of the Georg-August University School of Science (GAUSS)

Submitted by

Virginia Casasnovas Orus

from Boston

Göttingen, 2024

Thesis Advisory Committee

Prof. Dr. Alexander Gail
Sensorimotor Group, Cognitive Neuroscience Laboratory, German Primate Center, Göttingen

Prof. Dr. Hansjörg Scherberger
Neurobiology Laboratory, German Primate Center, Göttingen

Dr. Jorge Jaramillo
Department of Neurobiology, University of Chicago, Chicago (Il.)

Members of the Examination Board

Referee: Prof. Dr. Alexander Gail
Sensorimotor Group, Cognitive Neuroscience Laboratory, German Primate Center, Göttingen

Second referee: Prof. Dr. Hansjörg Scherberger
Neurobiology Laboratory, German Primate Center, Göttingen

Further members of the Examination Board

Dr. Jorge Jaramillo
Department of Neurobiology, University of Chicago, Chicago (Il.)

Prof. Dr. André Fiala
Department of Molecular Neurobiology of Behavior, University of Göttingen, Göttingen

Dr. Igor Kagan
Decision and Awareness Group, Cognitive Neuroscience Laboratory, German Primate Center, Göttingen

Prof. Dr. Tim Gollisch
Sensory Processing in the Retina, University Medical Center Göttingen

Date of oral examination: 12th of November, 2024

Acknowledgements

First and foremost, I would like to thank Alexander Gail for giving me the opportunity to join his group and embark on this exciting project. I am truly grateful for your thoughtful guidance and support throughout these years. I would also like to thank Hansjörg Scherberger and Jorge Jaramillo for their insightful feedback and the engaging discussions during our thesis committee meetings. Additionally, I am thankful to André Fiala, Igor Kagan and Tim Gollisch for kindly agreeing to be part of my examination board.

I would like to express my gratitude to Enrico Ferrea for laying the foundation for this project and for his willingness to assist with any doubts along the way. Moreover, I greatly appreciate the support provided by the lab's technical assistants, particularly by Sina Plümer, who was always available to help with monkey training and care. As well, I would like to thank the rest of the CNL lab, who consistently offered a helping hand by sharing their own experiences. Furthermore, I am grateful to the bachelor's and master's students I had the opportunity to supervise, whose contributions were of great value to this project.

Besides the scientific support, I would like to highlight the friendliness and openness of everybody in the lab. A big heartfelt thanks goes to Lukas Amann for being such an amazing collaborator. While there were many uncertainties in the project, I am certain that working with you has made this experience much more enjoyable.

Outside of the lab, I would like to thank the friends made along the way. Starting with Marta and Marcel, who warmly welcomed me in Göttingen. Juan Carlos, Giorgio, Morine, Karo and Daniel, thank you for sharing so many fun moments during these last years. From back in Spain, thank you to Pía, Elena, Isa, Laura F. and Laura B. for their continued invaluable friendship—hopefully it won't be long distance soon.

Lastly, I would like to thank my family, Begoña, Jose María and Guille, for their unwavering love and support. Above all, I would like to thank Christian, for truly being the kindest and most supportive partner that I could have ever hoped for. I was not expecting to find you here, but I am so happy I did.

Table of contents

For my grandparents

Chapter 1

General introduction

Movement enables us to interact with the world. However, this would be extremely difficult without sensory feedback coming from our limbs. When moving, we receive visual feedback, which is used to determine the position of our limbs relative to external objects, and somatosensory feedback, which provides information of the limb's configuration. Hence, incoming sensory feedback allows our brain to monitor how well outgoing motor commands are achieving the desired outcome, accordingly closing the control loop. Sensory feedback becomes essential when conditions change, which can be internal to our motor system, such as due to muscle fatigue or injury, or external, as when trying out a new tennis racket. Receiving feedback allows us to detect and potentially compensate for these changes by adjusting our movements, which would mean that, luckily, we are still able to win the tennis match. This compensation process is known as motor adaptation, and it is thought to involve updates of our brain's internal models that are used for motor control. Yet, sensory feedback can be noisy and unreliable. This can be due to our imperfect senses, such as using our less-accurate peripheral vision to assess how we hit the ball, or environmental conditions, like when playing a match in the dark at night. Given how dependent we are on sensory feedback to maintain adequate control, it becomes relevant to study how the underlying neural activity is affected when the quality of this feedback is poor. Even more so, deficient feedback particularly affects users of brain-computer interfaces (BCIs). This technology is aimed at restoring lost motor function by leveraging intact neural activity to control an external effector. However, users are currently, in most cases, only provided visual feedback to monitor their effector control. Therefore, evaluating conditions of visual feedback uncertainty is critical for BCI development.

This thesis examines the behavioral and neural consequences of using uncertain visual feedback to make reaching movements, with particular interest in the context of motor adaptation. The introduction will start with a behavioral perspective and review findings on human motor adaptation. The neural counterpart will follow, presenting research on non-human primate motor cortex during reaching behavior. As well, studies focusing on sensory feedback processing and motor adaptation will be assessed. Finally, the introduction will end by describing what BCIs are and how they have expanded our understanding of motor learning.

1.1 Computational models of sensorimotor control

An influential theory in neuroscience is that our brain holds internal representations of the body and the environment, known as internal models (McNamee & Wolpert, 2019). In a sensorimotor context, internal models can predict the consequences of issued motor commands (Jordan & Rumelhart, 1992; Miall & Wolpert, 1996). These are known as forward models, as they receive a copy of motor commands, known as an efference copy, and output the resulting sensory and motor states (Figure 1.1). Hence, they represent the relationship or mapping between the inputs and outputs of the limb. Forward models have been proposed to account for the limitations of sensory feedback (Miall & Wolpert, 1996; Wolpert & Flanagan, 2001). First, sensory feedback has inherent noise due to imperfect receptor transduction, and variability in action potential generation and synaptic transmission (Faisal et al., 2008). In this regard, integrating internal predictions with incoming sensory signals can reduce the uncertainty in the estimated state used for control. This integration process is known as state estimation. Second, internal predictions are important to compensate for temporal delays in the sensorimotor loop. Due to processing and pathway transmission times, it can take around 60 ms for somatosensory feedback and 90 ms for visual feedback to trigger a motor response (Scott, 2016). As a consequence, movement control would be greatly unstable if it only operated based on outdated sensory information (Jordan, 1996). Overall, internal models have been conceptualized to enable fast and robust movement control. While the precise neural implementation of internal models is still unclear, there is ample behavioral evidence that supports that such a predictive mechanism is used (Blakemore et al., 2000; Desmurget & Grafton, 2000; Flanagan & Wing, 1997; Körding & Wolpert, 2004; Wolpert et al., 1995).

Optimal feedback control (OFC) has been a prevalent theory to explain how our brain controls movement (Scott, 2004; Todorov & Jordan, 2002). OFC was proposed to solve the degrees-of-freedom problem that our motor system faces, namely the large number of possible muscle activation patterns that can be used to achieve a task goal. Under OFC, motor commands are based on the minimization of a cost function, which is thought to be based on task requirements and the motor system's biomechanical properties. In this manner, the motor system will choose a movement pattern that is accurate with respect to the task goal and requires the least energy expenditure or effort (Diedrichsen et al., 2010). Behavioral results in support of OFC show that movement variability is only corrected when it is task-relevant, i.e., it impedes achieving the task goal, known as the minimum-intervention principle (Latash et al., 2002; Todorov & Jordan, 2002). Importantly, OFC is based on continuous integration of sensory feedback. As a result, a key element of OFC is optimal state estimation, which relies on internal models for state predictions (Todorov & Jordan, 2002). In this case, optimal would mean that integration follows Bayesian principles (Körding & Wolpert, 2006). These dictate that each input signal is weighed by its relative reliability, implying that the higher the reliability of a signal, the higher its contribution to the final estimate. As a consequence, when integrating these weighed signals, the resulting final estimate is both more accurate

and reliable. Overall, OFC theory has served to bring forward the role of sensory feedback, showcasing its integration for effective movement control.

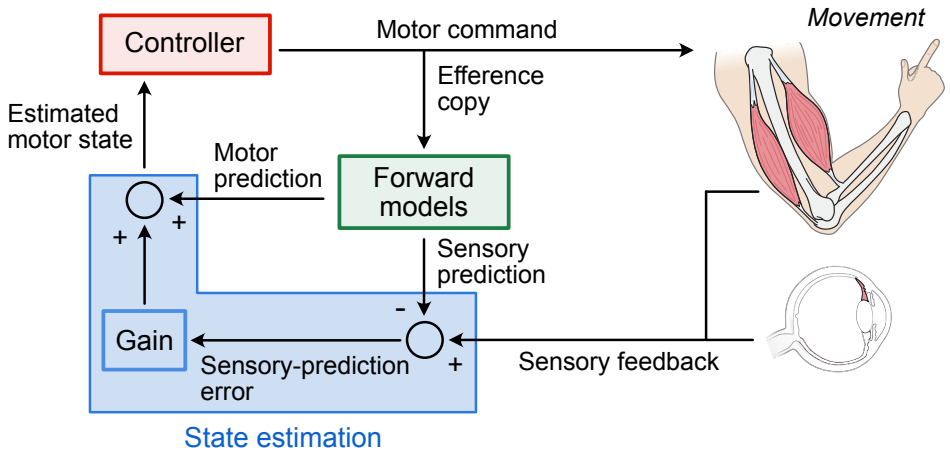

FIGURE 1.1: Computational model of motor control. A controller (red box) issues a motor command to the limb, which executes it. A copy of this command (efference copy) is sent to internal forward models (green box), which predict the sensory and motor state resulting from the motor command. At the same time, visual and somatosensory feedback is integrated and compared to sensory predictions. If these are discrepant, a sensory-prediction error is generated. This sensory-prediction error is scaled and integrated with the motor state prediction, known as the state estimation process (blue box). The resulting motor state estimate is provided back to the controller. Modified from (Wolpert et al., 1995). Graphical illustrations reproduced with permission from (Kandel et al., 2021).

1.2 Motor learning

A hallmark of our motor system is its flexibility. Motor learning can be divided into skill acquisition and motor adaptation. Skill acquisition involves *de novo* learning of a particular movement pattern, such as learning how to play tennis. Instead, motor adaptation is based on modifications to existing movement patterns to optimize performance, such as ultimately becoming a professional tennis player. At the same time, learning can be based on different processes (Huang et al., 2011; Wolpert et al., 2011). Error-based learning is a supervised process that aims to reduce an internal error signal over repetitions or trials. In this sense, it is supervised as the system has access to the expected outcome, with which it generates the error signal. On the other hand, reinforcement learning is based on maximising long-term reward or success through the exploration of the solution set (Dayan & Daw, 2008). Given its predominance in the field, I will focus on motor adaptation through the lens of error-based learning.

1.2.1 Internal models in motor adaptation

An important concept used to explain error-based motor adaptation is the internal forward model. As outlined in section 1.1, internal models would predict the sensory consequences

of a given movement command. When there is a discrepancy between the predicted and received sensory feedback, a sensory prediction error (SPE) is generated (Jordan & Rumelhart, 1992; Shadmehr et al., 2010). This SPE is thought to guide updates in the internal model, leading to motor adaptation (Miall & Wolpert, 1996). Thus, the adaptation process will be complete when predictions are back in line with the received sensory feedback. However, how much the SPE is considered can vary. SPEs are thought to be optimally integrated with internal predictions following Bayesian theory (Wolpert et al., 1995). In this way, when sensory feedback uncertainty is high, our motor system should rely more on internal predictions than on the SPE, and vice versa. Indeed, behavioral studies manipulating visual feedback uncertainty showed that movement corrections are smaller when visual feedback uncertainty is high (Burge et al., 2008; Körding & Wolpert, 2004; Wei & Körding, 2010). While internal prediction uncertainty is more difficult to experimentally manipulate, one study attempted to do so by allowing participants different levels of movement practice. The less the movement practice, the higher the internal prediction uncertainty. Their results showed that participants who sat idly in a dark room had increased movement corrections compared to participants who were allowed to practice (Wei & Körding, 2010). Therefore, behavioral results support that the integration of sensory-based updates or SPEs and internal predictions follows Bayesian principles.

1.2.2 Multiple processes of motor adaptation

Traditionally, motor adaptation was thought to only involve updates in our internal models, referred to as implicit adaptation. However, motor adaptation is now considered to be driven by multiple processes or components that develop at different timescales and/or are driven by different kinds of errors (Morehead & Orban de Xivry, 2021). In this regard, implicit and explicit adaptation are the two main processes that drive movement adjustments.

Implicit adaptation occurs in a slow, gradual and unconscious manner. This process is thought to be primarily driven by SPEs, the difference between expected and actual movement outcome (Shadmehr et al., 2010). However, more recent work suggests that implicit adaptation is also modulated by task performance measures (Al-Fawakhiri et al., 2023; Leow et al., 2018; Leow et al., 2020). As this process is considered to be automatic, implicit adaptation comes into effect at short reaction times. Error sensitivity refers to the magnitude of correction relative to the size of the previously experienced error. Implicit error sensitivity has been shown to be highest for small errors, and decrease with increasing error size (Hutter & Taylor, 2018; Kim et al., 2018; Marko et al., 2012). Therefore, implicit adaptation is best sought to correct small errors that likely originate from our nervous system (Wei & Körding, 2009), such as due to motor noise or fatigue. In line with this, implicit adaptation appears to reach an upper bound for large error sizes (Kim et al., 2018; Modchalingam et al., 2023), potentially reflecting a limited plasticity of our motor system (Tsay et al., 2021).

Explicit adaptation is based on fast strategic compensation of errors (Tsay et al., 2024), using procedures such as mental imagery or memory retrieval (Anguera et al., 2010; McDougle & Taylor, 2019). Moreover, this process is driven by task performance errors, such as the distance between movement endpoint and target (Morehead & Orban de Xivry, 2021). Since explicit adaptation is a conscious process, it requires cognitive resources that delay the initiation of the reach (Fernandez-Ruiz et al., 2011). Thus, long reaction times are typically associated with strategy use. Contrary to implicit adaptation, explicit adaptation is triggered by large and easily perceived errors, which more likely originate from external sources (Bond & Taylor, 2015; Neville & Cressman, 2018; Werner et al., 2015).

Implicit and explicit processes were initially thought to operate independently. This idea stemmed from a study showing that implicit adaptation can override an instructed explicit strategy, despite degrading task performance (Mazzoni & Krakauer, 2006). However, later evidence suggests that these two processes interact (Albert et al., 2022; Miyamoto et al., 2020). The source of this interaction could be task performance errors. In particular, target errors could be a driver of not only explicit, but also implicit adaptation, resulting in a competitive interaction between both (Albert et al., 2022). This would explain behavioral results showing that when explicit strategies are promoted, such as instructing participants how to reduce their movement error, implicit adaptation is reduced (Benson et al., 2011; Modchalingam et al., 2023; Neville & Cressman, 2018). Correspondingly, inhibiting explicit strategies increases implicit adaptation measures (Albert et al., 2021; Fernandez-Ruiz et al., 2011; Haith et al., 2015). While precisely how these two processes interact is still under investigation, current experimental paradigms make efforts to dissociate them, which will be presented below.

1.2.3 Motor adaptation paradigms

Motor adaptation is experimentally studied by perturbing the sensory feedback of a given movement. Classical experiments used prism glasses, which introduce a shift in the visual field (Helmholtz, 1867; Redding & Wallace, 1978; Welch, 1974). Right after donning the glasses, participants are unable to accurately reach towards a target. However, these reaching errors are gradually reduced with practise, and participants ultimately compensate for the visual shift. Remarkably, the adapted behavior is conserved even after taking the glasses off. This is known as the after-effect, which is the hallmark of implicit adaptation (Shadmehr & Mussa-Ivaldi, 1994). Nowadays, computer displays and movement tracking devices enable experimenters to introduce perturbations in a highly controlled and flexible manner. In this way, visual feedback presented on a display can be dissociated from the hand movement, which is typically occluded from view. Perturbations in the visual domain include rotations or shifts in the visual feedback of a movement, while perturbations in the proprioceptive domain can be implemented by applying a force field to the moving limb. Given that I am

mostly interested in the effects of visual feedback on movement, and rotations to the visual feedback are the most studied paradigm, I will focus on them here.

A visuomotor rotation (VMR) introduces an angle between the displayed visual feedback and hand movement directions (Figure 1.2). To compensate for the resulting visual errors, subjects should move in a direction counter to the imposed rotation. There are two main patterns in which VMRs can be applied, namely in a block design or at interspersed single-trials. In a block design, the VMR (same magnitude and direction) is applied continuously for a number of trials. This allows to evaluate behavioral changes after long-term exposure to the perturbation. Hence, the initial response to the perturbation, as well as the final adaptation level or after-effect can be quantified. To accurately measure the after-effect, visual feedback is typically removed upon starting the reach, which eliminates the influence of visual errors experienced on those trials. Another pattern is to apply different types of VMRs (different magnitudes and directions) randomly from trial to trial, resulting in minimal cumulative adaptation. This is known as single-trial learning, in which the response to the error experienced in the previous trial is measured. One practical advantage of this method is that it allows to test multiple conditions, such as different rotation sizes, on a single subject and session.

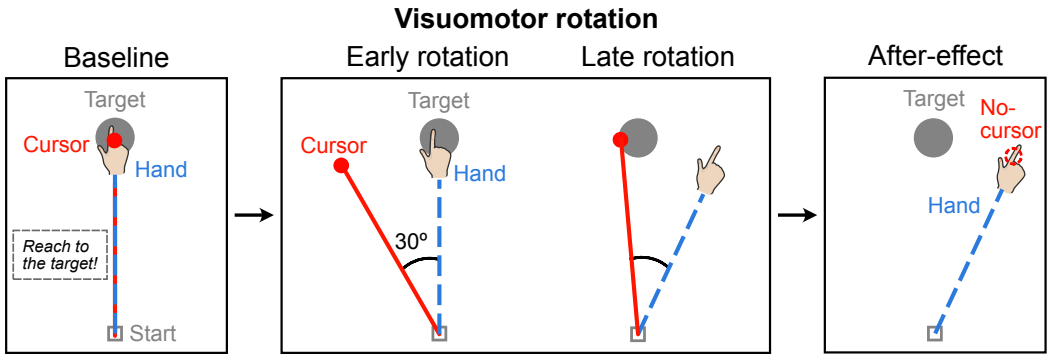

FIGURE 1.2: Visuomotor rotation paradigm to study motor adaptation. In an initial baseline block, participants perform reaches to a target by controlling a visual cursor representing their hand. Then, a visuomotor rotation is introduced. This perturbation rotates the visual cursor movement direction with respect to the hand movement direction. During early rotation, visual errors are large as the participants' baseline behavior is unchanged. After a number of trials (late rotation), visual errors are small as participants move the hand in a direction countering the rotation. How much the participant has adapted is assessed by removing the rotation and the visual cursor, and measuring how much of the adapted state is preserved (after-effect).

Given that motor adaptation is not a unitary process, studies now aim to appropriately dissociate implicit and explicit adaptation. One way to measure both is the process dissociation procedure (PDP), which assumes that explicit adaptation is controllable and can be disengaged at will (Werner et al., 2015). PDP involves removing visual feedback of the movement and providing specific instructions to participants for a short number of trials. To measure the implicit component, participants are asked to disengage any strategies and reach directly to the target. To measure the explicit component, they are asked to continue their previous

behavior, maintaining any strategy they had been using, and then the implicit component measure is subtracted.

Implicit and explicit adaptation can also be dissociated by providing aiming landmarks and asking participants to report their aiming direction, equivalent to the explicit component, prior to performing the reach (Bond & Taylor, 2015; Taylor & Ivry, 2011). Then, implicit adaptation is measured by subtracting the aiming direction from the performed reach direction. Thus, this procedure assumes that explicit adaptation can be verbalized (Maresch et al., 2021a). However, the use of aiming landmarks has been questioned as these appear to promote the use of a strategy (Maresch et al., 2021b). Furthermore, this method assumes that implicit and explicit adaptation are linearly additive processes, which may not always hold true ('t Hart et al., 2024).

One method to isolate implicit adaptation that has gained relevance is the error-clamp (Morehead et al., 2017). This method is based on implicit adaptation being a fully unconscious process. Contrary to the traditional or movement-contingent VMR, in which visual feedback direction is tied to hand reach direction, the error-clamp fixes the direction of the visual feedback. Therefore, participants experience a constant visual error, which they are instructed to ignore and to continue reaching towards the target. Consequently, the error-clamp is thought to only elicit SPEs, which would only result in implicit adaptation. Indeed, even though participants are told to ignore the constant visual error, it still elicits behavioral compensation (Kim et al., 2018; Morehead et al., 2017; Tsay et al., 2021; Zhang et al., 2024). While it is unclear whether the error-clamp engages the same adaptation mechanisms as the movement-contingent VMR (Albert et al., 2022; Zhang et al., 2024), it has proved useful to continuously monitor implicit adaptation.

1.3 Neurophysiology of movement

The previous sections showcased the behavioral relevance of sensory feedback, and its uncertainty, especially in the context of motor adaptation. This brings the question of how does sensory feedback uncertainty impact the neural correlates of movement. Movement control is distributed throughout the brain, involving both cortical and subcortical structures. In the case of voluntary goal-directed reaching, frontal and parietal cortical areas have a primary role. Posterior parietal cortex (PPC) associates sensory information to motor action (Andersen et al., 1997). In turn, frontal motor areas, including primary motor cortex (M1), premotor cortex, supplementary motor areas (SMA), and cingulate motor areas (CMA), contribute to the planning and execution of movement (Dum & Strick, 2002). Here, I will focus on M1 and dorsal premotor cortex (PMd), which I will jointly refer to as motor cortex. Given their high cognitive abilities and musculoskeletal similarity to humans, I will focus on studies using macaques as a model organism.

1.3.1 Motor cortex: Primary motor and dorsal premotor cortex

Primary motor cortex (M1) and dorsal premotor cortex (PMd) are frontal areas involved in motor control. M1 is anatomically located on the rostral bank of the central sulcus, and PMd lies rostral to M1 and medial to the spur of the arcuate sulcus (Figure 1.3, left). M1 receives input projections from primary somatosensory cortex, premotor cortex, SMA, CMA and more rostral areas of PPC (Stepniewska et al., 1993; Tokuno & Tanji, 1993; Wise et al., 1997). PMd is reciprocally connected to M1, SMA, CMA, prefrontal cortex and dorsal PPC areas (Caminiti et al., 1999; Caminiti et al., 1985; Ghosh & Gattera, 1995; Kurata, 1991; Wise et al., 1997). M1 is viewed as the primary source of cortical motor signals arriving to the spinal cord. Accordingly, neurons in the output layer of M1 form the corticospinal tract (Lemon, 2008), with axons terminating in intermediate regions of the spinal cord. M1 also projects directly to spinal motor neurons that innervate muscles via cortico-motoneuronal cells, mostly located in the caudal region of M1 (Rathelot & Strick, 2009). While PMd is considered to be higher in the control hierarchy than M1, PMd also projects to the spinal cord (Dum & Strick, 1991; Dum & Strick, 2002). Evidence of anatomical pathways from M1 and PMd to muscles is further supported by electrical intracortical stimulation of these areas (Godschalk et al., 1995; Stepniewska et al., 1993; Weinrich & Wise, 1982). This stimulation evokes muscle contraction, with higher electrical currents needed when targeting PMd, indicative of a more indirect connection.

Voluntary goal-directed reaching is typically divided into planning and execution stages. These two stages have been experimentally dissociated by imposing a delay between the goal or target presentation and movement initiation (instructed-delay task). As well, arm reaching behavior is classically studied by having monkeys perform reaches from the center of the workspace to radially placed visual targets (center-out reach task). In motor cortex, a functional rostro-caudal gradient has been found, with activity changing from being mostly planning-related to mostly execution-related (Johnson et al., 1996). Accordingly, results show that M1 is mostly active during movement execution, displaying little activity during the planning stage (Crammond & Kalaska, 2000; Riehle & Requin, 1989). In contrast, PMd is primarily involved in movement planning, but also contributes to execution (Godschalk et al., 1981; Riehle & Requin, 1989; Weinrich & Wise, 1982; Weinrich et al., 1984). Importantly, PMd does not reflect the sensory aspects of the visual target representing the motor goal, but rather the associated motor plan (Wise et al., 1992).

The study of motor cortex has evolved following advances in neural recording technology. Classical studies recorded from isolated neurons using single electrodes and focused on how the activity of each neuron related to given kinetic or kinematic parameters. Collectively, these studies sought to answer what information a neuron encodes or represents, taking what is known as a representational perspective (Figure 1.3, middle). With the advent of multi-electrode arrays, capable of recording from tens to hundreds of neurons simultaneously, research questions began to focus on the neural population as a whole. Along this line,

the dynamical systems framework has gained relevance to help understand how the neural population performs given computations (Vyas et al., 2020a) (Figure 1.3, right). Below, I will present findings of motor cortex under both the representational and dynamical systems perspective.

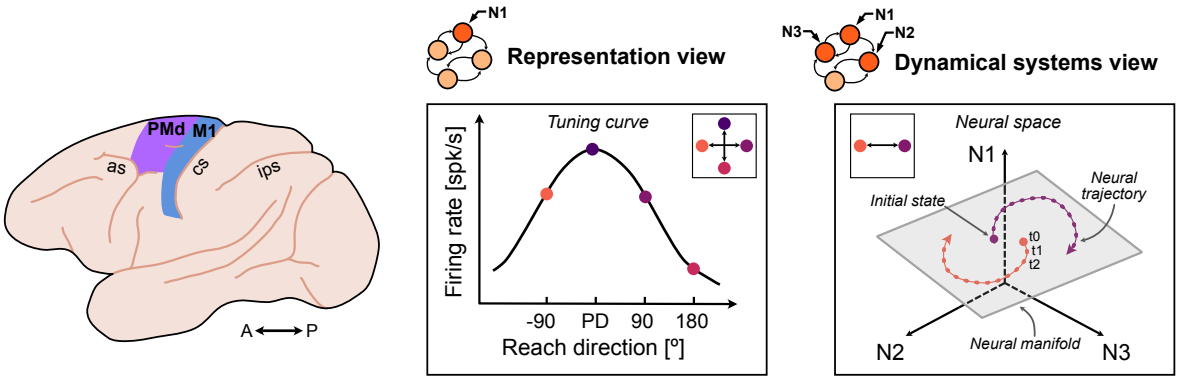

FIGURE 1.3: Motor cortex and study approaches. Left panel. Location of dorsal premotor cortex (PMd, purple) and primary motor cortex (M1, blue) in the macaque brain. *as* denotes the arcuate sulcus, *cs* the central sulcus and *ips* the intraparietal sulcus. Brain saggital view shown from anterior (A) to posterior (P). Middle panel. The representational view relates single-neuron activity to movement parameters. Single neurons typically display cosine tuning with respect to reach direction, being maximally active at their preferred direction (PD). Right panel. The dynamical systems view studies how neural population activity evolves in the neural state space. Each axis in this space represents the activity of a recorded neuron. Planning activity sets the initial state, from which a neural trajectory evolves over time during execution. Neural states do not explore the full space but are confined within a region of the neural space (neural manifold). Insets show potential reach targets.

Representational view

The representational view is based on single neurons representing or encoding information from given parameters. Thus, a neuron's activity should systematically change with the parameter, leading to the notion that this neuron is tuned to it. Single neurons in M1 have been found to encode low-level movement parameters, such as force, tightly linked with the required muscle activation to generate them (Cheney & Fetz, 1980; Evarts, 1968; Evarts et al., 1983; Kakei et al., 1999; Kalaska et al., 1989). Nevertheless, M1 single-neuron activity also consistently correlates with higher-level extrinsic parameters related to movement kinematics (Georgopoulos et al., 1982; Kakei et al., 1999), with similar findings for PMd neurons (Caminiti et al., 1991; Riehle & Requin, 1989). Most influential, M1 and PMd single-neuron activity relates to reaching direction (Caminiti et al., 1991; Crammond & Kalaska, 2000; Georgopoulos et al., 1982; Georgopoulos et al., 1986; Riehle & Requin, 1989). How the activity of these neurons relates to reaching direction is typically explained by a cosine curve, known as cosine tuning (Figure 1.3, middle). Thus, a neuron is maximally activated for a given reach direction, called its preferred direction (PD). Then, the neuron's activity lowers as the reach direction is further apart from its PD. This directional selectivity can be more or less prominent, which is captured by the neuron's modulation depth (MD). In this sense, the

lower the MD, the less distinguishable the activity at the PD from the activity at the rest of the reaching directions. Besides reach direction, M1 and PMd single-neuron activity has been shown to correlate with other kinematic parameters, such as reach extent (Messier & Kalaska, 2000; Riehle & Requin, 1989) or speed (Churchland et al., 2006b; Moran & Schwartz, 1999).

Focusing on directional tuning, the population response has also been evaluated by combining activity from multiple neurons. Thus, studies have inferred how the population represents a given reach direction based on the tuning properties of each individual neuron. For standard center-out reaches, neurons whose PD aligns with the instructed reach or target direction will be mostly active, driving the population response (Georgopoulos et al., 1986). However, when the target direction is made spatially uncertain, neurons whose PD is further apart to this direction are also active (Dekleva et al., 2016). This broadening of the population's target representation has been found in PMd, but not M1. Along this line, when there is an experimentally imposed bias towards a reach direction, neurons in PMd whose PD is close to the biased direction have increased activity prior to disclosing the reach direction (Glaser et al., 2018; Suriya-Arunroj & Gail, 2019). These findings highlight a functional separation between PMd and M1. PMd can represent the probability of an upcoming reach, whereas M1 is mainly reflects the selected action (Cisek & Kalaska, 2005; Dekleva et al., 2016; Glaser et al., 2018).

The representational view provided the first step to characterize motor cortex by relating single-neuron activity to movement parameters, trying to establish a direct link between neural processing and behavior (Kriegeskorte & Diedrichsen, 2019). However, this link has been rather difficult to determine (Churchland & Shenoy, 2007; Fetz, 1992). For instance, PDs have been observed to change between planning and execution (Churchland et al., 2010; Crammond & Kalaska, 2000), and even throughout execution (Churchland & Shenoy, 2007; Hatsopoulos et al., 2007; Sergio et al., 2005). Additionally, a given neuron may be related to multiple movement parameters or none at all (Churchland & Shenoy, 2007; Kakei et al., 1999; Kalaska et al., 1989). In this regard, mixed encoding was proposed, whereby neurons can encode multiple parameters as a mechanism to confer flexibility in the population readouts (Tye et al., 2024). Altogether, while conferring an intuitive description level, the complexity of single-neuron responses obscures the representational view. Therefore, there has been increased focus on studying the neural population as a whole, without considering individual tuning properties.

Dynamical systems view

Motor cortex is nowadays widely studied through the dynamical systems framework (Churchland & Shenoy, 2024; Shenoy et al., 2013; Vyas et al., 2020a). Within this framework, neural population activity is represented in an N-dimensional space, N being the number of neurons, where each axis represents the activity of a neuron (Figure 1.3, right). At each time step, the neural population takes a given point or state and, over time, follows a neural trajectory in

the space. Overall, this neural state space captures combinations of neuron activation, i.e., neural population activity patterns.

Assessing motor cortex activity in the neural state space, population activity patterns do not explore the full-dimensional space, but are confined to a lower-dimensional subspace or manifold (Gallego et al., 2017). Hence, the range of neural activity patterns used are well captured by a low number of independent patterns, called neural factors. Moreover, these neural factors appear similar across multiple motor behaviors despite requiring different muscle outputs (Altan et al., 2023; Gallego et al., 2018), and are conserved over long timescales (Gallego et al., 2020). Overlap between neural modes has even been found across monkeys performing the same behavior (Safaie et al., 2023). This preservation and stability of motor cortical activity patterns is hypothesized to result from constraints imposed by the neural network connectivity (Gallego et al., 2020; Safaie et al., 2023).

When conceptualizing motor cortex as a dynamical system, planning activity is thought to set the initial state upon which execution dynamics unfold (Churchland et al., 2010; Vyas et al., 2020a). Hence, the location of the initial state defines the subsequent movement. Neural variability has been shown to decline over the planning epoch, consistent with the idea that activity converges to an attractor-like initial state (Churchland, 2006). Furthermore, studies have shown that variability in the initial state correlates with variability in the reaching behavior (Afshar et al., 2011; Churchland et al., 2006a; Even-Chen et al., 2019), providing a link between planning states and subsequent behavior.

A longstanding question has been how can planning activity occur without generating motor output. Considering the mapping between neural and muscle activity, this can be divided into output-potent and output-null (Churchland & Shenoy, 2024). Output-potent neural activity produces muscle activity, whereas output-null neural activity does not. Following, the neural state space would have output-potent and output-null dimensions. Planning activity in PMd and M1 was seen to preferentially occupy output-null dimensions (Kaufman et al., 2014). In turn, execution activity occupied output-potent ones. Moreover, planning activity from PMd, thought to contribute more to the planning process, lied in the output-null space of M1. A later study extended this work by finding that planning and execution activity of motor cortex lie in orthogonal subspaces, but conserve the same task-related structure (Elsayed et al., 2016). The use of orthogonal subspaces would also help explain how planning can happen during execution, as has been seen when there is a sudden change in target (Ames et al., 2019) or performing a sequence of reaches (Zimnik & Churchland, 2021).

The transition from planning to execution has been proposed to be mediated by a trigger-like signal, possibly reflecting inputs from other brain areas (Kaufman et al., 2016). This is motivated by the finding that motor cortex exhibits a large activity response aligned to movement onset. Importantly, a component of this response is condition-independent, which means that it does not convey target direction or reach trajectory information. Instead, the condition-independent component carries movement timing information, being predictive of reaction

times on a single-trial basis (Kaufman et al., 2016; Michaels et al., 2015). Furthermore, this condition-independent component is also present when performing a sequential or corrective movement (Malonis et al., 2021; Zimnik & Churchland, 2021). Thus, it is possible that an input signal enables the transition from planning to execution dynamics.

When it comes to execution, population activity from motor cortex has been shown to have rotational dynamics during reaching (Churchland et al., 2012). The specific shape, namely amplitude and phase, of these rotations depends on the initial state set during planning. More recently, this rotational model was revisited to explain a more diverse set of reaches, and revealed that rotations occur in different planes and regions in the neural state space (Sabatini & Kaufman, 2024). Unlike muscle activity, motor cortex activity has been found to evolve in a smooth manner (Russo et al., 2018). Simulations showed that smooth dynamics confer robustness against noise. Thus, having these smooth dynamics would allow motor cortex to generate reliable outputs. Altogether, these findings are consistent with the view that motor cortex behaves as a dynamical system that generates movement (Churchland et al., 2012).

1.3.2 Motor cortex in sensory feedback processing

Motor cortex has been predominantly studied in relation to movement planning and initiation. Turning towards movement execution, understanding how limb sensory feedback is integrated becomes increasingly relevant. Indeed, motor cortex appears to take a role in sensory feedback processing. One approach to evaluate such processing has been to apply transient perturbations to limb sensory feedback. As a result, monkeys are required to make feedback-based movement corrections to achieve the task goal. Both mechanical and visual perturbations have been found to trigger changes in M1 population activity (Cross et al., 2024; Hatsopoulos & Suminski, 2011). In the case of mechanical perturbations, transient loads applied to the arm elicit an early task-independent, i.e., unaffected by behavioral goal, response in M1 that presumably reflects somatosensory inputs (Omrani et al., 2014; Pruszynski et al., 2014; Wolpaw, 1980). This is followed by a task-dependent response, likely responsible for goal-directed muscle activity. PMd also shows these task-dependent responses, albeit to a lower extent and at a longer time lag than M1 (Omrani et al., 2016). In addition, when PMd is temporarily deactivated through cortical cooling, corrections to mechanical loads are slower and less accurate (Takei et al., 2021). In the case of visual perturbations, these are typically shifts in the position of the visual cursor, representing the hand, which are applied during movement execution. These cursor shifts evoke a change in motor cortex activity (Cross et al., 2024) that has been divided into two phases (Stavisky et al., 2017). The early phase of the response does not influence downstream motor output, likely reflecting sensory processing. After this, the observed change in activity is responsible for driving corrective movements.

Motor cortex activity during feedback-based corrective movements has also been evaluated with a precision-reaching task. In this task, the target size is reduced to elicit small homing-in corrective movements, guided by visual feedback, after the larger initial movement is made. Results show that the PD of M1 neurons changed between initial and corrective movements (Schwartze et al., 2024). In terms of MD, a decrease in this parameter would be expected due to the smaller nature of the corrections. Nevertheless, when MDs were scaled by movement speed, neurons exhibited either increases or decreases for corrective relative to initial movements. Moreover, neural state space analyses revealed that neural states from initial or corrective movements were not fully overlapping (Lee et al., 2024; Schwartze et al., 2024). This indicates that different neural activity patterns are employed for each movement phase, which could be partly due to the difference in visual feedback reliance.

The effect of sensory feedback on motor cortex activity has also been studied by removing such feedback. In these studies, monkeys had to perform reaches with and without visual feedback of their hand. Relevant to this thesis, not having a cursor can be interpreted as having infinite visual feedback uncertainty. When reaching without a cursor, single neurons in M1 decreased their MD during the late phase of movement, that is, when coming close to the target (Suway & Schwartz, 2019). On the contrary, no tuning differences were found for the initial phase of movement, likely because visual feedback is mostly irrelevant at this time. Overall, motor cortex is involved in sensory feedback processing, most noticeable when feedback-based corrections are needed.

1.3.3 Motor cortex in motor adaptation

Motor adaptation appears to be dependent on the cerebellum, a subcortical structure thought to house internal models (Shmuelof & Krakauer, 2011). However, neural correlates of adaptation have also been found in motor cortex. Similar to human motor adaptation experiments, force-field (FF) perturbations to the moving limb, as well as VMRs, have been tested to uncover their neural counterpart.

In terms of reach direction tuning analysis, single neurons in motor cortex display shifts in PD when monkeys adapt to FF (Cherian et al., 2013; Gandolfo et al., 2000; Li et al., 2001; Perich & Miller, 2017) or VMR (Paz et al., 2003; Suway & Schwartz, 2019; Wise et al., 1998) perturbations. These shifts in PD could reflect a shift in the recruitment of neurons after adaptation (Arce et al., 2010a). Hence, for a given target direction, neurons whose baseline PD is aligned with the compensatory reach direction, and not the actual target direction, are mostly active. Notably, the shift in neuron recruitment appears to be modulated by the availability of visual feedback throughout the reach (Arce et al., 2010a; Arce et al., 2010b). When only showing visual feedback at movement endpoint, neurons with PDs between the compensatory and actual target direction are mostly active. This indicates a less-adapted neural population response, which is reflected in the behavioral measurements. Evaluating single-neuron PD shifts in M1 over the course of FF adaptation, these were found to appear

closely after the FF was introduced, and did not gradually increase following behavioral adaptation (Cherian et al., 2013; Perich & Miller, 2017). Moreover, the majority of these PD shifts disappeared after removing the FF. Thus, PD shifts in M1 are likely due to changes in the recruitment of neurons to compensate for the new kinetic requirements, implying that motor adaptation is implemented in upstream brain regions.

Planning activity has been the focus of multiple motor adaptation studies, as it provides a window to the neural adaptive state, dissociated from potential movement corrections during execution. In the neural state space, motor cortical planning states have been shown to gradually change throughout adaptation. These states move towards baseline states associated with reaching directions that would result in compensatory behavior (Sun et al., 2022; Vyas et al., 2018). Moreover, adequate planning states appear to be required for adaptation. Evidence shows that disruption of PMd activity through intracortical microstimulation close before movement initiation on a given trial caused visuomotor adaptation deficits in the next one (Vyas et al., 2020b). These deficits also occurred when stimulating M1, albeit to a lower degree. Thus, planning activity, more notable in PMd, is important for updates to the adapatation process.

Adaptation-related changes in functional connectivity within and between PMd and M1 have also been investigated with the help of modelling (Perich et al., 2018). For FF and VMR adaptation, no changes in functional connectivity between early and late adaptation were found within these areas. When assessing functional connectivity from PMd to M1, only PMd activity that was output-null to M1 activity during the planning period was affected, and only in the case of FF adaptation. This suggests that planning activity reserved to PMd specifically contributes to FF adaptation, whereas upstream inputs could mediate VMR adaptation. Supporting this, recurrent neural network (RNN) simulations showed that VMR adaptation is more likely due to changes in inputs from upstream areas to PMd and M1, than changes in local connectivity within these (Feulner et al., 2022).

Recent work has revealed an important role of planning activity in FF learning (Sun et al., 2022). Upon learning a FF, motor cortical planning states experienced a uniform shift, common to all reach directions, in the neural state space. Moreover, these uniform shifts persisted throughout washout, and did not happen for peri-movement neural states. Notably, when learning different FFs, the uniform shifts from each FF were orthogonal to each other. Thus, planning activity could be relevant for accessing and storing different motor behaviors without interference, as was previously suggested in a human behavioral FF experiment (Sheahan et al., 2016). Finally, uniform shifts of neural states did not happen after VMR adaptation, which adds to the evidence supporting that VMR and FF adaptation could be mediated by different neural mechanisms.

1.4 Brain-computer interfaces

Brain-computer interfaces (BCIs) transform neural activity into control signals for an external device (Andersen et al., 2022; Lebedev & Nicolelis, 2017; Wolpaw et al., 2000) (Figure 1.4). BCI technology emerged to help patients with disabilities by restoring lost visual, auditory or sensorimotor function. However, BCIs have also proven to be a useful experimental tool to study neural properties (Golub et al., 2016). Here, I will focus on intracortical BCIs designed to leverage motor cortex activity to control the movement of a cursor on a screen. As well, I will focus on closed-loop BCIs, with which the user receives concurrent feedback of their control that, in turn, potentially influences neural activity.

First, neural activity from a large number of neurons is recorded through microelectrode arrays implanted in motor cortex (Homer et al., 2013). These arrays enable high spatial and temporal recording resolution, so spikes of individual neurons can be detected on each electrode of the array. Then, this activity is provided as input to an algorithm or decoder, which defines the mapping that translates neural activity into motor commands for the cursor in real-time. Linear decoding methods have been proven successful, with the Kalman filter (Gilja et al., 2012; Malik et al., 2011) as one of the most commonly used decoding algorithms. Currently, decoding advances are geared towards implementing machine learning algorithms (Ali et al., 2024; Sussillo et al., 2016). Importantly, the decoder has to be trained or calibrated prior to use. Both manual reaches, as well as passive observation of computer-aided movements of the cursor, have been proven useful for decoder calibration, although, notably, the former is not an option for patients with lost motor function. Long-term stability is a central issue for BCIs, as neuronal dropout or unexpected shifts in neural activity can occur from day to day (Downey et al., 2018). Therefore, decoders are typically recalibrated each day in basic neurophysiology studies. However, a proposed approach to remedy this are adaptive decoders, which recalibrate throughout BCI use to aid with performance stability and learning (Orsborn et al., 2012; Orsborn et al., 2014; Rajeswaran et al., 2024; Shenoy & Carmena, 2014).

It is worth noting that one of the main advantages that BCIs provide, especially for basic neurophysiology studies, is that the decoder is predefined by the experimenter (Golub et al., 2016). This implies that the exact causal relationship between neural activity and behavior is known, which helps with its interpretation. Additionally, using a decoder removes the influence of additional brain structures or complex nonlinear arm dynamics, allowing to isolate the effect of the recorded neural activity on behavior.

Finally, the decoder outputs the position of the cursor, which is updated at each time step. Closing the loop, users receive sensory feedback of their control, which, in the case of the cursor on the screen and most other current applications, is in the visual domain. As a consequence, BCI users are particularly susceptible to conditions of high visual feedback uncertainty (Liu et al., 2024). The lack of somatosensory feedback can be considered an advantage

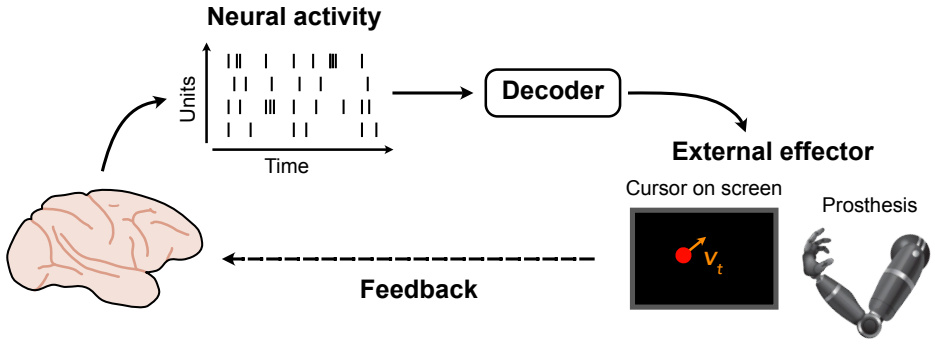

FIGURE 1.4: Brain-computer interface. Neural activity is recorded from the brain and passed into a decoder, which translates it into commands to control an external effector, such as a cursor on a screen or a prosthesis. Finally, the loop is closed by providing the user feedback on the effector control.

as it does not influence neural activity in basic neurophysiology studies. Nevertheless, additional artificial feedback is sought for clinical applications, as it has been shown to improve control performance (Dadarlat et al., 2015; Flesher et al., 2021; Suminski et al., 2010). Along this line, the development of bi-directional BCIs, which provide additional feedback to the brain in the form of electrical or optical stimulation, is underway (Bensmaia & Miller, 2014; Dadarlat et al., 2023).

1.4.1 BCIs in learning

BCI experiments have provided valuable insights into neural activity changes in motor cortex related to learning. To prepare for neuroprosthetic applications, neural changes related to learning to control a BCI *de novo*, akin to skill acquisition, have been investigated. During this process, neurons show changes in their tuning properties, which stabilize over days of training (Ganguly & Carmena, 2009). When assessing the neural population, it was found that each neuron independently varies its activity patterns early in learning, suggestive of an exploratory process (Athalye et al., 2017). As learning proceeds, this independent variability decreases, giving way to shared variability from coordinated population activity patterns. Thus, these results reflect the consolidation of a subspace containing the neural patterns that enable proficient BCI control. Moreover, experimenters found that recorded neurons whose activity was not used for decoding, and consequently did not directly influence behavior, also exhibited similar learning-related changes, albeit to a lesser degree (Ganguly et al., 2011; Zippi et al., 2022).

Similarly, BCI studies have explored how the population is affected by changes in the decoder, mimicking motor adaptation paradigms. A set of experiments rotated the directional contribution of a subset of neurons used for decoding, akin to a VMR. They found that the largest influence on behavioral adaptation came from global changes in all of the neurons, and was consistent with a re-aiming strategy to counter the rotation (Chase et al., 2012; Jarosiewicz et al., 2008). However, a smaller contribution came from changes in the tuning properties

of the rotated neurons, reflecting local adaptation. Evaluating these changes over a longer timescale, global changes initially contributed to a fast reduction in movement error, while small local changes built up over the course of weeks to optimize performance (Zhou et al., 2019).

Influential work tested how learning is constrained by the properties of the neural network. Monkeys started these experiments using an intuitive BCI mapping to control the movement of the computer cursor with M1 activity. Similar to manual reaches, the neural activity patterns used for control reside in a low-dimensional subspace, termed the intrinsic manifold, within the neural state space (Sadtler et al., 2014). To evaluate how learning was constrained by the intrinsic manifold, the BCI mapping was altered so that monkeys had to generate neural activity patterns within (within-manifold perturbation, WMP) or outside it (outside-manifold perturbation, OMP). Results showed that only after WMPs did monkeys regain proficient cursor control within a training session (Sadtler et al., 2014), while OMPs required multiple days of exposure (Oby et al., 2019). WMP learning was found to occur through re-association of existing activity patterns to different movement outputs, consistent with short-term motor adaptation (Golub et al., 2018). In contrast, OMP learning resulted from the formation of new activity patterns, reflecting *de novo* motor learning (Oby et al., 2019). Subsequent computational studies employing RNNs found that WMP may require smaller synaptic weight changes (Wärnberg & Kumar, 2019), and that WMP learning is more robust to noisy or sparse feedback, as well as to constraints in the number of plastic connections within the RNN network (Feulner & Clopath, 2021).

A follow-up study tested how neural activity had changed after the WMP in relation to the intuitive mapping (Losey et al., 2024). Thus, after the WMP was learnt, the intuitive mapping was reintroduced. Offline analysis revealed that this activity was still apt for control under the WMP, indicative of a memory trace of the learnt behavior. The memory trace was shown to not influence behavior under the intuitive mapping, residing in its null-space, adding to the evidence that this could be a potential mechanism to store multiple behaviors without interference (Sun et al., 2022). Furthermore, BCIs have also enabled the study of how changes in internal states, such as arousal or engagement, influence learning (Hennig et al., 2021). Large abrupt fluctuations in trial-to-trial M1 activity were found after changing the BCI mapping, as well as after long pauses, hypothesized to be indicative of changes in the monkeys internal state. Moreover, these fluctuations either facilitated or hindered behavioral improvements for moving towards given targets, suggesting that internal state can influence how behavior proceeds with learning.

1.5 Thesis aims and overview

Visual feedback of our limbs is used for adequate movement control. As a consequence, when this visual feedback is uncertain, control is impaired. This is notable when adjustments to our movements are required, such as during motor adaptation. However, since motor adaptation is greatly multifaceted, more precise inspection of the effects of visual feedback uncertainty is warranted. At the same time, little is known about the neural underpinnings of the behavioral impairments caused by visual feedback uncertainty. In this regard, assessing how visual feedback uncertainty affects neural activity is critical for BCI users, who mostly do not have any other sources of additional feedback for effector control. The overarching goal of this thesis is to gain understanding on the behavioral and neural consequences of using uncertain visual feedback for movement. This will be addressed in two related aims: 1) Extend behavioral findings on the effect of visual feedback uncertainty on human motor adaptation, and 2) test how motor cortex activity is affected by visual feedback uncertainty when reaching using the arm or via a BCI.

Chapter 2 provides new insights into human motor adaptation under visual feedback uncertainty. While adaptation has been shown to be attenuated under high visual feedback uncertainty for small visual errors (Burge et al., 2008; Wei & Körding, 2010), how it affects adaptation to large errors is still an open question. Recent studies isolating implicit adaptation by making visual feedback task-irrelevant, found no attenuation under high feedback uncertainty for large errors (Tsay et al., 2021; Tsay et al., 2023). However, we show that attenuation still happens when visual feedback is task-relevant.

As a first step to understand the neural counterpart, in Chapter 3 we studied how visual feedback uncertainty affects motor cortical activity during reaching. The manuscript related to this work has a shared first authorship with a fellow PhD student. Detailed author contributions are presented at the beginning of the chapter. This study compared how target and feedback uncertainty affect motor goal representations during reach planning and early execution. To increase the reliance on visual feedback, precluding the use of somatosensory feedback, we included a condition in which reaches were made through a BCI. This chapter includes a supplementary section with additional findings that have not been included in the manuscript, but expand on the effect of visual feedback uncertainty on reach planning and execution.

As an appendix, this thesis includes an additional co-authored published article. This work studies multisensory integration of visual and vibrotactile cues during reach planning in human participants.

Chapter 2

Task-relevant visual feedback uncertainty attenuates visuomotor adaptation

Virginia Casasnovas, Lukas K. Amann, Gianna L. Haas, and Alexander Gail

Published in *Journal of Neurophysiology* (Casasnovas et al., 2024)

Author contributions:

VC, LKA, and AG conceived and designed research.

VC and GLH performed experiments.

VC analyzed the data.

VC, LKA, and AG interpreted results of experiments.

VC prepared figures and drafted the manuscript.

VC, LKA, GLH, and AG edited and revised the manuscript.

VC, LKA, GLH, and AG approved the final version of the manuscript.

american physiological society

JNP JOURNAL OF NEUROPHYSIOLOGY

J Neurophysiol 132: 879–889, 2024.
First published August 7, 2024; doi:10.1152/jn.00180.2024

RESEARCH ARTICLE

Control of Movement

Task-relevant visual feedback uncertainty attenuates visuomotor adaptation

Virginia Casasnovas,[1,2] Lukas K. Amann,[1,2] Gianna L. Haas,[2] and Alexander Gail[1,2,3,4]

[1]*Sensorimotor Group, German Primate Center – Leibniz Institute for Primate Research, Göttingen, Germany;* [2]*Faculty of Biology and Psychology, University of Göttingen, Göttingen, Germany;* [3]*Leibniz ScienceCampus Primate Cognition, Göttingen, Germany; and* [4]*Bernstein Center for Computational Neuroscience, Göttingen, Germany*

Abstract

Motor adaptation is attenuated when sensory feedback about the movement is uncertain. Although this was initially shown for small visual errors, attenuation seems not to hold when visual errors are larger and the contributions of implicit adaptation are isolated with the error-clamp method, which makes visual feedback task-irrelevant. Here we ask whether adaptation to a similarly large perturbation is attenuated when task-relevant visual feedback is uncertain. In a first experiment, we tested participants on a 30° movement-contingent visuomotor rotation under both low (cursor) and high (cloud of moving dots) visual feedback uncertainty. In line with optimal integration, we found that the early increase in adaptation and final extent of adaptation were reduced with high feedback uncertainty. In a second experiment, we included several blocks of no-feedback trials during the perturbation block to quantify the contribution of implicit adaptation. Results showed that implicit adaptation was smaller with high compared to low feedback uncertainty throughout the perturbation block. The estimated contribution of explicit adaptation was overall small, particularly for high feedback uncertainty. Our results demonstrate an influence of task-relevant visual feedback, and the resulting target errors, on implicit adaptation. We show that our motor system is sensitive to the feedback it receives even for larger error sizes and accordingly adjusts its learning properties when our ability to achieve the task goal is affected.

NEW & NOTEWORTHY Motor adaptation is linked to the estimation of our actions. Whereas uncertainty of task-irrelevant visual feedback appears not to influence implicit adaptation for errors beyond a certain size, here we tested whether this is still the case for task-relevant feedback. We show that implicit adaptation is attenuated when task-relevant visual feedback is uncertain, suggesting a dependency on the assessment of not just sensory prediction errors but also target errors.

motor adaptation; task-relevant error; visual feedback uncertainty

INTRODUCTION

Movements result in sensory feedback, allowing us to assess how we are interacting with the world. For adequate control, it is thought that our motor system internally predicts movement-associated feedback and compares it with the actually received feedback (1–3). A sensory prediction error (SPE) arises when changes happen internally in our motor system or in the external environment, which result in our movements not providing the sensory feedback we expect. The process by which we compensate for these changes is called motor adaptation (4, 5). However, sensory feedback can be noisy and unreliable because of our imperfect senses (6) or environmental conditions, such as the limited accuracy in peripheral vision or when moving under low-light conditions. How uncertain we are about incoming sensory feedback should then modulate how much we take into account the corresponding SPE to drive adaptation (7). Indeed, it has been shown that motor corrections are reduced when visual feedback of hand position is uncertain, implying that our motor system integrates incoming feedback with internal predictions in a statistically optimal manner (8–10). Although studies that supported this optimal integration model focused on small visual errors, the size of the error has also been shown to modulate adaptation (11–14).

Motor adaptation results from multiple processes (15). Implicit adaptation is thought to be driven by SPEs in a

Correspondence: A. Gail (agail@gwdg.de).
Submitted 25 April 2024 / Revised 30 July 2024 / Accepted 1 August 2024

0022-3077/24 Copyright © 2024 The Authors. Licensed under Creative Commons Attribution CC-BY 4.0.
Published by the American Physiological Society.

Downloaded from journals.physiology.org/journal/jn (077.025.034.247) on October 1, 2024.

gradual and unconscious manner, whereas explicit adaptation is driven by task performance errors, which give rise to intentional strategies that require cognitive effort (16–18). In this way, implicit adaptation appears to fully correct for small errors that are more easily attributed to our motor system. As error sizes increase, implicit error sensitivity is reduced (13, 14). Moreover, larger errors can elicit not only implicit adaptation but also explicit action selection strategies to compensate for them (19–21). Here, we focus on adaptation to errors above the size range that is fully compensated by implicit adaptation and large enough to trigger explicit adaptation, and we test how the implicit and explicit components depend on visual feedback uncertainty.

To see whether optimal integration of sensory feedback is independent of error size, a recent study (22) tested the effect of visual feedback uncertainty on both small and large errors. In contrast to previous studies that assessed visual feedback uncertainty (8–10), the experiments specifically targeted implicit adaptation. Implicit adaptation was isolated with the error-clamp method, in which visual feedback is fixed at a given error size while participants are instructed to ignore it (23). This type of perturbation maintains a constant SPE, independent of the state of adaptation of the behavior. Moreover, since the provided feedback is task-irrelevant, the error-clamp method is believed to eliminate target errors, the difference between visual feedback and the target. Results showed that increased visual feedback uncertainty did attenuate implicit adaptation when error sizes were small ($\leq$18°) but not when errors were large ($\geq$30°). These results held in a second study in which participants had visual impairments, i.e., when visual feedback uncertainty originated from intrinsic sources (24). The authors argued that our motor system has limited plasticity, so that for large errors the issued motor correction is already maximal and thus unaffected by uncertainty (but see Ref. 25). At the same time, another study saw uncertainty-induced attenuation in single-trial learning with large error sizes using the error-clamp method (26), which leaves the conditions under which attenuation to feedback uncertainty is observed an open question.

Measuring similar levels of implicit adaptation when having different levels of visual feedback uncertainty for larger error sizes could be due to the types of errors the system experiences. Although the error-clamp method is thought to only measure the consequences of SPEs, implicit adaptation has also been shown to be sensitive to task performance (27–29). Hence, it is possible that the task-irrelevance of the feedback and the lack of target errors inherent to the error-clamp method are responsible for the fact that high visual feedback uncertainty does not attenuate implicit adaptation in the case of large errors. Moreover, recent work suggests that implicit adaptation is also driven by target errors and even competes with explicit processes for such (30). This competition hypothesis would explain the empirical observation that measured implicit adaptation is higher when explicit strategies are suppressed, as target errors are then mostly available to the implicit system. In fact, a recent online study pointed toward such effect, in which participants with and without visual impairment adapted to a movement-contingent 45° rotation (31). Although the results showed no differences in implicit aftereffect, this could be due to higher explicit learning in participants without visual impairment, which we more thoroughly assess here.

In this study, to expand past findings in favor of optimal integration for small errors (8–10), we evaluated the effect of visual feedback uncertainty on motor adaptation when error sizes are large. Importantly, unlike in error-clamp experiments, visual feedback was contingent on the participants' reaching direction, making it relevant to achieve the task goal. In a first experiment (*experiment 1*), we applied a contingent visuomotor rotation (VMR) with a large perturbation size (30°). We chose a 30° rotation since, first, Refs. 22, 24 had found no differences in implicit adaptation between uncertainty conditions for this perturbation size in a similar block design with error-clamp feedback. Second, 30° is substantially larger than the error sizes used in previous movement-contingent studies (<8°) showing attenuation of learning by feedback uncertainty. In *experiment 2*, we further dissociated implicit and explicit adaptation by introducing interspersed no-feedback trials over the course of adaptation. In both experiments, we found that visual feedback uncertainty decreases overall adaptation, as well as the isolated implicit adaptation. Although our task elicited rather small explicit adaptation, we also inferred a reduction of this component with high feedback uncertainty. Our results show that implicit adaptation to large errors is attenuated with high feedback uncertainty, provided that this feedback is relevant to achieve the task goal.

MATERIALS AND METHODS

Participants

Sixty healthy individuals (39 females, 10 left-handed; age = 24.3 ± 5.5 yr, mean ± SD) participated in either one of two experiments. All participants had normal or corrected-to-normal vision. They gave written informed consent before starting the experiment and were financially compensated for their participation. After receiving instructions, each session began with a short training block to familiarize participants with the experimental setup and task, and, after a short break, they started the main experiment. The study was approved by the local ethics committee of the Georg-Elias-Müller-Institute for Psychology at the University of Göttingen and was in accordance with the Declaration of Helsinki.

Experimental Setup

Participants performed the experiment seated in a two-dimensional (2-D) stereoscopic augmented-reality environment (32) (Fig. 1A). Two computer monitors (BenQ XL2720T, Matrox DualHead2Go DisplayPort splitter; screen size 590 × 338 mm, 60 Hz refresh rate, distance 450 mm) were placed on either side of the participant with the screens facing each other. Participants had to look into a pair of mirrors that were angled at 45° relative to the screens, and a 2-D projection of the screen images was shown in front of them. The mirrors were opaque, so vision of the arm was occluded. Arm movements were recorded through a haptic manipulandum (Delta.3, Force Dimension; 2 kHz sampling rate) with participants holding and moving a spherical handle with their dominant hand. The haptic manipulandum and screen spaces had

Downloaded from journals.physiology.org/journal/jn (077.025.034.247) on October 1, 2024.

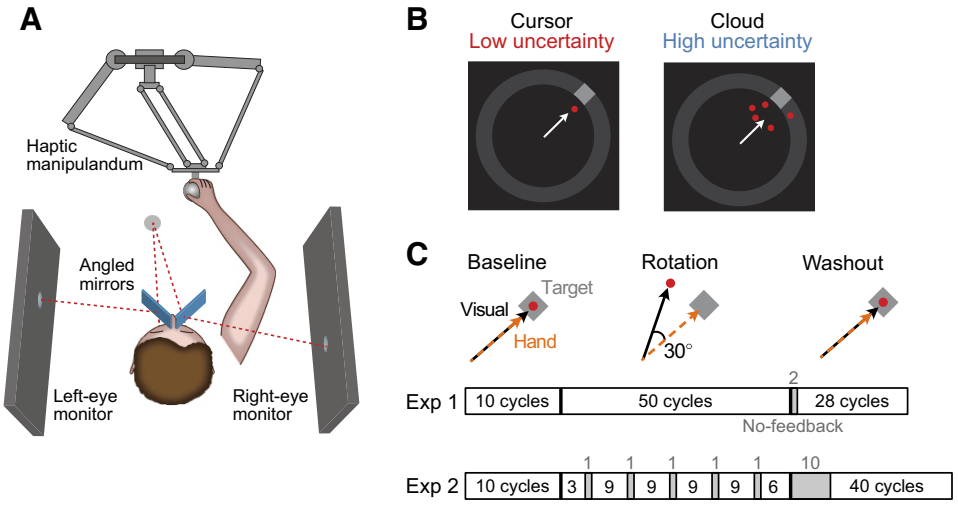

Figure 1. Experimental setup and design. *A*: representation of participant performing the experiment. *B*: visual feedback uncertainty conditions: low-uncertainty cursor (*left*) and high-uncertainty cloud (*right*). *C*: visuomotor rotation blocks: baseline (hand and visual feedback direction aligned), rotation (visual feedback direction rotated by 30° counterclockwise with respect to hand direction), and washout (hand and visual feedback direction aligned). Below are cycle numbers and block progression for *experiments 1* and *2*. Numbers in gray indicate no-feedback cycles.

a 1:1 scaling. The movement of the manipulandum was constrained to a vertical 2-D plane. The experiment was run through custom-written software (C++, OpenGL), which also saved task and kinematic data.

Experimental Design

We modulated the spatial uncertainty of visual feedback of the participant's hand position (Fig. 1*B*). There were two feedback uncertainty conditions. In the low-uncertainty condition participants controlled a single red dot or cursor (2-mm radius), whereas in the high-uncertainty condition participants controlled a cloud of five moving red dots (each had a 2-mm radius). The initial position of each dot was drawn from a 2-D Gaussian distribution with a 20-mm standard deviation around the true hand position. Additionally, each dot was assigned a random velocity direction (fixed speed of 100 mm/s) and had a 250-ms lifetime. This meant that the cloud's centroid was not fixed, ensuring that hand position uncertainty remained high throughout the trial.

The behavioral task consisted of center-out reaches from a central circle (10-mm radius) to one of four potential targets (20-mm arc) positioned at a 100-mm distance from the center at the diagonal directions (45°, 125°, 225°, and 315°). Targets appeared on a dark gray ring (90-mm inner radius, 110-mm outer radius) that remained visible throughout the experiment. Each trial started by the participant moving the cursor or cloud into the central circle. Participants managed to do this with similarly high accuracy for cursor and cloud (mean initial position SD, averaged across experiments: cursor: 2.9 mm and cloud: 3.5 mm). After participants held the central position for 500 ms, one of the targets appeared, staying visible until the trial ended. Participants were instructed to reach into the direction of the target as soon as they saw it. The trial was aborted if participants took longer than 500 ms in *experiment 1* or 1,000 ms in *experiment 2* to start their movement. Movement start was defined as the time when a speed threshold of 20 mm/s was crossed or the central circle was exited. Participants were asked to perform fast and straight reaches, attempting to slice through the target. Importantly, participants controlling the cloud were instructed that the center of the cloud had to cross the target, not just one of the cloud's individual points. If participants did not manage to reach 100 mm away from the center (target distance) within 400 ms, the target turned blue, indicating a failed trial. This criterion applied in 15.56% and 11.06% of trials in *experiments 1* and *2*, respectively. A trial was also considered failed in the rare case when participants entered the target area but dropped to a low speed (50 mm/s) before crossing the target distance (*experiment 1*: 1.83%, *experiment 2*: 0.84% of trials). These strict time and speed constraints were introduced to encourage ballistic reaches and avoid slow corrective movements for homing into the target. Additionally, we checked the hand angle relative to the target direction at the moment when the reach crossed the target distance. If this angle was larger than 40°, which could indicate that participants were not correctly aiming at the target, the trial was considered failed, but no feedback about this was given to the participant, i.e., the target did not turn blue. Such trials hardly happened (*experiment 1*: 0.11%, *experiment 2*: 0.03%). During data collection, each target direction was selected in a pseudorandom manner, not counting failed trials. This meant that target directions were repeated until there was one successful trial for each target direction. In this way, a cycle was defined as four successful trials, one for each target direction, plus any interleaving failed trials. We note that this ultimately resulted in participants performing different numbers of reaches, which we account for in our analysis.

Upon crossing the target distance, the visual feedback froze for 100 ms and then disappeared. In this manner, different from most related previous studies, which only employed mid- or end-point feedback, we continuously provided visual feedback during the reach. We did not provide any binary signal to indicate whether the participants hit or missed the target, to avoid binary reward contributions to adaptation, as we expected more hits with the cursor compared to the cloud. The movement back to the center was without visual feedback and physically constrained by a force channel that guided participants toward the center. Visual feedback reappeared when participants entered the central circle.

We performed two experiments in which we assigned participants to the low or high visual feedback uncertainty condition, with $N = 15$ participants per uncertainty condition in each experiment. Both experiments consisted of a VMR

Downloaded from journals.physiology.org/journal/jn (077.025.034.247) on October 1, 2024.

adaptation paradigm with a 30° counterclockwise perturbation (Fig. 1*C*). A VMR rotates the direction of the visual feedback with respect to that of the hand, where the center position is the pivot point. This perturbation elicits a visual error during reach, which participants have to compensate by physically moving their hand at an angle that is countering the imposed rotation.

Experiment 1 ($N = 15$/condition) revisited the effect of visual feedback uncertainty on VMR adaptation. The experiment started with a baseline block of 10 cycles. The baseline was followed by a rotation block of 50 cycles and a washout block of 30 cycles. There were two no-feedback cycles at the beginning of the washout block to quantify aftereffects without the contribution of visual errors.

In *experiment 2* ($N = 15$/condition), we further dissociated adaptation into its implicit and explicit components to test how these were individually affected by feedback uncertainty. For this, we removed visual feedback during reach on a number of cycles in the rotation block (*cycles 4*, *14*, *24*, *34*, and *44*) and instructed participants to focus on their physical hand and directly move it through the target, ignoring any strategies they might have been applying in the previous feedback trials. The color of the feedback turned yellow at the start of the no-feedback trials to make participants aware of the change in condition. We considered reaches in these no-feedback trials to be a measure of implicit adaptation, as they reflected the participant's hand representation without a compensation strategy and the influence of visual errors. *Experiment 2* had 10 baseline cycles, 50 rotation cycles, and 50 washout cycles. Compared to *experiment 1*, we extended the no-feedback phase at the beginning of the washout to 10 cycles to better evaluate retention behavior.

Data Analysis

Behavioral analyses were performed using MATLAB (R2018b), and plots were created with the GRAMM toolbox (33).

For offline analysis of the movement data, we included all trials that reached the lower end of the outer ring (90-mm distance). We decided to include failed trials in which participants had almost completed the reach, as these likely contributed to adaptation. This excluded 7.49% and 6.4% of total trials across all participants in *experiments 1* and *2*, respectively. Additionally, we removed trials in which major online corrections occurred. We defined online corrections as strongly curved trajectories that showed more than a 25° difference between the hand angles at 25 mm and maximum distance from the center. This constraint removed 0.9% and 0.73% of total trials in *experiments 1* and *2*, respectively, indicating that participants complied well with the instruction to conduct ballistic straight reaches.

To quantify adaptation, we extracted different behavioral parameters during offline analysis. As primary measure, we computed the reach angle on each trial, i.e., the angle between the target direction and the vector pointing from the center position to the hand position at peak speed of the reach. For each participant, we additionally removed outliers, defined as reach angles that deviated more than three times the interquartile range from the participant median, which applied to 0.08% and 0.04% of total trials in *experiments 1* and *2*, respectively. Reach angles were then corrected for individual directional biases by subtracting the average reach angle for each target during the baseline block from all trials to that target. To compute the reach angle per cycle, we averaged the reach angle of four consecutive successful trials, one to each target, and any interleaving failed trials. Additionally, we measured reaction times. The reaction time was defined as the delay between target presentation and the time when the hand reached a speed of 20 mm/s and increased monotonically for 50 ms.

For *experiment 1*, the final extent of adaptation was measured by both averaging the reach angles from the last four cycles of the rotation block (*cycles 67–60*) and averaging the first two no-feedback cycles of the washout block (*cycles 61* and *62*). The change in reach angle was quantified for the early phase of the rotation and washout blocks, as we wanted to evaluate behavior when error sizes were still large. For this, we averaged the difference in reach angles between the first four consecutive cycles of the rotation (*cycles 11–14*) and washout (*cycles 64–67*), excluding the no-feedback cycles at the beginning of washout. Specifically, the first cycle difference for rotation was taken relative to the last baseline cycle, whereas the first cycle difference for washout was taken relative to the first feedback washout cycle. For visualization, we flipped the sign of the change in reach angle during washout. As an alternative, we recomputed the extent and early change in reach angle based on the number of experienced trials. We now binned data by averaging four consecutive reaches, not necessarily one to each target, including both successful and failed trials. The extent of adaptation was then based on *bins 196–200*, which would have been the end of the rotation block if failed trials would have been considered during data collection.

For *experiment 2*, we focused on the analysis of implicit and explicit adaptation. We refer to a given no-feedback cycle and its previous feedback cycle as a probe block (see Fig. 3*A*, dashed box). We considered the reach angle in the no-feedback cycles as a measure of implicit adaptation. We calculated explicit adaptation as the difference between the total adaptation (previous feedback cycle) and the implicit adaptation (no-feedback cycle) within a given probe block. Furthermore, we inferred a potential effect of the VMR on cognitive load by evaluating the reaction times (34, 35). Employment of cognitive resources would lead to an increase in reaction times, indicating the formation of an explicit strategy. We expected cognitive load to be highest at the beginning of the rotation and washout blocks (36), when participants experienced large errors and could form an initial strategy to counteract them. For the rotation block, we averaged the reaction time of the first three rotation cycles and subtracted the reaction time average of all ten baseline cycles. We did similarly for the washout block, taking the average of the first three cycles of the washout with visual feedback and subtracting the average of the preceding ten cycles. Finally, given that *experiment 2* included a longer no-feedback washout phase, we more closely evaluated the differences in washout behavior. For visualization, reach angles during washout were normalized with respect to the first no-feedback washout hand angle. We measured changes in reach angle during washout for both the no-feedback and feedback phases by again averaging

Downloaded from journals.physiology.org/journal/jn (077.025.034.247) on October 1, 2024.

the difference in reach angle of the first four consecutive cycles of each phase.

As a control, we checked whether the differences in the number of performed reaches for each participant would affect adaptation measures. We first quantified success rates for each participant based on the total number of performed trials before any offline exclusion criteria and tested for differences between uncertainty conditions for each experiment. We then similarly computed success rates but only considering the baseline and rotation blocks, as differences in those could subsequently affect adaptation measures taken over rotation and early washout. These success rates were correlated with the adaptation measures computed for *experiment 1* (after offline trial exclusions), namely the average reach angle during late rotation and no-feedback washout and the change in reach angle during early rotation and washout. We also calculated these adaptation measures for *experiment 2* and correlated them with the success rates, with the only difference that the early rotation change in reach angle included the difference in hand angles between the first three cycles of rotation, as the fourth cycle was a no-feedback one.

Statistics

For all measures, we were mainly interested in comparing high- and low-feedback uncertainty conditions. We first checked for normality and homogeneity of variance of the data, using the Shapiro–Wilk test and Levene's test, respectively. If the data passed these tests, an independent-samples unpaired t test was performed. Otherwise, the nonparametric Wilcoxon rank-sum test was used. For both, the significance level was $\alpha = 0.05$. These statistical tests were done in MATLAB (R2018b).

We evaluated implicit and explicit reach angles throughout adaptation by fitting two generalized linear mixed models (GLMMs) with beta error distributions (37, 38). Reach angles were transformed into a proportion ([0,1]) from the range of possible reach angles ([−180°, 180°]). Hence, a reach angle of zero had a value of 0.5 after the transformation, positive reach angles had values between 0.5 and 1, and negative reach angles had values between 0.5 and 0. The circularity of the reach space could be ignored here, since absolute reach angles were always much smaller than 180°. We included probe block number (z transformed), uncertainty, and their interaction as fixed effects. In the implicit reach angle model we also included probe block number squared and its interaction with uncertainty as fixed effects. This was because we expected a steeper increase in reach angle for the first probe blocks, which would level off for the last probe blocks. Participant identity was set as random intercept and probe block number as a random slope within participant (39, 40). We did not include parameter estimation for the correlation between the random intercepts and slope. Both implicit and explicit reach angle models were compared to a null model lacking fixed effects with a likelihood-ratio test. If this difference was significant, we tested significance of the interaction terms. In the case that the interaction was not significant, we fitted a reduced model without interaction terms and tested significance of the main effects. The significance of each main and interaction effect term was tested with a likelihood-ratio test. Models were fitted in R (version 4.2.3) using the "glmmTMB" package (version 1.1.8). Overdispersion of the models was not observed. We assessed model stability by excluding participants one at a time, fitting the full model to each of the subsets, and comparing the range of estimates obtained with those obtained for the full dataset. The models showed good stability. Confidence intervals of model estimates and fitted values were obtained with a parametric bootstrap (N = 1,000; "simulate" function from the "glmmTMB" package). The sample for each model comprised a total of 150 reach angles, obtained from 30 participants who performed five probe blocks each.

RESULTS

Participants were able to perform either experiment controlling either the cursor or the cloud feedback. Success rates were not significantly different between high- and low-uncertainty conditions in *experiment 1* (cursor: 81.7 ± 7.9%, cloud: 84.7 ± 6.8%, $t_{28} = -1.11$, $P = 0.28$, $d = -0.41$, unpaired t test). In *experiment 2*, success rates were lower for high feedback uncertainty (cursor: 90.5 ± 5.4%, cloud: 84.9 ± 8%, $z = 2.24$, $P = 0.03$, Wilcoxon rank-sum test). Nevertheless, when correlating our primary adaptation measures (adaptation extent and early changes) with the success rates (computed only over baseline and rotation blocks), we did not find significant correlations in either experiment (Supplemental Fig. S1). The independence of adaptation measures from success rate makes it unlikely that differences in success rate, and hence in the number of actually performed reaches between participants, were responsible for differences in adaptation between uncertainty conditions.

Visual Feedback Uncertainty Attenuates Adaptation for Large Errors

In *experiment 1*, we tested the effect of visual feedback uncertainty on adaptation when presenting this feedback continuously throughout the reach and applying a 30° movement-contingent perturbation. Participants in the cursor and cloud conditions adapted to the VMR, reaching increasingly toward a compensatory direction (Fig. 2*A*). After the VMR perturbation was removed, reach behavior gradually regressed to baseline. The range of error sizes (interquartile range across participants) experienced during the early phases of rotation and washout was highly overlapping between cursor and cloud conditions. For early rotation, the range was [32.67°, 18.63°] for the cursor group and [33.5°, 21.55°] for the cloud group. For early washout, the range was [24.71°, 9.05°] for the cursor group and [19.3°, 9.08°] for the cloud group.

We found clear differences in adaptation between high- and low-visual feedback uncertainty conditions. The final level of adaptation at the end of the rotation block was higher in the cursor group (Fig. 2*B*; cursor: 24.67 ± 2.28°, cloud: 20.82 ± 2.49°, $t_{28} = 4.41$, $P < 0.001$, $d = 1.61$, unpaired t test), and the same was found for the aftereffect, measured in the no-feedback washout cycles (cursor: 22.99 ± 2.37°, cloud: 18.79 ± 3.16°, $t_{28} = 4.12$, $P < 0.001$, $d = 1.5$, unpaired t test). Consistent with this, the change in reach angle was higher for the cursor group during early rotation (Fig. 2*C*;

Downloaded from journals.physiology.org/journal/jn (077.025.034.247) on October 1, 2024.

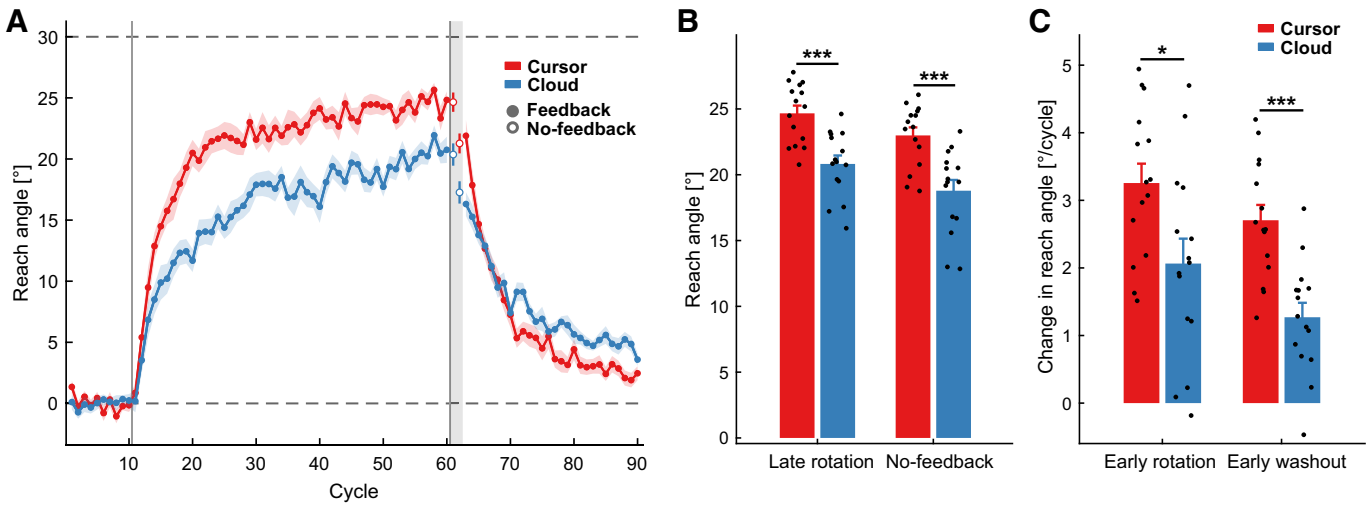

Figure 2. Adaptation is reduced under high visual feedback uncertainty (*experiment 1*). *A*: average hand reach angle with cycle number. Red color corresponds to cursor group ($N = 15$) and blue to cloud group ($N = 15$). Gray vertical lines indicate start and end of rotation block. Gray vertical shaded area and open circles cover no-feedback cycles. *B*: average reach angle during late rotation (*cycles 57–60*) and no-feedback washout (*cycles 61* and *62*). *C*: average change in reach angle during early rotation (*cycles 11–14*) and early washout (*cycles 64–67*). Black points in bar plots represent individual participants. Colored shaded areas and error bars indicate SE across participants. *$P < 0.05$ and ***$P < 0.001$ from unpaired *t* tests.

cursor: 3.26 ± 1.11°/cycle, cloud: 2.07 ± 1.43°/cycle, $t_{28} = 2.55$, $P = 0.02$, $d = 0.93$, unpaired *t* test) and early washout (cursor: 2.71 ± 0.88°/cycle, cloud: 1.27 ± 0.83°/cycle, $t_{28} = 4.61$, $P < 0.001$, $d = 1.68$, unpaired *t* test). As a control, we found similar results if we computed cycles by grouping four successively performed trials, irrespective of whether they were considered failed or not (Supplemental Fig. S2).

Implicit Adaptation Is Affected by Task-Relevant Feedback Uncertainty

Since explicit and implicit adaptation were not dissociated in *experiment 1*, we performed a second experiment in which we used no-feedback cycles to measure implicit adaptation repeatedly over the course of adaptation (Fig. 3*A*) and estimated explicit adaptation by subtraction of implicit adaptation from total adaptation. We fitted GLMMs to the implicit (Fig. 3*B*) and explicit (Fig. 3*C*) reach angles to evaluate differences between uncertainty conditions over time (model results in Supplemental Table S1). Analyzing implicit reach angles, the model revealed significant fixed effects compared to the null model [$\chi^2_5 = 125.82$, $P < 0.001$, likelihood-ratio test]. Specifically, the model showed a significant interaction between uncertainty and quadratic probe block number [$\chi^2_1 = 8.79$, $P = 0.003$, likelihood-ratio test]. Model fits of implicit reach angles indicated a reduced adaptation of reach angle with high feedback uncertainty as well as a steeper increase in reach angle with probe block number in the case of low feedback uncertainty. When assessing the difference between uncertainty conditions at each probe block, model fits showed nonoverlapping confidence intervals for all probe blocks except the first one.

Compared to no-feedback cycles, the reach angles in the preceding feedback cycles were barely larger, leading to small estimates of reach angles accountable to explicit adaptation across probe blocks (cursor: 1.51 ± 1.56° and cloud: 0.04 ± 1.34°). Nevertheless, the explicit reach angle model was also significantly different from the null model [$\chi^2_3 = 8.55$, $P = 0.04$, likelihood-ratio test]. The interaction term between uncertainty and probe block number was not significant [$\chi^2_1 = 0.28$, $P = 0.67$, likelihood-ratio test]. Therefore, we fitted a reduced model without this interaction term, which showed a significant effect of uncertainty [$\chi^2_1 = 7.28$, $P = 0.007$, likelihood-ratio test] but not of probe block number [$\chi^2_1 = 0.99$, $P = 0.32$, likelihood-ratio test]. Model fits of explicit reach angles showed lower reach angles with high uncertainty feedback.

Additionally to the reach angles, we quantified reach reaction times, which potentially reflect the use of cognitive resources linked to explicit adaptation. When comparing the reaction times over the course of the experiment, we observed different trends for each feedback uncertainty condition (Fig. 4*A*). The cursor group displayed marked increases in reaction times during early rotation and feedback washout that gradually decreased back to baseline, whereas the cloud group showed a moderate increase in reaction time at the start of the rotation that remained constant for the rest of the experiment. Capturing these differences, we observed significantly higher reaction time changes at the start of rotation block relative to baseline in the cursor group (45.42 ± 23.24 ms) compared to the cloud group (Fig. 4*B*; 17.73 ± 18.53 ms, $t_{28} = 3.61$, $P = 0.001$, $d = 1.32$, unpaired *t* test). The equivalent was observed at the start of the washout block with visual feedback compared to the washout without feedback (cursor: 24.27 ± 30.18 ms, cloud: −0.14 ± 20.3 ms, $t_{28} = 2.6$, $P = 0.01$, $d = 0.95$, unpaired *t* test). This slowing of reaction times in the early phase after introducing or removing the perturbation could suggest stronger contributions of explicit adaptation in the low- compared to the high-feedback uncertainty group. The same trend was observed for the reaction times in *experiment 1*, though the difference of the change at the start of rotation between uncertainty conditions did not reach significance, which could be due to the tighter reaction time constraint during data collection (Supplemental Fig. S3).

Downloaded from journals.physiology.org/journal/jn (077.025.034.247) on October 1, 2024.

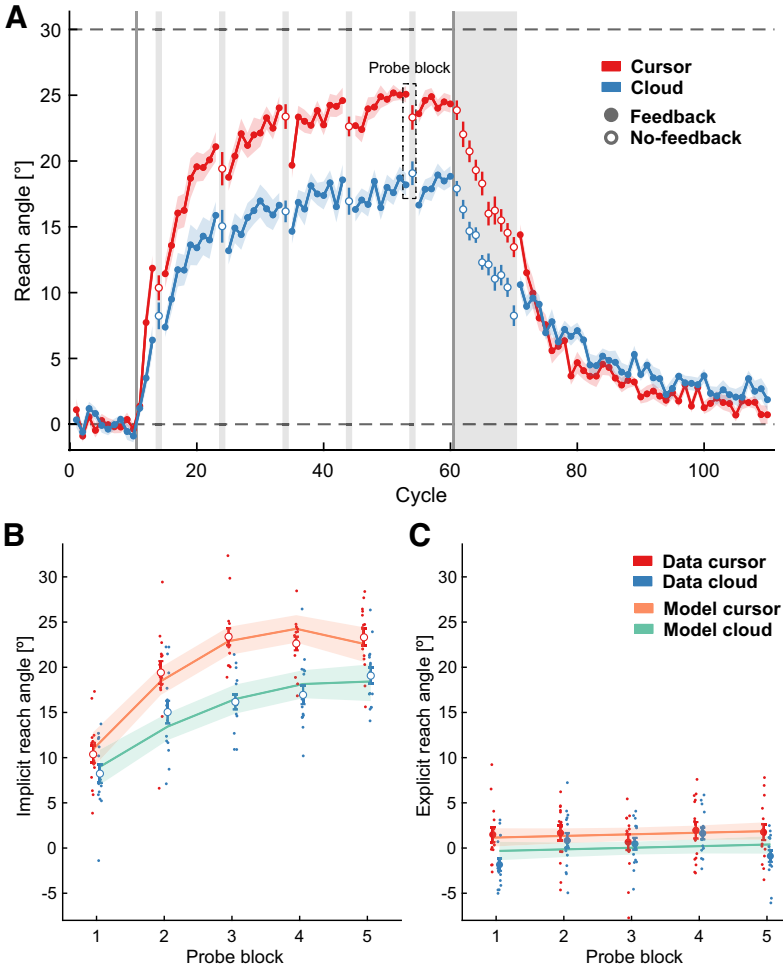

Figure 3. Implicit adaptation is reduced with high visual feedback uncertainty (*experiment 2*). *A*: average hand reach angle with cycle number. Red color corresponds to cursor group ($N = 15$) and blue to cloud group ($N = 15$). Gray vertical lines indicate start and end of rotation block. Gray vertical shaded areas and open circles cover no-feedback cycles. Dashed box marks the last probe block. Error bars and shaded areas indicate SE across participants. *B*: and *C*: implicit (*B*) and explicit (*C*) reach angles with probe block number during rotation. Implicit adaptation corresponds to no-feedback cycles, and explicit adaptation was calculated by subtraction to the previous feedback adaptation cycle. Red (cursor) and blue (cloud) large points and error bars correspond to participant means and SE. Small points represent individual participants. Orange (cursor) and green (cloud) lines and shaded areas show generalized linear mixed model (GLMM) fits with their 95% confidence intervals (reduced model for explicit reach angles; bootstrap $N = 1{,}000$).

Visual Feedback Uncertainty Does Not Affect Retention Properties

Finally, *experiment 2* included a longer no-feedback washout in order to better evaluate retention behavior. During the no-feedback phase of the washout, we observed no differences in the reach angles when these were normalized to the first no-feedback washout cycle (Fig. 5*A*). Moreover, the change in reach angles over the no-feedback washout showed no significant difference between uncertainty conditions (Fig. 5*B*; cursor: $1.39 \pm 0.72°$/cycle, cloud: $1.4 \pm 0.76°$/cycle, $t_{28} = -0.03$, $P = 0.97$, $d = -0.01$, unpaired t test). In other words, the speed of readaptation without visual feedback was not affected by the feedback uncertainty experienced during

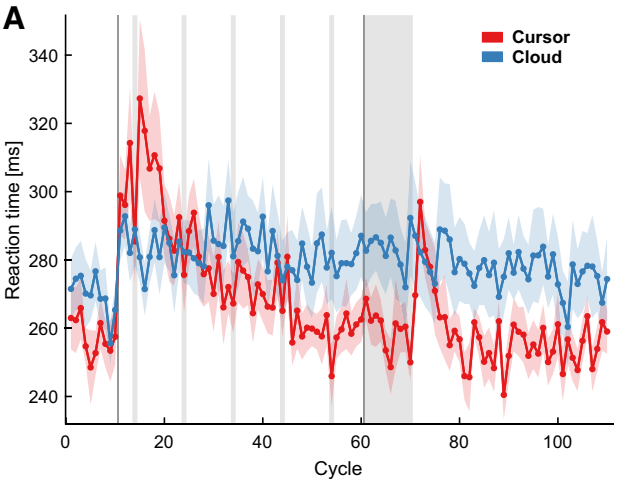

Figure 4. Reaction time increases during early rotation and feedback washout are more prominent with low visual feedback uncertainty (*experiment 2*). *A*: average reaction time with cycle number for cursor (red, $N = 15$) and cloud (blue, $N = 15$) groups. Gray vertical lines indicate start and end of rotation block. Gray vertical shaded areas cover no-feedback cycles. *B*: reaction time change during early rotation and early feedback washout, relative to baseline and no-feedback washout, respectively. Black points in bar plots represent individual participants. Colored shaded areas and error bars indicate SE across participants. $^*P < 0.05$ and $^{**}P < 0.01$ from unpaired t tests.

Downloaded from journals.physiology.org/journal/jn (077.025.034.247) on October 1, 2024.

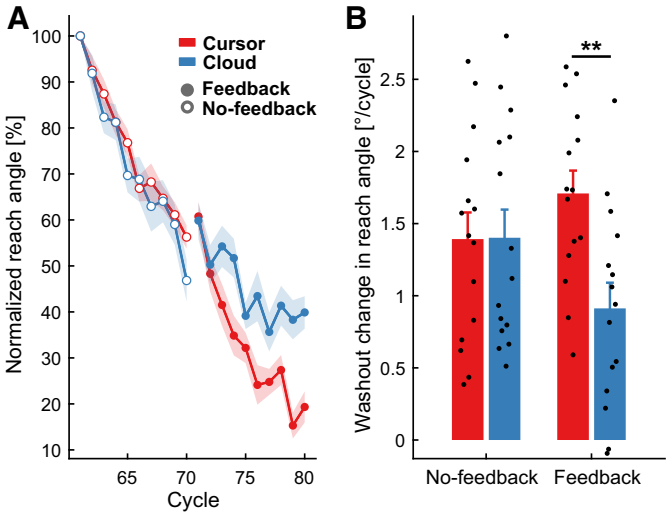

Figure 5. Retention properties without visual feedback are similar for low- and high-uncertainty conditions (*experiment 2*). *A*: average normalized hand reach angle with washout cycle number. Normalization with respect to the first no-feedback washout cycle, presented as a percentage. Red color corresponds to the cursor group ($N = 15$) and blue to the cloud group ($N = 15$). *B*: average change in reach angle for early no-feedback and feedback phases of washout. Black points represent individual participants. Colored shaded areas and error bars indicate SE across participants. $^{**}P < 0.01$ from unpaired *t* test.

adaptation and the difference in achieved final level of adaptation. In contrast, when visual feedback was shown, consistent with *experiment 1*, washout behavior showed faster readaptation in the cursor compared to the cloud condition (Fig. 5*B*; cursor: $1.71 \pm 0.61°$/cycle, cloud: $0.91 \pm 0.69°$/cycle, $t_{28} = 3.34$, $P = 0.002$, $d = 1.22$, unpaired *t* test). This shows that learning but not retention is affected by visual feedback uncertainty.

DISCUSSION

Tracking sensory feedback enables subsequent motor adaptation, with previous work showing that when visual feedback is made uncertain adaptation is attenuated (8–10). In this study, we tested whether this effect holds for large perturbation sizes. In our first experiment, we saw that high visual feedback uncertainty resulted in a slower increase in adaptation, reflecting smaller corrective responses in the early rotation and washout phases. As well, we found smaller adaptation levels in the late rotation phase and smaller aftereffects, corresponding to a reduced cumulative effect of adaptation. Since the attenuated adaptation could be due to a reduced explicit strategy, in a second experiment we separately estimated the implicit and explicit components of adaptation by introducing no-feedback trials. We found that the attenuation of adaptation for the large perturbation was prominent in the measured implicit component. Indications of a reduced explicit component were observable as well, though its contribution to adaptation seems rather small. Moreover, readaptation behavior during washout under no-feedback conditions did not differ between uncertainty conditions, suggesting that feedback uncertainty specifically affects the learning and not retention properties of our motor system.

Our results contrast recent studies testing visual feedback uncertainty with the error-clamp method (22, 24, 41). These previous studies did not find uncertainty-related attenuation of implicit adaptation with large error sizes, neither when visual feedback uncertainty was experimentally manipulated (22, 41) nor when participants had intrinsic visual impairments (24). One explanation was that the implicit system has limited plasticity, so there is a maximum trial-to-trial correction that our motor system can issue (22, 24). When error sizes are large, the issued correction is already maximal and, as a result, unaffected by variations in feedback uncertainty. As an alternative explanation, a reduced effect of feedback uncertainty for large error sizes was shown to be in line with predictions from a divisive normalization model (41). Other recent work that also used the error-clamp method instead found attenuated adaptation with higher feedback uncertainty for large but not small error sizes. The authors propose a model in which a perceptual error, based on Bayesian combination of visual feedback, proprioceptive feedback, and sensory predictions, drives implicit adaptation (26).

Although this discrepancy between experimental results may be due to nuanced differences in task design, it is important to consider the impact the error-clamp method might have. Specifically, since the error clamp makes feedback irrelevant to the task goal, it is unclear whether implicit adaptation proceeds in a different manner than with task-relevant feedback. Findings in error-clamp experiments show that implicit adaptation reaches a common final value (~20°) over a wide range of error sizes (1.75° to 95°) (14, 23). Thus, imposed visual errors below this asymptotic value are overcompensated, putatively because there is no feedback signal to halt the adaptation process when it should be "complete," i.e., when the level of adaptation reaches the size of the perturbation. This opens the question of whether, in the error-clamp paradigm, proprioceptive feedback takes higher importance than the task-irrelevant visual feedback and, as a result, adaptation is bounded by proprioceptive limits (25). Therefore, it may be that error-clamped compared to contingent VMR paradigms are measuring different levels or subcomponents of implicit adaptation, and that these are not majorly affected by the properties of the presented visual feedback, such as uncertainty.

In the present study, we considered 30° to be a large perturbation size. Although there is no strict definition, large error sizes are often those considered to elicit strong explicit adaptation. In contrast, a 30° perturbation results in little explicit adaptation (19, 21, 42) and could be regarded as small. When focusing on the implicit system, as in our study, a different criterion seems more relevant. The size of trial-to-trial corrections has been found to increase with error size but remains constant for error sizes above 20° (13, 14). This is in line with the idea that the implicit system is in charge of correcting small errors that are attributed to our motor system, i.e., that are assumed to be intrinsic to the system. Recent work has also shown that a visual cursor with a 30° rotation is clearly perceived to be rotated with respect to the hand movement (43), and so it is unlikely to be only assigned to our motor system. Moreover, implicit adaptation seems to reach a final extent of ~20° for perturbation sizes above this

Downloaded from journals.physiology.org/journal/jn (077.025.034.247) on October 1, 2024.

level (14, 44), suggesting that the total amount of implicit adaptation is limited to below 30°. Thus, whereas our choice of perturbation is recognized to be small for the explicit system, it can be considered large for the implicit system.

A consequence of using a movement-contingent block design is that the error sizes experienced gradually changed throughout the experiment. This meant that responses to large errors were mainly captured during the early rotation phase, when error sizes were mostly still larger than 20°. Indeed, we found reduced changes in reach angle with high feedback uncertainty for this period in *experiment 1*. When we isolated implicit adaptation in *experiment 2*, differences between uncertainty conditions in the first implicit cycle at early rotation did not become evident. At the same time, we observed that this first implicit cycle showed higher reach angle adaptation than the previous total adaptation cycle for high feedback uncertainty (with an equivalent trend for the last implicit cycle). We therefore think that there was effectively no explicit component for high feedback uncertainty, and that this unexpectedly high first implicit cycle was probably due to other factors, such as insufficient knowledge of the workspace or an impaired sense of hand position. Consequently, we believe that differences in implicit adaptation between feedback uncertainty conditions hold throughout the perturbation period.

Based on our task design, we think that two different types of errors contributed to the observed dependence of adaptation on feedback uncertainty, namely SPEs and task performance errors (15). Given that the VMR was movement contingent and the ballistic nature of the reaches, these two types of error are not independent in our experiments. First, SPEs result from the difference between received and expected sensory feedback, in this case the difference between the visual feedback and the aiming direction. In our experiments, we continuously presented visual feedback throughout the reach to maximize its availability or relevance, as showing feedback continuously results in increased adaptation by potentially strengthening SPEs (17, 45). A point to consider is that, for a given angular error, its arc length increases with distance from the center. As the amount of uncertainty provided by the cloud did not change with this distance, we can expect that participants controlling the cloud could not detect that there was an angular deviation until later in the reach. This would lead to a reduced sampling time of the SPE within a trial compared to the low-uncertainty condition, where the deviation would become clear early in the reach. In this sense, the higher uncertainty in the SPE together with the potentially smaller duration of experiencing it within a trial could have contributed to the observed attenuation in adaptation.

Second, participants experienced task performance errors in the form of target errors, namely the observed discrepancy between the visual feedback and target direction, primarily apparent at the end of the reach. Our uncertainty manipulation also affected these target errors, given that they are based on estimation of feedback position. Influencing target errors becomes relevant, as it has been found that the implicit system is also sensitive to task performance, which could lead to an interaction with the explicit learning process (28, 30). In this line, a recent study proposed that the implicit system also learns from target errors, competing with the explicit system for this source (30), which would explain why implicit adaptation is reduced when explicit strategies are promoted (20, 46). In our task, there was little elicited explicit adaptation, meaning that target errors were mostly available to the implicit system and likely influenced its progress. This fact could be relevant for the present results, as a recent online study tested a movement-contingent 45° perturbation in participants with and without visual impairment and did not find differences in the implicit (no feedback) aftereffect between the two groups (31). However, the observed pattern of adaptation was in line with higher rates of both explicit and implicit learning for participants with intact vision compared to those with impaired vision. Thus, higher explicit learning in participants with intact vision could have hindered the progression of implicit adaptation and reduced the measured aftereffect of this group. Here, in a more controlled laboratory setting and experimentally manipulating visual feedback uncertainty, we find further evidence for this idea, revealing differences in implicit adaptation as a function of visual feedback uncertainty.

Furthermore, prior work has shown that seeing the visual feedback hit or intersect the target reduces implicit adaptation (27, 29). Thus, mistakenly perceiving more hits with high uncertainty feedback may have also contributed to the reduced adaptation. However, this effect would primarily impact the extent of adaptation in the phase of the experiment when participants have mostly compensated for the rotation and hence target error sizes are small. Nevertheless, we see reduced adaptation with high uncertainty in the early phase of the perturbation, when errors are still large. This is in contrast with studies in which target errors were eliminated with the error-clamp method (22, 24, 41). As a consequence, having a target error additional to the SPE in the present study could have contributed to the discrepancy in the found effects of feedback uncertainty on implicit adaptation to large perturbation sizes. In this sense, our data suggest that the sensitivity of implicit adaptation to target errors could explain the dependence of adaptation on visual feedback uncertainty.

Regarding explicit adaptation, we expected that this component would also be reduced with high visual feedback uncertainty, as strategies should be based on estimation of target errors. We found that this was the case, although our task constraints elicited rather reduced explicit measurements, in line with previous studies testing a 30° perturbation (19, 21, 42). One caveat is our method to extract explicit adaptation, computing it by subtraction of measured implicit to total adaptation. Recent work suggests that the addition of explicit and implicit measures might not always equal total adaptation (42, 47), potentially making our explicit measures less accurate. We additionally inferred explicit processing from the reaction times. The low-uncertainty group exhibited longer reaction times compared to the high-uncertainty group during early rotation and early washout. As longer reaction times have been previously related to the required cognitive processing of strategy employment (34, 35, 48), we consider our results to support reduced explicit adaptation with high feedback uncertainty. Nevertheless, future work should consider using methods to directly measure the explicit component (49), as well as testing larger perturbation sizes (20, 21, 50) or using delayed end-point feedback (51, 52)

Downloaded from journals.physiology.org/journal/jn (077.025.034.247) on October 1, 2024.

to promote explicit adaptation and better evaluate how it is affected by visual feedback uncertainty.

Altogether, we think that the combination of uncertainty in SPEs and target errors resulted in impaired implicit adaptation. We acknowledge that since we used a movement-contingent perturbation design and the measured explicit adaptation was small, the aiming direction probably coincided with the target direction, implying that we cannot fully tease apart contributions from the SPE and target error. Still, we think that the fact that the visual feedback was task-relevant, and thus important for task performance, contributed to our results. Related to this, we also point out that having little explicit adaptation potentially did not mask changes in the implicit system, which highlights the importance of considering the interplay between these two processes when studying motor adaptation. Implicit adaptation relates to small gradual corrections that result from the adjustment of our internal models for movement control. Correspondingly, the size of these corrections decreases with increasing error size (11, 12). Although having this kind of inverse relationship is not in accord with optimal integration theory, which predicts a linear scaling of corrections with error size, here we show that principles of optimal integration do hold when considering uncertainty of sensory feedback. In this line, our motor system reduces its adaptation when receiving uncertain sensory feedback, even when error sizes are large. To conclude, assessment of sensory feedback plays a key role in motor learning, ultimately guiding us in order to achieve our movement goals.

DATA AVAILABILITY

Data are available at https://doi.org/10.25625/NMU5P3.

SUPPLEMENTAL MATERIAL

Supplemental Material: https://doi.org/10.25625/NMU5P3.

ACKNOWLEDGMENTS

We thank Enrico Ferrea for help with study conceptualization, Lukas Dorsch for assistance with data collection, and Roger Mundry for assistance with GLMM design and analysis.

GRANTS

This work was funded by grants from the European Commission, Plan4Act consortium (H2020-FETPROACT-16 732266 WP1) to A.G., the State of Lower Saxony, Deep Movement Diagnostics consortium (ZN3422) to A.G., and the German Research Foundation, Collaborative Research Center "Cellular mechanisms of sensory processing" (DFG SFB-889 C4) to A.G.

DISCLOSURES

No conflicts of interest, financial or otherwise, are declared by the authors.

AUTHOR CONTRIBUTIONS

V.C., L.K.A., and A.G. conceived and designed research; V.C. and G.L.H. performed experiments; V.C. analyzed data; V.C., L.K.A., and A.G. interpreted results of experiments; V.C. prepared figures; V.C. drafted manuscript; V.C., L.K.A., G.L.H., and A.G. edited and revised manuscript; V.C., L.K.A., G.L.H., and A.G. approved final version of manuscript.

REFERENCES

1. **Jordan MI**, **Rumelhart DE.** Forward models: supervised learning with a distal teacher. *Cogn Sci* 16: 307–354, 1992. doi:10.1207/s15516709cog1603_1.
2. **Wolpert DM**, **Ghahramani Z.** Computational principles of movement neuroscience. *Nat Neurosci* 3, Suppl: 1212–1217, 2000. doi:10.1038/81497.
3. **Wolpert DM**, **Flanagan JR.** Motor prediction. *Curr Biol* 11: R729–R732, 2001. doi:10.1016/S0960-9822(01)00432-8.
4. **Shadmehr R**, **Smith MA**, **Krakauer JW.** Error correction, sensory prediction, and adaptation in motor control. *Annu Rev Neurosci* 33: 89–108, 2010. doi:10.1146/annurev-neuro-060909-153135.
5. **Wolpert DM**, **Diedrichsen J**, **Flanagan JR.** Principles of sensorimotor learning. *Nat Rev Neurosci* 12: 739–751, 2011. doi:10.1038/nrn3112.
6. **Faisal AA**, **Selen LP**, **Wolpert DM.** Noise in the nervous system. *Nat Rev Neurosci* 9: 292–303, 2008. doi:10.1038/nrn2258.
7. **Wolpert DM**, **Miall RC.** Forward models for physiological motor control. *Neural Netw* 9: 1265–1279, 1996. doi:10.1016/S0893-6080(96)00035-4.
8. **Körding KP**, **Wolpert DM.** Bayesian integration in sensorimotor learning. *Nature* 427: 244–247, 2004. doi:10.1038/nature02169.
9. **Burge J**, **Ernst MO**, **Banks MS.** The statistical determinants of adaptation rate in human reaching. *J Vis* 8: 20.1–20.19, 2008. doi:10.1167/8.4.20.
10. **Wei K**, **Körding K.** Uncertainty of feedback and state estimation determines the speed of motor adaptation. *Front Comput Neurosci* 4: 11, 2010. doi:10.3389/fncom.2010.00011.
11. **Wei K**, **Körding K.** Relevance of error: what drives motor adaptation? *J Neurophysiol* 101: 655–664, 2009. doi:10.1152/jn.90545.2008.
12. **Marko MK**, **Haith AM**, **Harran MD**, **Shadmehr R.** Sensitivity to prediction error in reach adaptation. *J Neurophysiol* 108: 1752–1763, 2012. doi:10.1152/jn.00177.2012.
13. **Hutter SA**, **Taylor JA.** Relative sensitivity of explicit reaiming and implicit motor adaptation. *J Neurophysiol* 120: 2640–2648, 2018. doi:10.1152/jn.00283.2018.
14. **Kim HE**, **Morehead JR**, **Parvin DE**, **Moazzezi R**, **Ivry RB.** Invariant errors reveal limitations in motor correction rather than constraints on error sensitivity. *Commun Biol* 1: 19, 2018. doi:10.1038/s42003-018-0021-y.
15. **Morehead JR**, **Orban de Xivry JJ.** A synthesis of the many errors and learning processes of visuomotor adaptation (Preprint). *bioRxiv* 2021.03.14.435278, 2021. doi:10.1101/2021.03.14.435278.
16. **Mazzoni P**, **Krakauer JW.** An implicit plan overrides an explicit strategy during visuomotor adaptation. *J Neurosci* 26: 3642–3645, 2006. doi:10.1523/JNEUROSCI.5317-05.2006.
17. **Taylor JA**, **Krakauer JW**, **Ivry RB.** Explicit and implicit contributions to learning in a sensorimotor adaptation task. *J Neurosci* 34: 3023–3032, 2014. doi:10.1523/JNEUROSCI.3619-13.2014.
18. **McDougle SD**, **Ivry RB**, **Taylor JA.** Taking aim at the cognitive side of learning in sensorimotor adaptation tasks. *Trends Cogn Sci* 20: 535–544, 2016. doi:10.1016/j.tics.2016.05.002.
19. **Modchalingam S**, **Vachon CM**, **'t Hart BM**, **Henriques DY.** The effects of awareness of the perturbation during motor adaptation on hand localization. *PLoS One* 14: e0220884, 2019. doi:10.1371/journal.pone.0220884.
20. **Neville KM**, **Cressman EK.** The influence of awareness on explicit and implicit contributions to visuomotor adaptation over time. *Exp Brain Res* 236: 2047–2059, 2018. doi:10.1007/s00221-018-5282-7.
21. **Bond KM**, **Taylor JA.** Flexible explicit but rigid implicit learning in a visuomotor adaptation task. *J Neurophysiol* 113: 3836–3849, 2015. doi:10.1152/jn.00009.2015.
22. **Tsay JS**, **Avraham G**, **Kim HE**, **Parvin DE**, **Wang Z**, **Ivry RB.** The effect of visual uncertainty on implicit motor adaptation. *J Neurophysiol* 125: 12–22, 2021. doi:10.1152/jn.00493.2020.
23. **Morehead JR**, **Taylor JA**, **Parvin DE**, **Ivry RB.** Characteristics of implicit sensorimotor adaptation revealed by task-irrelevant clamped feedback. *J Cogn Neurosci* 29: 1061–1074, 2017. doi:10.1162/jocn_a_01108.

Downloaded from journals.physiology.org/journal/jn (077.025.034.247) on October 1, 2024.

24. **Tsay JS**, **Tan S**, **Chu MA**, **Ivry RB**, **Cooper EA.** Low vision impairs implicit sensorimotor adaptation in response to small errors, but not large errors. *J Cogn Neurosci* 35: 736–748, 2023. doi:10.1162/jocn_a_01969.
25. **Tsay JS**, **Kim H**, **Haith AM**, **Ivry RB.** Understanding implicit sensorimotor adaptation as a process of proprioceptive re-alignment. *eLife* 11: e76639, 2022. doi:10.7554/eLife.76639.
26. **Zhang Z**, **Wang H**, **Zhang T**, **Nie Z**, **Wei K.** Perceptual error based on Bayesian cue combination drives implicit motor adaptation. *eLife* 13: RP94608, 2024. doi:10.7554/eLife.94608.
27. **Leow LA**, **Marinovic W**, **de Rugy A**, **Carroll TJ.** Task errors contribute to implicit aftereffects in sensorimotor adaptation. *Eur J Neurosci* 48: 3397–3409, 2018. doi:10.1111/ejn.14213.
28. **Miyamoto YR**, **Wang S**, **Smith MA.** Implicit adaptation compensates for erratic explicit strategy in human motor learning. *Nat Neurosci* 23: 443–455, 2020. doi:10.1038/s41593-020-0600-3.
29. **Al-Fawakhiri N**, **Ma A**, **Taylor JA**, **Kim OA.** Exploring the role of task success in implicit motor adaptation. *J Neurophysiol* 130: 332–344, 2023. doi:10.1152/jn.00061.2023.
30. **Albert ST**, **Jang J**, **Modchalingam S**, **'t Hart BM**, **Henriques D**, **Lerner G**, **Della-Maggiore V**, **Haith AM**, **Krakauer JW**, **Shadmehr R.** Competition between parallel sensorimotor learning systems. *eLife* 11: e65361, 2022. doi:10.7554/eLife.65361.
31. **Tsay JS**, **Asmerian H**, **Germine LT**, **Wilmer J**, **Ivry RB**, **Nakayama K.** Large-scale citizen science reveals predictors of sensorimotor adaptation. *Nat Hum Behav* 8: 510–525, 2024. doi:10.1038/s41562-023-01798-0.
32. **Morel P**, **Ulbrich P**, **Gail A.** What makes a reach movement effortful? Physical effort discounting supports common minimization principles in decision making and motor control. *PLoS Biol* 15: e2001323, 2017. doi:10.1371/journal.pbio.2001323.
33. **Morel P.** Gramm: grammar of graphics plotting in Matlab. *J Open Source Softw* 3: 568, 2018. doi:10.21105/joss.00568.
34. **Fernandez-Ruiz J**, **Wong W**, **Armstrong IT**, **Flanagan JR.** Relation between reaction time and reach errors during visuomotor adaptation. *Behav Brain Res* 219: 8–14, 2011. doi:10.1016/j.bbr.2010.11.060.
35. **McDougle SD**, **Taylor JA.** Dissociable cognitive strategies for sensorimotor learning. *Nat Commun* 10: 40, 2019. doi:10.1038/s41467-018-07941-0.
36. **Anguera JA**, **Reuter-Lorenz PA**, **Willingham DT**, **Seidler RD.** Contributions of spatial working memory to visuomotor learning. *J Cogn Neurosci* 22: 1917–1930, 2010. doi:10.1162/jocn.2009.21351.
37. **Bolker BM.** *Ecological Models and Data in R*. Princeton, NJ: Princeton University Press, 2008.
38. **Baayen RH.** *Analyzing Linguistic Data: a Practical Introduction to Statistics using R*. Cambridge, UK: Cambridge University Press, 2008.
39. **Barr DJ**, **Levy R**, **Scheepers C**, **Tily HJ.** Random effects structure for confirmatory hypothesis testing: keep it maximal. *J Mem Lang* 68: 10.1016/j.jml.2012.11.001, 2013. doi:10.1016/j.jml.2012.11.001.
40. **Schielzeth H**, **Forstmeier W.** Conclusions beyond support: overconfident estimates in mixed models. *Behav Ecol* 20: 416–420, 2009. doi:10.1093/beheco/arn145.
41. **Makino Y**, **Hayashi T**, **Nozaki D.** Divisively normalized neuronal processing of uncertain visual feedback for visuomotor learning. *Commun Biol* 6: 1286, 2023. doi:10.1038/s42003-023-05578-4.
42. **'t Hart BM**, **Taqvi U**, **Gastrock RQ**, **Ruttle JE**, **Modchalingam S**, **Henriques DY.** Measures of implicit and explicit adaptation do not linearly add (Preprint). *bioRxiv* 2022.06.07.495044, 2024. doi:10.1101/2022.06.07.495044.
43. **Ebrahimi S**, **Ostry DJ.** Persistence of adaptation following visuomotor training. *J Neurophysiol* 128: 1312–1323, 2022. doi:10.1152/jn.00164.2022.
44. **Modchalingam S**, **Ciccone M**, **D'Amario S**, **'t Hart BM**, **Henriques DY.** Adapting to visuomotor rotations in stepped increments increases implicit motor learning. *Sci Rep* 13: 5022, 2023. doi:10.1038/s41598-023-32068-8.
45. **Schween R**, **Taube W**, **Gollhofer A**, **Leukel C.** Online and post-trial feedback differentially affect implicit adaptation to a visuomotor rotation. *Exp Brain Res* 232: 3007–3013, 2014. doi:10.1007/s00221-014-3992-z.
46. **Benson BL**, **Anguera JA**, **Seidler RD.** A spatial explicit strategy reduces error but interferes with sensorimotor adaptation. *J Neurophysiol* 105: 2843–2851, 2011. doi:10.1152/jn.00002.2011.
47. **Maresch J**, **Mudrik L**, **Donchin O.** Measures of explicit and implicit in motor learning: what we know and what we don't. *Neurosci Biobehav Rev* 128: 558–568, 2021. doi:10.1016/j.neubiorev.2021.06.037.
48. **Haith AM**, **Huberdeau DM**, **Krakauer JW.** The influence of movement preparation time on the expression of visuomotor learning and savings. *J Neurosci* 35: 5109–5117, 2015. doi:10.1523/JNEUROSCI.3869-14.2015.
49. **Maresch J**, **Werner S**, **Donchin O.** Methods matter: your measures of explicit and implicit processes in visuomotor adaptation affect your results. *Eur J Neurosci* 53: 504–518, 2021. doi:10.1111/ejn.14945.
50. **Werner S**, **van Aken BC**, **Hulst T**, **Frens MA**, **van der Geest JN**, **Strüder HK**, **Donchin O.** Awareness of sensorimotor adaptation to visual rotations of different size. *PLoS One* 10: e0123321, 2015. doi:10.1371/journal.pone.0123321.
51. **Hinder MR**, **Tresilian JR**, **Riek S**, **Carson RG.** The contribution of visual feedback to visuomotor adaptation: how much and when? *Brain Res* 1197: 123–134, 2008. doi:10.1016/j.brainres.2007.12.067.
52. **Schween R**, **Hegele M.** Feedback delay attenuates implicit but facilitates explicit adjustments to a visuomotor rotation. *Neurobiol Learn Mem* 140: 124–133, 2017. doi:10.1016/j.nlm.2017.02.015.

Downloaded from journals.physiology.org/journal/jn (077.025.034.247) on October 1, 2024.

Supplementary material

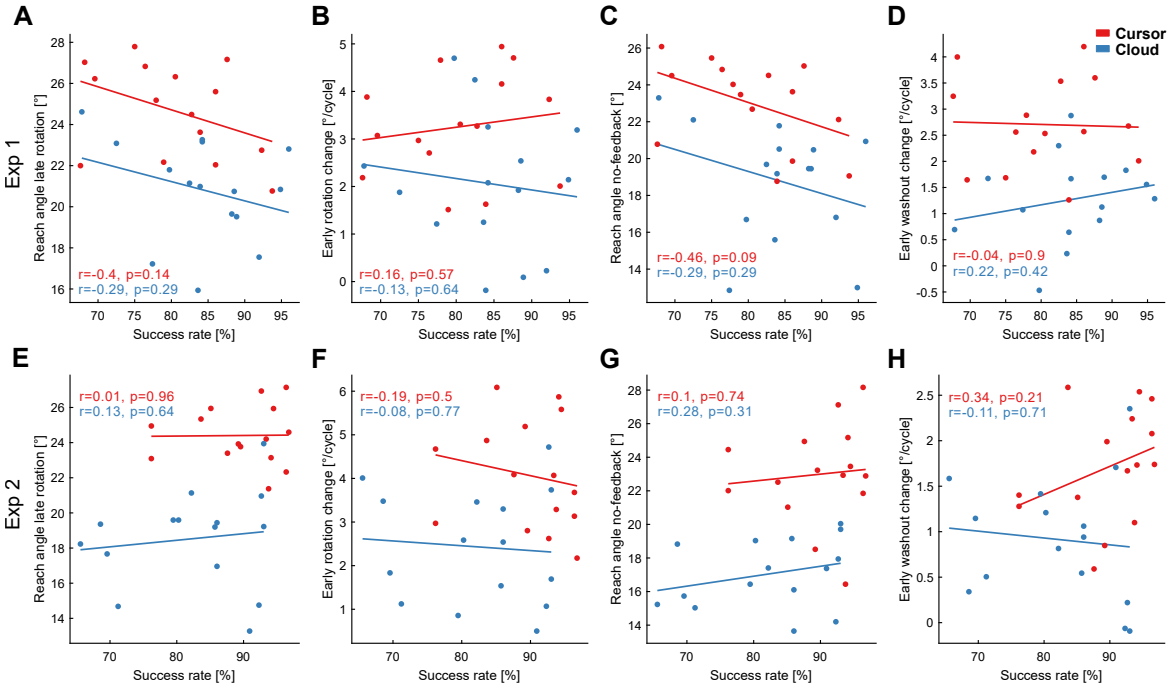

FIGURE S1: **No significant correlation between adaptation measures and success rates (Experiment 1 and 2).** Points represent success rate during baseline and rotation blocks against **A:** reach angle during late rotation (cycles 57-60), **B:** early rotation change in reach angle (cycles 11-14), **C:** reach angle during no-feedback washout (cycles 61-62), and **D:** early washout change in reach angle (cycles 64-67) for each participant in Experiment 1. **E, F, G, H:** Same as A, B, C, D but for Experiment 2; only including cycles 11-13 for the early rotation change in reach angle, and using cycles 72-75 for the early washout change in reach angle. Colored lines represent best linear fit for each uncertainty group (red for cursor and blue for cloud). Shown is the Pearson correlation coefficient (r) and p-value (p) for each line.

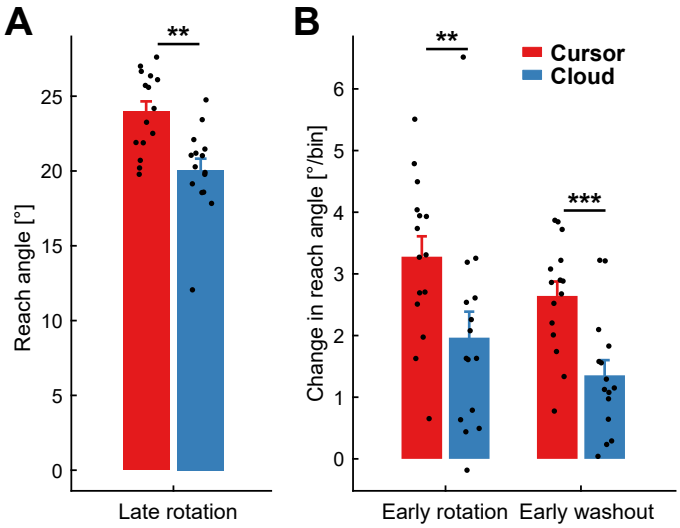

FIGURE S2: **Adaptation measures based on the number of experienced trials still reflect attenuation with high feedback uncertainty (Experiment 1). A:** Average reach angle during late rotation (cursor: 23.97±2.66, cloud: 20.08±2.89, z 3.19, p 0.001, Wilcoxon rank-sum test). **B:** Average change in reach angle during early rotation (cursor: 3.28±1.28/cycle, cloud: 1.97±1.63/bin, z 2.70, p 0.007, Wilcoxon rank-sum test) and early washout (cursor: 2.64±0.9/bin, cloud: 1.36±0.95/bin, $t_{(28)}$ 3.80, $p < 0.001$, d 1.39, unpaired t-test). Red color corresponds to cursor group and blue to cloud group. Black points represent individual participants. Error bars indicate SEM across participants. $^{**}p < 0.01$, $^{***}p < 0.001$.

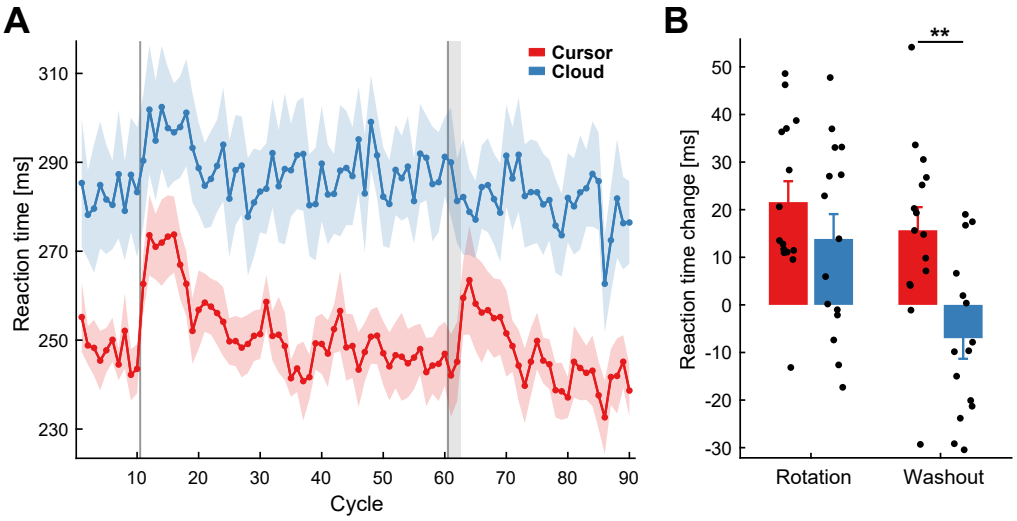

FIGURE S3: **Reaction times over the session show different modulation between low and high visual feedback uncertainty conditions (Experiment 1). A:** Average reaction time with cycle number for cursor (red) and cloud (blue) groups. Gray vertical lines indicate start and end of rotation block. Gray vertical shaded areas cover no-feedback cycles. **B:** Reaction time change during early rotation relative to baseline (cursor: 21.3±16.12ms, cloud: 13±19.87ms, $t_{(28)}$ 1.26, p 0.22, d 0.46, unpaired t-test), and early feedback washout relative to preceding late rotation and no-feedback washout (cursor: 15.87±19.08ms, cloud: -7.28±16.14ms, $t_{(28)}$ 3.59, $p < 0.01$, d 1.31, unpaired t-test). Black points in bar plots represent individual participants. Colored shaded areas and error bars indicate SEM across participants. **$p < 0.01$.

Predictor	Estimate	Std	2.5% CL	97.5% CL	Df	Chisq	p	Min	Max
Implicit reach angle model									
Intercept	0.256	0.009	0.238	0.274				0.252	0.261
Uncertainty	-0.072	0.013	-0.1	-0.047				-0.078	-0.068
Probe block	0.046	0.005	0.037	0.055				0.045	0.049
Probe block^2	-0.035	0.004	-0.043	-0.026				-0.037	-0.033
Probe block x uncertainty	-0.009	0.007	-0.022	0.005	1	1.74	0.187	-0.012	-0.006
Probe block^2 x uncertainty	0.019	0.006	0.006	0.031	1	8.79	0.003	0.017	0.021
Explicit reach angle model									
Intercept	0.017	0.004	0.008	0.024				0.015	0.019
Uncertainty	-0.016	0.006	-0.027	-0.005				-0.018	-0.014
Probe block	0.001	0.004	-0.006	0.009				-0.001	0.003
Probe block x uncertainty	0.003	0.006	-0.008	0.014	1	0.28	0.6	0.001	0.005
Explicit reach angle model reduced									
Intercept	0.017	0.004	0.009	0.024				0.015	0.019
Uncertainty	-0.016	0.006	-0.027	-0.005	1	7.28	0.007	-0.018	-0.014
Probe block	0.003	0.003	-0.003	0.008	1	0.99	0.32	0.002	0.004

TABLE S1: **GLMM model results for implicit and explicit reach angles.** Estimate corresponds to mean value. Std for standard deviation. Lower (2.5%) and upper (97.5%) confidence levels from bootstrap estimation (N 1000). Degrees of freedom (Df), Chi-square value (Chisq) and p-value from likelihood ratio test. Minimum and maximum value from model stability results. Uncertainty predictor had the low uncertainty condition as reference.

Chapter 3

Visual target and task-critical feedback uncertainty impair different stages of reach planning in motor cortex

Lukas K. Amann, Virginia Casasnovas*, and Alexander Gail*

* Lukas K. Amann and Virginia Casasnovas are shared first authors.

Please note that this manuscript will also be part of Lukas K. Amann's dissertation upon agreement of all authors. The individual contributions of each author are listed in detail below.

Author contributions:

LKA, VC, and AG conceptualized the project.

LKA planned array surgery for monkey Z.

LKA designed and programmed the target uncertainty task, trained both monkeys, and recorded the data.

VC designed and programmed the manual feedback uncertainty task, trained both monkeys, and recorded the data.

VC adapted BCI framework for the BCI feedback experiment.

LKA recorded the BCI feedback uncertainty dataset for monkey Z.

VC recorded the BCI feedback uncertainty dataset for monkey Y.

LKA analyzed the target uncertainty dataset and performed neural decoding analyses for the manual feedback dataset.

VC analyzed the BCI feedback uncertainty dataset and performed behavior and neural dPCA analyses for the manual feedback dataset.

LKA, VC, and AG interpreted the data.

LKA assembled figures 1, 4, S1, S2, and S4.

VC assembled figures 2, 3, 5, and S3.

LKA wrote paragraphs concerning target uncertainty in the introduction and discussion.

VC wrote paragraphs concerning feedback uncertainty in the introduction and discussion.

LKA and VC wrote the abstract and methods sections.

LKA wrote sections presenting the single unit and decoding analyses in the results.

VC wrote sections presenting the behavior and dPCA analyses in the results.

LKA, VC, and AG edited and critically reviewed the manuscript.

Please note that since this manuscript is prepared for submission to *Nature Communications*, the Methods section will appear after the Discussion section.

Abstract

Sensory uncertainty jeopardizes accurate movement. During reaching, visual uncertainty can affect the estimation of hand position (feedback) and the desired movement endpoint (target). While impairing motor learning, it is unclear how either form of uncertainty affects cortical reach goal encoding. We show that reach trajectories vary more with higher visual uncertainty of the target, but not the feedback. Accordingly, cortical motor goal activities in rhesus monkeys were less accurate during planning and movement initiation under target but not feedback uncertainty. Yet, when monkeys critically depended on visual feedback to conduct reaches via a brain-computer interface, then visual feedback uncertainty did impair reach accuracy and neural motor goal encoding around movement initiation. Neural state space analyses revealed a dimension that separated population activity by uncertainty level in all tested conditions. Our findings demonstrate that while both target and feedback uncertainty always reflect in neural activity, uncertain feedback only deteriorates neural reach goal information and behavior when it is task-critical, i.e., when having to rely on the sensory feedback and no other more reliable sensory modalities are available. Further, uncertain target and feedback impaired reach goal encoding in a time-dependent manner, suggesting that they are integrated during different stages of reach planning.

Keywords

Visual uncertainty, brain-computer interface, motor goal

Introduction

Sensory signals from different modalities provide information about the state of our body and the environment, allowing us to plan and execute movements accurately (Cross et al., 2024; Pruszynski et al., 2014; Sober & Sabes, 2003; Wolpert et al., 1995). However, these sensory signals present a challenge for motor control, as they are inherently corrupted by uncertainty (see Faisal et al., 2008 for review). Visual accuracy is reduced in the periphery of the visual field, for instance, or due to external like low-light conditions or visual blur. When performing a reach towards a visual target, uncertainty can affect both sensory information about the current, time-varying position of the effector (feedback uncertainty) and the desired movement endpoint (target uncertainty). Target and feedback uncertainty both should compromise accurate movement planning and execution. Previous work has shown that visual target uncertainty results in increased reach errors (Amann et al., 2024; Dekleva et al., 2016) and that visual feedback uncertainty attenuates corrections to movement perturbations (Burge et al., 2008; Casasnovas et al., 2024; Tsay et al., 2021; Zhang et al., 2024). Both of these findings have been interpreted through the lens of optimal integration. To control an effector (e.g., hand position) it is necessary to know its current and its future desired state. It is thought that to estimate this state, sensory information from different modalities and internal predictions of the limb's state are integrated, weighing them according to their relative reliabilities (Angelaki et al., 2009; Bays & Wolpert, 2007). Thus, the greater the uncertainty in the visual input, the less influence it should have on the computation of a final state estimate used for control. While the behavioral consequences are evident for both cases of uncertainty, their neural underpinnings in motor cortex remain unclear. Here, we directly compare how target and feedback uncertainty shape the neural dynamics underlying reach planning and test under which circumstances these neural effects translate to reduced behavioral performance.

Target and feedback uncertainty both impair the computation of the motor vector from a potentially uncertain starting point (effector feedback about current hand position) to a potentially uncertain endpoint (target). In this sense, both could be expected to impair movement accuracy and underlying neural motor goal encoding during planning and execution of a reach, until an endpoint is reached. Yet, target and feedback uncertainty also differ.

First, target and feedback uncertainty differ with respect to the possibility of sensory cross-modal compensation. While a visually instructed target comes with its inherent uncertainty, unreliable visual information about the hand may be partly compensated by somatosensory input following optimal integration principles (Alais & Burr, 2004; Amann et al., 2024; Bayramova et al., 2021; Dadarlat et al., 2015; Ernst & Banks, 2002; Ferrea et al., 2022a; Moscatelli et al., 2019; Sober & Sabes, 2003; van Beers et al., 2002). To prevent cross-modal compensation, we leverage a brain-computer interface (BCI). BCI-controlled movements allow to experimentally determine the sensory feedback the user receives. BCIs translate recorded

neural activity directly into a behavioral readout, such as the movement of an external effector (Ferrea et al., 2024; Ganguly & Carmena, 2009; Golub et al., 2018; Velliste et al., 2008). As this movement is controlled through the BCI and not the physical arm, movement-contingent proprioceptive feedback becomes unavailable. By only providing visual feedback about the BCI-controlled movement, the effects of visual feedback uncertainty on neural activity can be isolated (Golub et al., 2016) and compared to those during physical arm reaches. At the same time, BCIs have also been successfully employed to restore lost motor function in patients (Aflalo et al., 2015; Ajiboye et al., 2017; Bouton et al., 2016; Braun et al., 2024; Collinger et al., 2013; Hochberg et al., 2006; Willett et al., 2021). From this clinical perspective, the lack of relevant proprioceptive inputs could make BCI users particularly vulnerable to visual feedback uncertainty. Thus, studying this condition under BCI control also provides insights for optimizing its clinical application.

Second, target and feedback uncertainty likely differ with respect to the time at which they become most relevant even if persisting throughout the planning and execution process. To make a reach, the motor system is thought to compute the associated motor goal and translate it into muscle activity (see Kim et al., 2021; Wong et al., 2015 for reviews). When a delay is imposed between target presentation and movement initiation, different areas in frontoparietal motor-associated cortical areas have been found to contain sustained information about the pending motor goal (i.e., desired state of the body) from target selection to movement execution (e.g., Batista et al., 2007; Churchland et al., 2010; Crammond and Kalaska, 2000; Elsayed et al., 2016; Riehle and Requin, 1989; Sabatini and Kaufman, 2024). The effects of uncertain target locations have been previously examined by presenting either two visual target cues or a single noisy cue. When two mutually exclusive potential targets are offered, the two associated motor goals are co-represented in motor areas during planning until the final target identity is disclosed, provided animals consider both options as equipotent and do not select a reach goal prematurely (Cisek & Kalaska, 2005; Coallier et al., 2015; Klaes et al., 2011; Suriya-Arunroj & Gail, 2019). Comparably, when the target location has to be estimated from a noisy visual cue, motor goal representations in the dorsal premotor cortex (PMd) cover a wider range of possible reach directions (Dekleva et al., 2016). Therefore, target uncertainty is likely to mainly affect the target selection process and planning, as long as the action is still undefined.

In contrast to target uncertainty, feedback uncertainty might primarily affect action execution itself. For example, previous work showed that when hand visual feedback is unavailable, which can be seen as maximal feedback uncertainty, motor-associated spatial selectivity in motor cortex neurons is reduced only during the final stages of reach execution (Suway & Schwartz, 2019). Yet, that motor goals are, at least partly, computed relative to the hand starting position in frontal lobe motor areas (Caminiti et al., 1991; Caminiti et al., 1990; Hatsopoulos et al., 2007; Pesaran et al., 2006). Therefore, it remains elusive what stages of movement planning might also be compromised by uncertain feedback information and how

these effects might differ from the ones observed for uncertain targets.

Here, we evaluate when and how visual uncertainty of target and effector feedback affects neural population activity in motor cortex during movement planning and execution. We trained two male rhesus monkeys (*Macaca mulatta*) to perform memory-guided center-out reaches towards different target directions while recording neural activity from PMd and primary motor cortex (M1). In each session, we compared high and low levels of visual target or feedback uncertainty. Additionally, we tested feedback uncertainty during manual reaches (manual control – MC) and when performing reaches through a BCI (brain control – BC) to account for compensatory proprioceptive input. Using a decoding approach, our results show that neural motor goal representations were less well-defined during early planning and movement initiation when the target direction was uncertain. In contrast, when feedback was uncertain, representations were only impaired under BC during movement initiation. Both finding reflect in corresponding behavioral variability during early and late movement execution, respectively. Moreover, population activity can be separated by uncertainty level along an uncertainty dimension in neural state space at any time for both uncertainty types. This suggests that while target and feedback uncertainty are always encoded in motor cortex, they only impact motor goal representations at specific stages during reach planning in a behaviorally relevant way.

Results

Sensory uncertainty can increase movement variability and movement time

Monkeys performed center-out reaches controlling a visual cursor either by using a haptic manipulandum (manual control, MC) or via a brain-computer interface (brain control, BC; velocity-based Kalman filter, see Methods for details) in a vertical 2D workspace (Fig. 1a). They had to remember the location of a briefly flashed visual target cue while keeping gaze and hand position fixed at the center before initiating the movement in response to a 'go' cue (Fig. 1b). Monkeys performed reaches under different uncertainty types to investigate the effect of visual target and visual feedback uncertainty about the spatial location of the target or effector (Fig. 1c).

Across daily sessions, we varied the type of uncertainty, target or feedback, to test for their respective effects on motor planning. Additionally, in the case of feedback uncertainty, we also varied the control mode, MC or BC, to vary the behavioral relevance of the visual feedback. This resulted in a total of three task conditions: target MC, feedback MC, and feedback BC. We did not test target uncertainty under BC because target information would be provided only visually during the cue period. Therefore, removing movement-contingent proprioceptive inputs would likely only have minor influences on directional encoding during reach planning.

Within each task condition, we tested two fixed uncertainty levels (low and high). The low level of target uncertainty was implemented by presenting the true target, the high level by showing an array of five bars distributed along a ring (high; Fig. 1c, left panel). The low level of feedback (effector position) uncertainty was implemented by having monkeys control a focal cursor, the high level by controlling a cloud of five moving dots (high; Fig. 1c, middle and right panels).

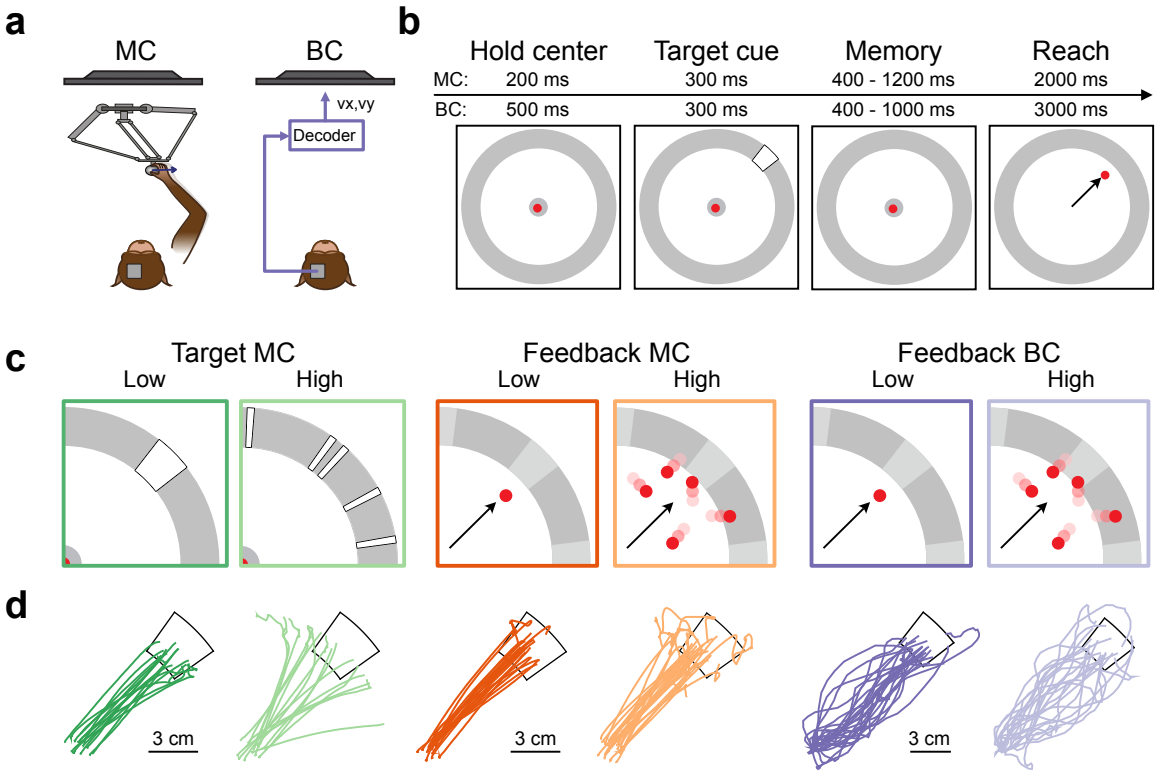

FIGURE 1: **Experimental setup and task design. a.** Monkeys performed center-out reaches by controlling a cursor via a haptic manipulandum (manual control – MC) or a brain-computer velocity decoder (brain control – BC). **b.** Task design. After acquiring and holding the central hand and eye fixation (gray disk), a brief visual cue indicated the location of a target (white arc) along an outer target ring (gray ring). Following a variable delay period, in which hand and eye movements had to be withheld and which ended with disappearance of the hand and eye fixation stimulus, monkeys were required to move the cursor (red circle) towards the remembered target location. **c.** Implementation of target and feedback uncertainty. In target uncertainty sessions, either the true target location was revealed during cue period (low uncertainty, dark green) or the target was cued using five bars drawn from a Gaussian distribution centered on the true target location (high uncertainty, light green). Feedback uncertainty was varied by monkeys controlling a cursor (low, dark orange and purple) or a cloud of five moving dots each of which had the same visual appearance as the cursor (high, light orange and purple). The initial position of each dot of the cloud was drawn from a 2D Gaussian centered on the true hand position. Each dot was assigned a random velocity direction and had a short lifetime of 300 ms before re-initializing. **d.** Example trajectories. Monkey Z reached towards a target located at 45°. Examples with varied target uncertainty in green, feedback MC in orange, and feedback BC in purple. Low uncertainty in dark color, high uncertainty in light color.

Monkeys were able to perform the task in all three task conditions. Average success rates were reduced for high compared to low uncertainty levels, especially for target MC (monkey Y: low: 62%, high: 31%; monkey Z: low: 77%, high: 38%). For feedback MC (monkey Y: low: 94%, high: 84%; monkey Z: low: 94%, high: 89%) and BC (monkey Y: low: 95%, high: 87%; monkey Z: low: 94%, high: 82%) performance reductions were less pronounced. To evaluate the behavioral consequences of uncertainty in more detail, we analyzed the monkeys' reach trajectories (Fig. 1d).

First, we used early (25% eccentricity) and late (75%) absolute angular reach errors to characterize reach planning and execution, respectively (Fig. 2a). Large early reach errors indicate that the planned reach direction is incorrect (planning error). This is because movement corrections at that time are not possible due to slow visual feedback processing. In contrast, late reach errors do not only capture an incorrectly planned reach direction, but also an inability to use effector feedback to properly guide reach execution (execution error). We found that high target uncertainty caused larger early reach errors (Fig. 2b; paired t-test, monkey Y: $t_{(7)}$=-13.09, p=3.53e-06; monkey Z: $t_{(7)}$=-7.75, p=1.11e-04), while early reach errors were neither affected in feedback MC (monkey Y: $t_{(9)}$=1.36, p=0.21; monkey Z: $t_{(9)}$=-1.34, p=0.21) nor BC conditions (monkey Y: $t_{(9)}$=-2.18, p=0.06; monkey Z: $t_{(9)}$=-0.85, p=0.4). Late reach errors were higher for high target uncertainty (monkey Y: p=4.36e-07; monkey Z: p=1.22e-06). In the case of feedback uncertainty, late reach errors were not different between uncertainty levels in MC (monkey Y: $t_{(9)}$=1.67, p=0.13; monkey Z: : $t_{(9)}$=-0.24, p=0.82) but were larger for high uncertainty in BC (monkey Y: $t_{(9)}$=-5.83, p=2.51e-04; monkey Z: $t_{(9)}$=-5.26, p=5.22e-04). Therefore, target uncertainty decreases both early and late movement accuracy, while feedback uncertainty only decreases late movement accuracy, and only in BC.

Second, we evaluated speed profiles aligned to the go cue (Fig. 2c). For MC conditions, reaches started with a steep, transient speed increase, followed by a much smaller increase and decrease in speed. This suggests that reaches were composed by an initial "ballistic" component to bring the hand close to the target, likely in a feedforward manner. If the monkey did not directly enter the target area after this initial component, smaller homing-in movements were made, putatively guided by incoming sensory feedback. This observation also reflects in the traces of the traveled distance, which show a steep increase followed by a plateau (Fig. 2d). In contrast to MC, speed and distance for BC reaches changed more gradually, suggesting that movements were predominantly feedback-based throughout the movement. Moreover, we observed that the reduction between early and late reach errors was larger for feedback BC compared to MC (Fig. 2b), indicating that feedback-based corrections were more prominent under BC. There were no evident differences between uncertainty levels regarding speed and traveled distance-from-the-center as a function of time.

Reach reaction times were longer with high target uncertainty (Fig 2e; paired t-test, monkey

Y: $t_{(7)}$=-5.96, p=5.64e-04; monkey Z: $t_{(7)}$=-5.47, p=9.35e-04) and high feedback uncertainty in MC (monkey Y: $t_{(9)}$=-7.97, p=2.28e-05; monkey Z: : $t_{(9)}$=-9.89, p=3.94e-06). We also estimated reaction times in BC (but see Methods for limited interpretability), which did not show differences between feedback uncertainty levels in monkey Y ($t_{(9)}$=0.57, p=0.57) but were increased for low uncertainty in monkey Z ($t_{(9)}$=5.04, p=7.05e-04). Finally, movement times increased with higher uncertainty across all conditions (Fig 2f; paired t-test; target MC: monkey Y: $t_{(7)}$=-8.11, p=8.34e-05; monkey Z: $t_{(7)}$=-11.44, p=8.74e-06; feedback MC: monkey Y: $t_{(9)}$=-9.68, p=4.71e-06; monkey Z: $t_{(9)}$=-9.69, p=4.66e-06; feedback BC: monkey Y: $t_{(9)}$=-2.68, p=0.03; monkey Z: $t_{(9)}$=-4.32, p=0.002).

Together, the behavioral results suggest that target and feedback uncertainty affect behavioral accuracy during selective phases of the trial. Target uncertainty is visible in early execution already, suggesting a planning error, while feedback uncertainty becomes evident during later execution only. This is the case even though both types of uncertainty in the sensory input persist from beginning to the end of the trial.

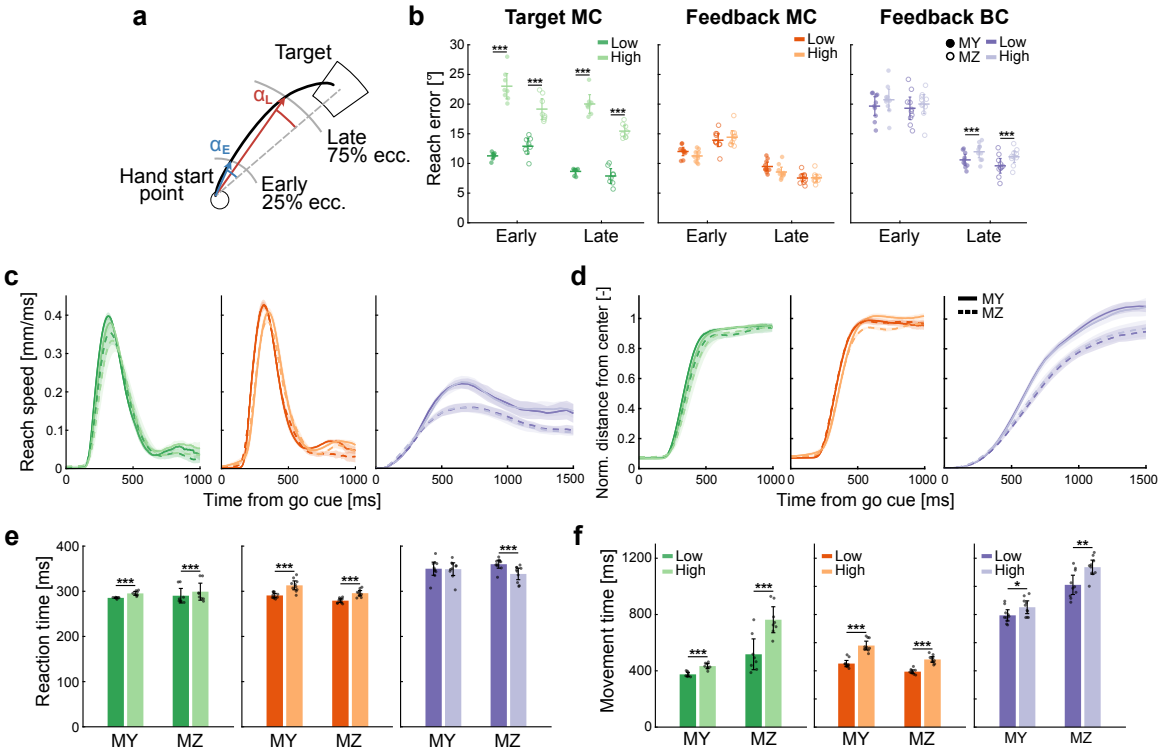

FIGURE 2: **Behavioral results.** **a.** Absolute directional reach error. Reach error was computed relative to the initial hand position when the trajectory crossed 25% (Early, $_E$, blue) and 75% (Late, $_L$, red) of the target eccentricity. **b.** Early and late reach errors. High uncertainty in light and low uncertainty in dark color. Target MC in green, feedback MC in orange, and feedback BC in purple. Circles correspond to individual sessions. Filled circles correspond to monkey Y and open ones to monkey Z. **c.** Reach speed in time from go cue. Solid lines correspond to monkey Y and dotted ones to monkey Z. **d.** Distance from the center in time from go cue. Distance was normalized by the target eccentricity. Line styles are the same as in (**c**). **e.** Reaction times. **f.** Movement times. Black dots correspond to individual sessions in (**e**) and (**f**). Error bars and shaded areas in all panels depict 95% CIs across sessions. *p<0.05, **p<0.01, ***p<0.001 for paired t-tests.

Target and feedback uncertainty modulate single-neuron and population-level neural responses

We recorded neural activity from motor cortex using chronically implanted floating microelectrode arrays (FMAs) in PMd for monkey Z and PMd and M1 for monkey Y (Fig. 3a). We refer to M1 and PMd jointly as motor cortex. Taking all sessions into account, we recorded a range of 35 – 83 single neurons in monkey Y and 32 – 54 neurons in monkey Z per session. A summary of the number of recorded units and trials can be found in Supplementary Table S1. Since data from the two monkeys led to the same conclusions, we report the combined results for the two monkeys. Individual results can be found in Supplementary Fig. S1-3.

Most neurons were selective ("tuned") for the target direction (Fig. 3b-c). Neural spike densities varied with target direction after target cue (monkey Y: 41%, monkey Z: 52% tuned units), before go cue (monkey Y: 53%, monkey Z: 49% tuned units).

Uncertainty levels had diverse effects on neural activity. For example, spike densities suggest reduced amplitude and directional selectivity during the onset of the target cue and early planning stages when target uncertainty was high, with less noticeable differences during late planning (Fig. 3b). Uncertainty modulations were less prominent in the feedback MC condition (Fig. 3c). Similarly, there were varied response differences for high and low in feedback BC (Fig. 3d).

Observing larger behavioral reach errors for target MC and feedback BC at different stages of the reach is in line with our hypothesis that the two types of uncertainty affect neural activity for movement planning and execution in distinct ways. Specifically, larger reach errors during early movement, as observed with target uncertainty (Fig. 2b), are linked to increased planning errors, which we expect to be the consequence of less informative neural motor planning activity. Therefore, we predict that neural representations of reach directions are less well separated in neural space. Larger behavioral reach errors during late movement, instead, as observed in target MC and feedback BC indicate increased execution errors. These errors could result from the cumulative effect of less informative neural planning activity and/or less informative neural movement-associated activity.

To decide between these two possibilities, we trained a series of support vector machines (SVMs) and decoded the reach direction based on spike densities over the course of the trial (Fig. 4a). We decoded the executed reach direction, as compared to the instructed target direction, to account for large deviations between these two in the case of target uncertainty. In a first approach, we trained decoders on trials with different uncertainty levels independently to assess the separability of directional representations in each uncertainty level (Fig. 4b, 'within-level'). We analyzed the decoding performance during two time intervals with sliding windows (100 ms duration, 50 ms shift; see Methods), aligned to target cue onset (-100 to 600 ms) or go cue (-200 to 600 ms). In all task conditions for both uncertainty levels, decoders achieved higher-than-chance performances shortly after target cue (Fig. 4c-e),

providing the basis for testing the effect of visual uncertainty on the quality of directional information at the neural level.

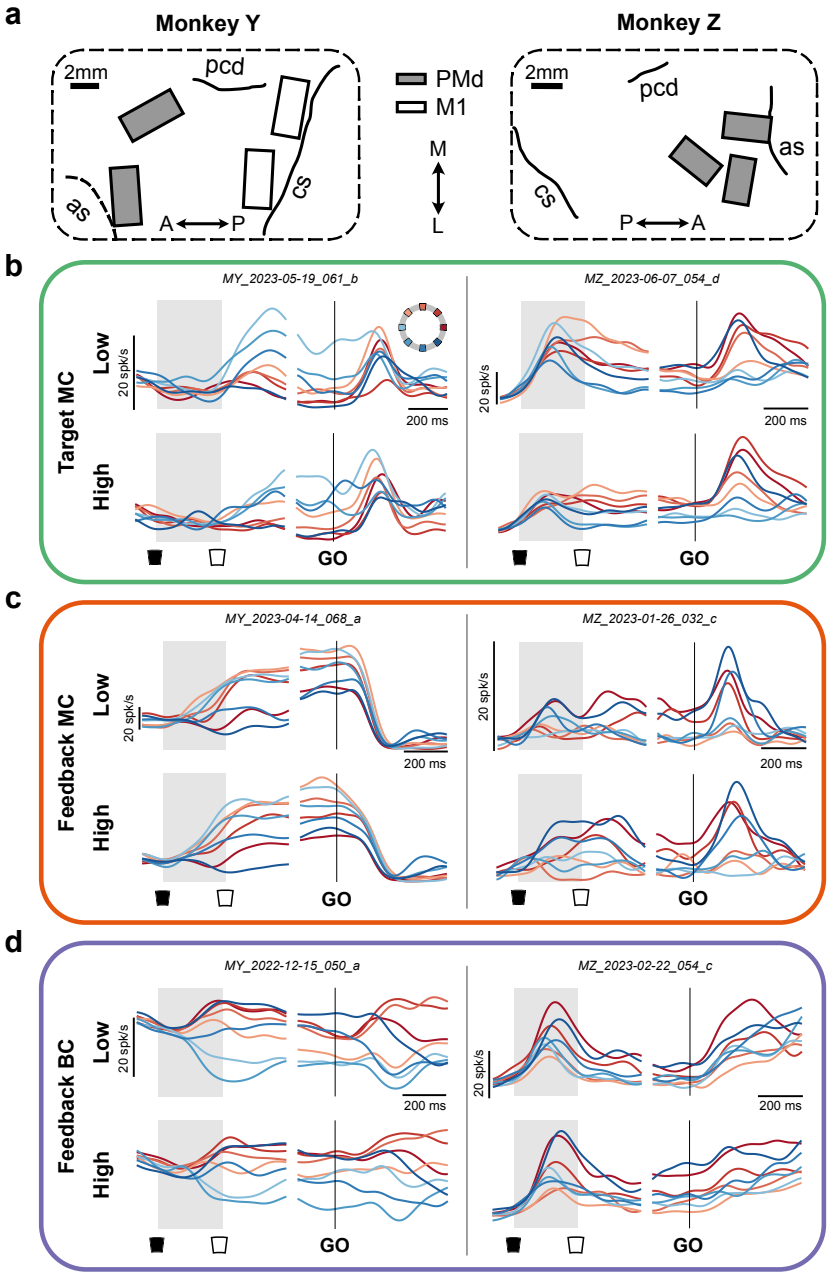

FIGURE 3: **Recording sites and example responses of single neurons. a.** Illustration of recordings sites for monkey Y (left) and monkey Z (right). Monkey Y was implanted in the right hemisphere, monkey Z in the left. Gray boxes depict 32-channel multielectrode arrays in dorsal premotor cortex (PMd), while white boxes show arrays in primary motor cortex (M1). as: arcuate sulcus, pcd: precentral dimple, cs: central sulcus. **b.** Example responses of two single neurons in trials with low (top row) and high (bottom row) uncertainty for target MC. Each trace shows the trial-averaged firing rate for a given target direction indicated by color (target direction color map shown in inset). Filled black arc: target cue onset, empty arc: target cue offset, and GO: go cue. Gray shaded area indicates time the target cue was visible. Vertical line marks go cue. Vertical scale bars correspond to 20 spikes/s, and horizontal scale bars to 200 ms. **c.** Same as in (**c**) but for feedback MC. **d.** Same as (**b**) and (**c**) but for feedback BC.

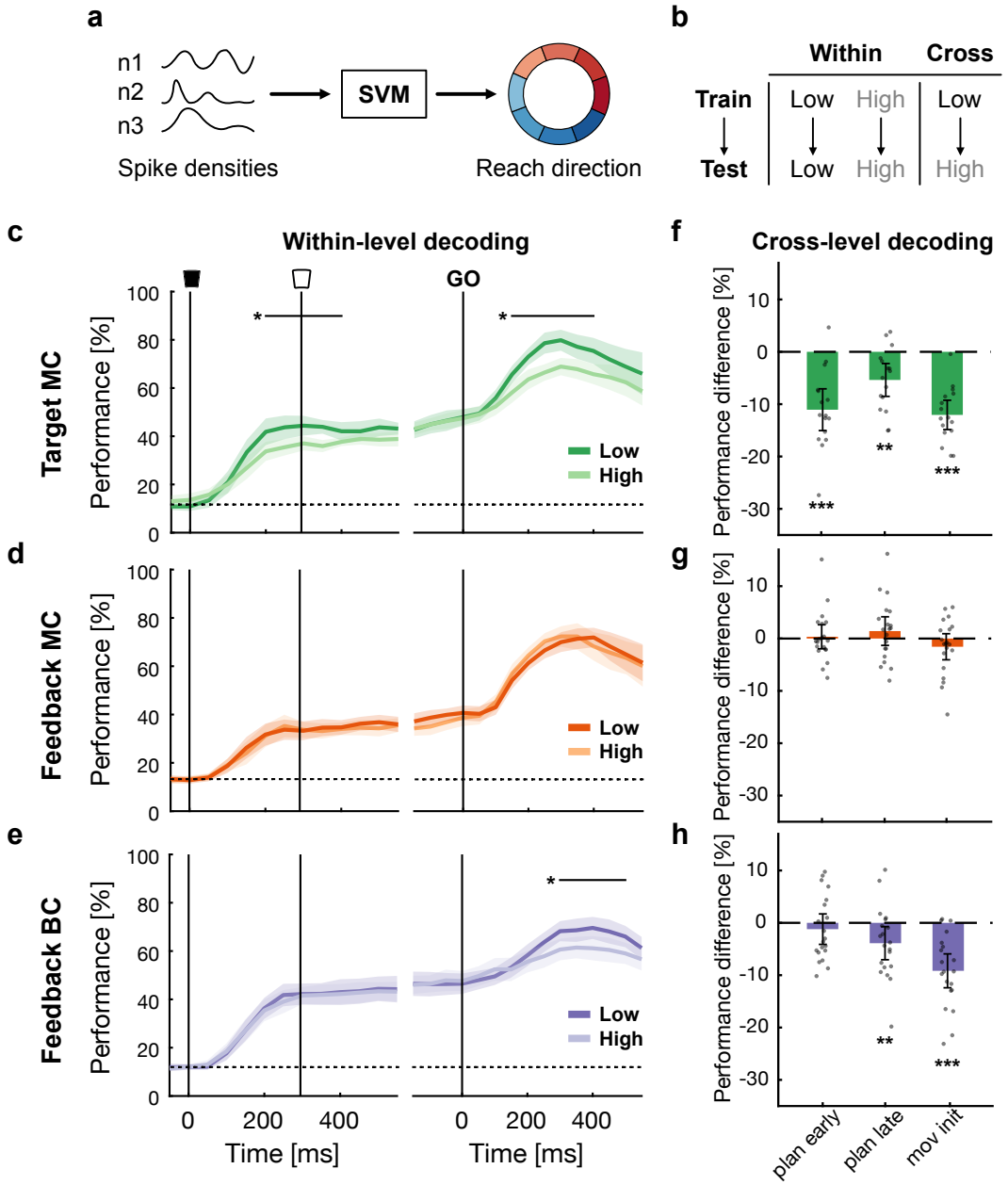

FIGURE 4: **Decoding of reach direction. a.** Schematic drawing of decoding procedure. Spike densities were input to a support vector machine (SVM) to decode the reach direction. **b.** Decoding modes. For within-level decoding, SVMs were trained on spike densities from low or high uncertainty trials and tested on the same uncertainty level. For cross-level decoding, SVMs were trained on low uncertainty trials and tested on high uncertainty trials. **c.** Decoding performance of decoders trained on spike densities of 100 ms time intervals shifted by 50 ms for target MC. Performance was computed for each session and uncertainty level independently using 5-fold cross-validation. Performance was then averaged across folds for each session. Shaded areas depict 95% CIs for the average performance across sessions and monkeys. Dotted lines indicate chance level at 12.5%. Lightness indicates uncertainty level (low: light, high: dark). Filled black arc: target cue onset, empty arc: target cue offset, and GO: go cue. Horizontal bars indicate time windows in which performances of SVMs trained on different uncertainty levels were significantly different (*$p<0.05$, permutation test). **d.** Same as in (**c**) but for feedback MC. **e.** Same as in (**c**) and (**d**) but for feedback BC. **f.** Performance difference between decoders tested and trained on low uncertainty trials and cross-level decoding for target MC. Negative values indicate lower performance in cross-level decoding. Performance was evaluated at three 200 ms time windows spanning from early planning to movement initiation. Black dots depict individual sessions. Error bars depict 95% CIs across sessions. *$p<0.05$, **$p<0.01$, ***$p<0.001$ for one-tailed one-sample t-tests. **g.** Same as in (**f**) but for feedback MC. h. Same as in (**f**) and (**g**) but for feedback BC.

We hypothesized that target and feedback uncertainty modulated decoding performance of directional information differently during planning and early execution of movement. In line with this idea, when manipulating target uncertainty, decoders trained on trials with high uncertainty achieved significantly lower performances during planning, 200 to 400 ms after target cue onset, and during movement initiation, around 150 to 400 ms after go cue (Fig. 4c; permutation test (Maris & Oostenveld, 2007), $p<0.05$). In contrast, in feedback MC, there was no uncertainty-associated difference in decoding performance in either of the two time windows (Fig. 4d; $p>0.05$). However, in feedback BC, decoders trained on high-uncertainty trials performed significantly worse than those trained on low-uncertainty trials during movement initiation, around 300 to 500 ms after go cue (Fig. 4e; $p<0.05$). Thus, while target uncertainty impairs directional neural coding during both, early planning and movement initiation, feedback uncertainty does so only during movement initiation and only if visual feedback is exclusive for controlling movements, as no movement-contingent proprioception is available in BC.

Separate but similar neural subspaces for different levels of uncertainty

The above within-level decoding analyses showed that high uncertainty can lead to less distinct representations of reach directions. Yet, similar within-level decoding performances do not necessarily mean that directional representations are conserved between uncertainty levels. In fact, we observed single neuron response differences (Fig. 3c) between uncertainty levels in feedback MC despite similar within-level decoding results. To characterize the effects of uncertainty on reach direction representations, we conducted two further analyses. First, we conducted cross-level decoding to test for generalization of reach direction coding between uncertainty levels (Fig. 4f-h). At the same time, uncertainty might affect neural activity irrespectively of reach direction. Thus, second, we analyzed neural state spaces between both uncertainty levels to test for potential non-alignment of neural dynamics (Fig. 5).

For the cross-level decoding, first, SVM decoders to classify the reach direction based on spike densities were trained and tested exclusively on low-uncertainty trials to determine the reference performance. Second, spike densities from high-uncertainty trials were used as test trials for the same decoders trained on low-uncertainty trials and the resulting classification cross-level performance was determined (Fig. 4b, 'cross'). If cross-level decoders perform poorly, it would suggest that neural directional coding is indeed qualitatively different between uncertainty levels. We expect this to occur at least during intervals with different within-level performances. Conversely, if the cross-level decoders perform similar to the reference performance, it indicates that the underlying representation of reach direction is preserved between uncertainty levels. We tested cross-level decoding performance in three non-overlapping 200 ms time windows ranging from early planning (-50 to 150 ms aligned to target cue offset) over late planning (-150 to 50 ms aligned to go cue) to movement initiation (-50 to 150 ms

aligned to movement onset). We chose these time epochs because they capture the temporal progression from early formation of a motor plan to its convergence, and execution.

The cross-level decoding performances differed from the reference decoding performances in target MC and in feedback BC conditions (Fig. 4f-h). In the MC (Fig. 4f), we found lower cross-level decoding performances during all three epochs (one-tailed one-sample t-test, early planning: $t_{(15)}$=-3.90, p=7.09e-04; late planning: $t_{(15)}$=-2.82, p=0.007; movement initiation: $t_{(15)}$=-6.79, p=2.99e-06). In contrast, cross-decoding performances were similar to the reference performance for feedback MC (Fig. 4g), not showing significant performance differences in any of the tested epochs (early planning: $t_{(19)}$=-1.08, p=0.15; late planning: $t_{(19)}$=1.80, p=0.98; movement initiation: $t_{(19)}$=-0.92, p=0.18). Finally, for feedback BC, performances during late planning and movement initiation were significantly lower in cross-level compared to reference decoding (Fig. 4h; late planning: $t_{(19)}$=-3.44, p=0.001; movement initiation: $t_{(19)}$=-4.29, p=1.98e-04). We did not find a difference in the cross-level decoding performance in feedback BC during early planning ($t_{(19)}$=-1.12, p=0.13). As expected, reduced within-decoding performances for high uncertainty (Fig. 4c-e) are accompanied by reduced generalization of direction decoding between uncertainty levels (Fig. 4f-h). However, we also found periods of non-correspondence (i.e., during late planning for target MC and feedback BC), suggesting that visual uncertainty can affect neural activity without impairing reach goal representations.

With neural state space analyses, we further investigated the influence of uncertainty on the neural activity. We used demixed principal component analysis (dPCA) to find latent dimensions exclusively influenced by uncertainty. To do so, we concatenated neural activity from three non-overlapping time epochs, aligned to target cue onset (-100 to 600 ms), go cue (-200 to 600 ms) and movement onset (-200 to 400 ms), and fitted the dPCA to the full matrix (see Methods). Then, we projected neural activity into the dPCA space. The top 20 demixed principal components (dPCs) captured variances of 86.3% (84.3%) for target MC, 87.8% (88.1%) for feedback MC, and 86.3% (90.3%) for feedback BC in monkey Y (Z) on average across sessions.

For visualization purposes, we plotted time- and trial-averaged neural states for each reach direction and uncertainty level (-50 to 150 ms from movement onset) in the space constructed by the first two direction dPCs and the first uncertainty dPC (Fig. 5a). These neural states had a radial organization according to reach direction in the direction dPC plane (see Supplementary Fig. S4 for the distributions of the neural states in direction dPC space). At the same time, states for all reach directions were separated along the uncertainty dPC in all task conditions. This indicates that uncertainty itself is also reflected in neural population activity, regardless of whether it affects the target or effector location.

The variances explained by dimensions related to uncertainty was overall low with 3.1% (7.2%) for target MC, 3.1% (5.3%) for feedback MC, and 5.6% (4.3%) for feedback BC in monkey Y (Z) on average across sessions (Fig. 5b). We also found an interaction effect of

reach direction and uncertainty, with interaction dPCs accounting for 11.6% (14.8%) of the explained variance in target MC, 11.2% (14.5%) in feedback MC, and 13.9% (11.4%) in feedback BC. This indicates that most neural variance is explained by reach direction in all task conditions. At the same time, in all task conditions, including those where cross-level decoding indicated very good generalization between high- and low-uncertainty levels, there was a significant, similar-sized uncertainty component and its interaction with the reach direction component.

We analyzed the projections onto the first uncertainty dPC to investigate potential differences in the time course of their separation. We time-averaged projections over the same short time windows as for the cross-level decoding, namely early and late planning, and movement initiation (Fig. 5c). We additionally time-averaged a baseline window. This window included the hold period before the target was shown (-100 to 0 ms from target cue), i.e., before directional information was revealed.

The neural projections over the time windows were separated by uncertainty level, but we also observed differences in time courses of this separation between task conditions. To test for the significance of the separation, we used a repeated-measures ANOVA on the distance between low and high uncertainty neural states. We tested if this distance was different from zero and if it is depended on the time epoch. For all uncertainty types, the test revealed a significant intercept, indicating a significant difference in neural states between uncertainty levels (target MC: $F_{(1,15)}=112.9$, $p=2.24e\text{-}08$; feedback MC: $F_{(1,19)}=64.4$, $p=1.6e\text{-}07$; feedback BC: $F_{(1,19)}=139.2$, $p=3.45e\text{-}10$). In case of feedback uncertainty, the separation was already present during the baseline epoch, following that the uncertainty level was already known at that time due to the visual appearance of the cursor/cloud. Moreover, target MC and feedback BC had a significant effect of time epoch (target MC: $F_{(3,45)}=52.2$, $p=1.08e\text{-}14$; feedback BC: $F_{(3,57)}=10.5$, $p=1.35e\text{-}05$), whereas this was not the case for feedback MC ($F_{(3,57)}=0.92$, $p=0.44$). Compared to baseline, the effect of target uncertainty increased for the rest of the epochs, peaking at early planning shortly after the target was cued. In contrast, the effect of uncertainty in feedback BC was already present during baseline, but gradually increased after early planning (see Supplementary Table S2 for post-hoc results). Thus, uncertainty in target MC had the largest effect during early planning, when the monkey starts to integrate target information and selects its reach direction, even though target uncertainty persists throughout the remainder of the trial until the end of the movement. Conversely, uncertainty in feedback BC becomes more prominent towards the start of the movement, when the monkey begins to integrate visual effector information for control, even though uncertainty about the hand position exists already from the beginning of the trial prior to movement planning.

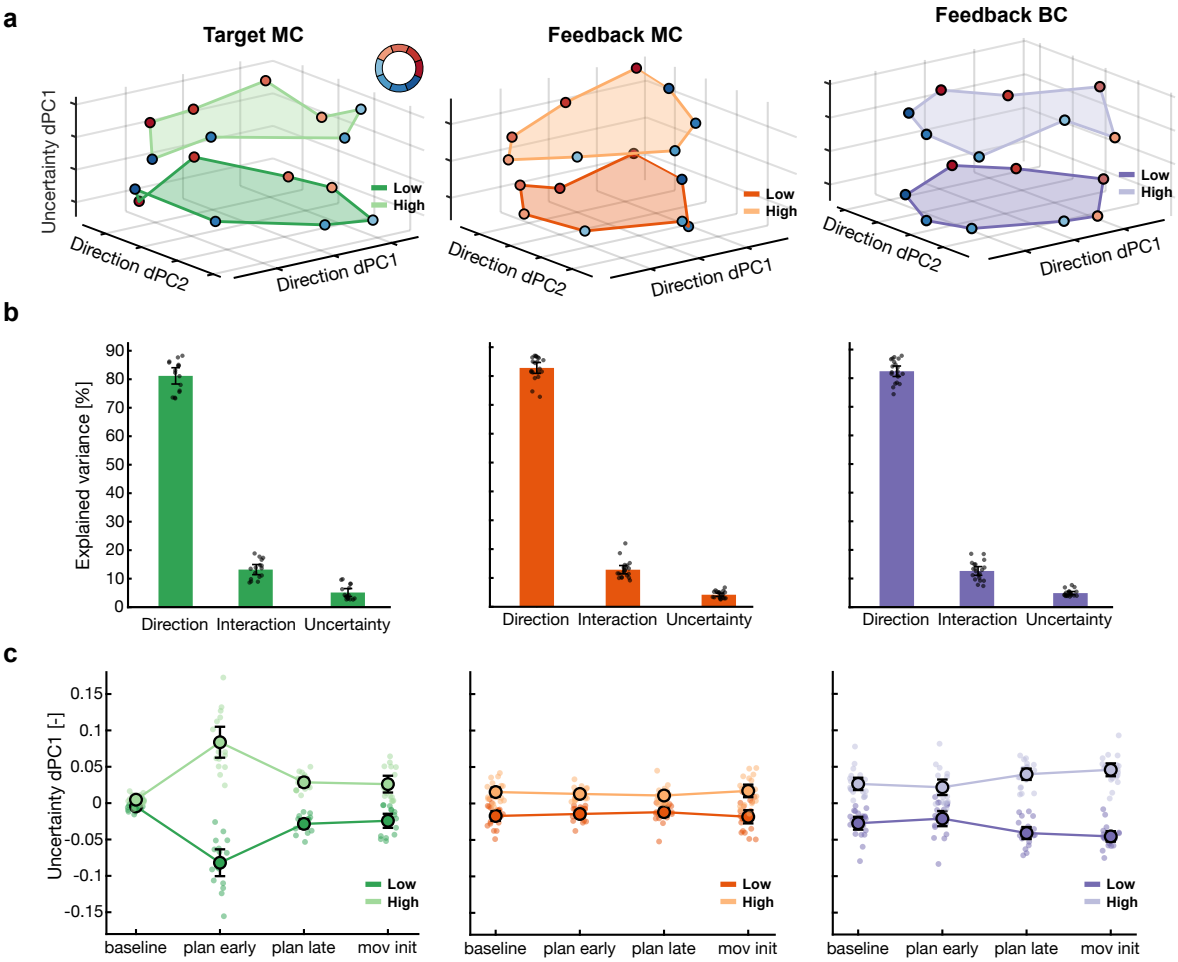

FIGURE 5: **Uncertainty in neural state space. a.** Projections of neural states into the space spanned by the first two direction dPCs and the first uncertainty dPC from one example session in monkey Y on average over the movement initiation time window of all trials of each task condition (reach direction x uncertainty x trial type). Circle colors indicate reach direction (color map shown in inset). Lightness indicates uncertainty level (low: light, high: dark). Columns show different task types: target MC in green (left), feedback MC in orange (middle), and feedback BC in purple (right). Note that dPCs are displayed as orthogonal for easier visualization but orthogonality is not enforced by dPCA. Trial-to-trial variability around means is omitted for clarity. **b.** Average variance explained by dPCs related to each task parameter (direction, uncertainty, and their interaction) across monkeys. **c.** Projection onto first uncertainty dPC for different time intervals. Same uncertainty color and lightness scheme as in (**a**). Points depict individual session averages. Error bars indicate 95% CIs across sessions and monkeys.

Discussion

We tested how visual uncertainty in either the visual target or effector position affects neural coding of reach goals in frontal motor areas of rhesus monkeys. When the position of the target was uncertain, population-level neural decoding of the reach goals revealed impaired spatial representations, notable during early planning and around movement onset. When feedback about the effector position was uncertain, reach representations appeared

unchanged during manual reaches (MC), i.e., when additional movement-contingent proprioceptive information was available. Instead, when monkeys performed brain-controlled (BC) reaches that could only be controlled by visual feedback, reach goal representations were impaired around the time of movement onset in the case of high visual uncertainty. These patterns were highly consistent with decreased directional accuracy of reach behavior in early and late phases of the movements due to target or feedback uncertainty, respectively. While signatures of uncertainty were similarly present in all task conditions in the neural state space, the generalization of reach goal representations between uncertainty conditions was reduced throughout planning and movement initiation for target uncertainty, and for late planning and movement initiation for feedback uncertainty in BC.

The consequences of uncertainty have been mostly discussed in the context of optimal integration of the internal state and sensory inputs (Bays & Wolpert, 2007; Shadmehr et al., 2010). Behavioral studies showed that manual motor adaptation under visual feedback uncertainty is impaired (Burge et al., 2008; Casasnovas et al., 2024; Körding & Wolpert, 2004; Tsay et al., 2021). Despite its behavioral relevance, the neural consequences of visual uncertainty have been largely unexplored in the sensorimotor domain. For instance, it was unclear whether motor goal representations are compromised during the planning of a reach due to feedback uncertainty. Previous research showed that when removing visual feedback, which is as an extreme form of uncertainty, a subset of neurons in M1 decreased their modulation depth, i.e., the strength of their directional selectivity was lower (Suway & Schwartz, 2019). Notably, these changes were only prominent towards the end of the reach. However, the effect of visual feedback uncertainty could have been masked by greater reliance on proprioceptive feedback. Here, we show that visual feedback uncertainty affected movement-associated direction representations at reach initiation, but only when no proprioceptive feedback was available, i.e., under BC, but not MC conditions. This effect could arise because proprioceptive feedback can be used to compensate for visual uncertainty in MC or because BC involves a more feedback-based mode of control, whereas MC is predominantly feedforward. Thus, the effect of uncertain visual feedback is apparent when this information becomes critical for task performance.

Humans and monkeys have been shown to integrate inputs from two sensory modalities by adjusting the sensory weights according to the relative reliability of the signals (Alais & Burr, 2004; Angelaki et al., 2009; Ernst & Banks, 2002; van Beers et al., 2002). Furthermore, experimental and theoretical work has demonstrated that corrective responses to mechanical perturbations initially exhibit similar dynamics regardless of visual feedback availability (Crevecoeur et al., 2016; Kasuga et al., 2022). These studies, grounded in optimal feedback control theory, proposed that motor control relies on an optimal estimate of the moving limb's state, accounting for long visual delays and sensory uncertainty (Crevecoeur et al., 2016; Hoffmann & Crevecoeur, 2024; Kasuga et al., 2022). Extending these behavioral and modeling findings, a recent study demonstrated that overlapping populations of motor cortex

neurons respond to both visual and mechanical perturbations (Cross et al., 2024). This suggests that motor cortex might receive the final result of a state estimator located in upstream regions such as the parietal cortex, where sensory inputs are suggested to be optimally integrated (Gamberini et al., 2018; Mulliken et al., 2008). In our case, high feedback uncertainty under MC likely shifted sensory weights towards proprioception. In contrast, only uncertain visual information was available for state estimation under BC, resulting in behavioral and neural impairments. Also, while state estimation for movement control could make use of cross-modal integration, in our experiment, target information was exclusively available in the visual domain. Thus, there were no alternative sources of information to compensate for high target uncertainty, leading to the most prominent impairments.

We additionally observed differences in the way reaches were performed between MC and BC. MC reaches were composed by a large initial feedforward component, followed by smaller corrective sub-movements to enter the target area, if necessary. This entails that monkeys did not need to rely on sensory feedback to control the movement during the initial component, as this could be majorly based on internal predictions of the limb's state (Miall & Wolpert, 1996; Shadmehr et al., 2010). In contrast, BC reaches were predominantly feedback-based, as proper BC requires of continuous monitoring of visual feedback. Thus, the nature of movement (feedforward vs. feedback-based) was also different between MC and BC, which could have contributed for the differences in effects of visual feedback uncertainty. Numerous studies have demonstrated that movement control can be effectively modeled using a Kalman filter, which combines the internal prediction of the limb's state with sensory evidence (Izawa & Shadmehr, 2008; Kasuga et al., 2022; Saunders & Knill, 2004; Wolpert et al., 1995). Consequently, the shift in control policy between MC and BC may reflect a change in the Kalman gain, altering the degree to which the final state estimate relies on sensory input. Future studies could use a BCI paradigm incorporating controlled perturbations (Chase et al., 2012; Ferrea et al., 2024; Golub et al., 2018; Stavisky et al., 2017) to investigate how motor cortical activity reflects state estimation processes under uncertainty and varying access to sensory information.

Visual feedback and target uncertainty separate neural activity patterns, consistent with previous studies showing that neural dynamics evolve within distinct neural manifolds for various task parameters and contexts (Mante et al., 2013; Remington et al., 2018; Sun et al., 2022). This separation was present across all experimental conditions, including the feedback MC condition, even though feedback uncertainty during MC did not affect reach accuracy or reach goal encoding. It has been hypothesized that independent dimensions in neural space allow computations to occur without influencing ongoing movements (Ames et al., 2019; Elsayed et al., 2016; Kaufman et al., 2014). In our study, such dimensions could potentially integrate uncertainty information. However, we found that uncertainty affects behavioral movement variability when related to the target location or feedback under BC. Thus, while some of the baseline level uncertainty-related information might be encoded

along independent dimensions, additional neural variance associated with uncertainty also interacts with directional encoding, ultimately affecting behavioral outcome. Similar effects have been suggested for reward signals interacting with motor preparation, which can lead to poor performance when reward expectation is exceptionally high (Smoulder et al., 2024).

We found that the effect of target uncertainty evolves over the planning epoch, with decoding results showing impairment during early but not late planning. Studies that manipulated the uncertainty of target identity showed that population activity reflects two potential discrete and spatially separated targets until one of them is specified (Cisek & Kalaska, 2005; Coallier et al., 2015; Klaes et al., 2011; Suriya-Arunroj & Gail, 2019). This strategy has been linked to the decision-making process where two choices compete against each other (Cisek, 2007; Thura et al., 2022; Thura & Cisek, 2014). When target uncertainty instead is introduced by a spatially probabilistic broadening of a single target position, as in our study, previous findings showed widespread reach representations in PMd and reduced decoding performance, consistent with our results (Dekleva et al., 2016). This effect of uncertainty was present from early to late planning. In contrast, we found reduced decoding performances only during early planning. The differing time courses of uncertainty-induced reductions in neural motor goal specificity observed across studies may stem from variations in task design. While Dekleva et al., 2016 used an instructed-delay paradigm, we used a memory-guided task in which the visual target cue was presented only briefly. The memory-guided design likely encourages a quick decision to reduce the memory load from a broad stochastic distribution of target cues to a single selected target direction. Thus, in our study, monkeys might have made the final decision during the early planning stage, leading to well-represented but distinct neural states later.

Our results suggest that when spatial information—whether it pertains to current hand position or target location—is available solely through the visual domain, increased visual uncertainty leads to less precise motor goal representations in the monkey motor cortex. For target uncertainty, this is the case during movement planning and initiation, while for feedback uncertainty, only during movement initiation. This highlights that both target and effector location are necessary components for making a goal-directed movement. Frontoparietal reach areas encode motor goals in different spatial reference frames that combine effector and target positions, along with other potential parameters like gaze direction (Batista et al., 1999; Batista et al., 2007; Bremner & Andersen, 2012; Cisek & Kalaska, 2002; McGuire & Sabes, 2011; Pesaran et al., 2006). If motor goal representations were exclusively affected by target uncertainty, this would suggest an endpoint encoding scheme. On the other hand, if also feedback uncertainty affects these goal representations, this would argue in favor of reach vector encoding. Based on our findings, both encoding schemes could be implemented in a serial manner (Hudson & Landy, 2012; Thaler & Todd, 2009), aligning with findings of changing encoding schemes depending on task demands (Bremner & Andersen, 2014; Taghizadeh et al., 2024). During early planning, endpoint information is primarily used to

compute the motor plan. However, close to reach initiation, the current hand position is also used, likely continuing to influence representations throughout execution.

During BC, when additional proprioceptive inputs are not relevant for task performance, uncertainty had a detrimental effect on both behavioral performance and decoding accuracy of neural reach representations. From a translational perspective, our findings highlight how BCI users are particularly susceptible to visual feedback uncertainty. This underscores the crucial role of proprioceptive feedback in stabilizing motor goal representations by providing additional redundant information to compensate for unreliable visual inputs (Amann et al., 2024; Dadarlat et al., 2015; Risso et al., 2019; Suminski et al., 2010). Given that movements are often performed in environments with unreliable visual conditions, such as dim lighting or occlusions, our findings emphasize the need for developing bi-directional BCIs that provide additional somatosensory feedback (see Klaes et al., 2014 for review). Along this line, several studies have shown that bi-directional BCIs significantly enhance control under full vision (Flesher et al., 2016; Flesher et al., 2021; Suminski et al., 2010), which would likely extend to conditions of visual uncertainty.

In conclusion, we have shown that goal representations are less well-defined when the reach target is uncertain. This also happens when the visual feedback of the effector is uncertain, given that there is no proprioceptive information to compensate for it and the movement is conducted under feedback control. Therefore, our findings suggest that target and feedback uncertainty influence motor cortex activity depending on their behavioral relevance. Our study highlights the importance of considering conditions of uncertainty in the development of BCIs, given their negative impact on sensorimotor planning, especially under unimodal sensory feedback conditions.

Methods

Animals and implants

Two male rhesus macaques (*Macaca mulatta*, monkey Y: 16 years, monkey Z: 15 years) performed the experiments. Both monkeys had been implanted with a custom-fit titanium head post. Later, both monkeys were implanted with intracortical 32-channel floating microelectrode arrays (FMAs; 250 m spacing, impedance 0.1 to 0.4 MΩ; MicroProbes for Life-Science, Gaithersburg, Maryland, USA). Details on surgical procedures and implant design can be found in (Ahmed et al., 2022; Berger et al., 2020). In brief, craniotomy coordinates were calculated from pre-surgical MRI scans. Final array locations were based on subdural anatomical landmarks at the time of the surgery. The array connectors (Omnetics, Connector Corporation, Minneapolis, Minnesota, USA) were placed in a custom-designed array chamber (Ahmed et al., 2022) contralateral to the craniotomy. Monkey Y was implanted with six FMAs (M1: 2, PMd: 2, PRR: 2) in the left hemisphere seven years prior to the experiments. Monkey Z was implanted with eight FMAs (M1: 2, PMd: 3, PRR: 3) in the right hemisphere

one year prior to the experiments (Fig. 3a). Unit counts for the PRR arrays of both monkeys, as well as for the M1 arrays of monkey Z, were too low to extract meaningful conclusions and were consequently excluded from analysis. Arrays in M1 and PMd were targeted at distal arm regions. Electrode lengths of M1 arrays in monkey Y were staggered and ranged from 2.5-7.1 mm, with the longer electrodes on the side of the central sulcus. Electrode lengths of PMd arrays ranged from 2.9-4.5 mm in monkey Y and 2.3-3.8 mm in monkey Z.

Both animals were housed in social groups with one male conspecific in facilities of the German Primate Center. Cage sizes exceeded requirements by German and European regulations. Animals were provided with an enriched environment, including wooden structures, toys, and enrichment devices. All procedures and experiments were approved by the responsible regional government office (Niedersächsisches Landesamt für Verbraucherschutz und Lebensmittelsicherheit [LAVES]) under permit numbers 3392 42502-04-13/1100 and 33.19-42502-04-18/2823 and complied with German Law and the European Directive 2010/63/EU regulating the use of animals in research.

Apparatus

Monkeys sat in a primate chair placed in front of a screen (27-inch diagonal, 60 Hz refresh rate; XL2720T, BenQ, Taipei, Taiwan) at 75 cm eye-screen distance. A custom software (C++, OpenGL) was used for task control and kinematic hand and eye data recording (Morel et al., 2017). For manual-control tasks, monkeys used a haptic manipulandum constrained in a 2D vertical plane (2 kHz sampling rate, 2:3 screen:haptic scale; Delta.3, Force Dimension, Nyon, Switzerland) to perform reaching movements using the arm contralateral to the implantation site. BCI decoder calibration and velocity estimation (for details see below) was run in MATLAB 2015 (Mathworks Inc.) on a separate computer which communicated with the task controller computer through a virtual-reality peripheral network (Ferrea et al., 2022b). The head of the animals was fixed in position via the head post implant, while the animal was free to move the rest of its body. Gaze direction was tracked using a video-based eye tracker (1 kHz sampling rate; EyeLink 1000 plus, SR Research, Ottawa, Canada).

Behavioral tasks

Manual control (MC)

Monkeys performed a memory-guided center-out reach task in a 2D workspace using the haptic manipulandum. Each trial started with the monkey moving the hand visual feedback into a fixation point (gray circle, 10 mm radius) in the center of the workspace on the black screen. A red square (5 mm side) was displayed in the center of the fixation point to indicate that the animal had to maintain a fixed gaze at this location (20 mm tolerance radius, corresponding to 1.5° visual angle). The fixation point was surrounded by a well-visible dark gray ring (80 mm inner radius, 100 mm outer radius) within which targets appeared. This ring

remained visible throughout the trial. After holding the hand and eye fixation for 200 ms, a target (white, 20 mm arc, corresponding to 12.5° opening angle for the reach direction) was cued for 300 ms. When testing target uncertainty, there were 16 possible target directions (cardinal, oblique, and intermediate, all spaced 22.5°) for both monkeys. We chose a discrete set of target directions to ensure a sufficient number of trials for later analyses, while maintaining spatial proximity between them to cover the whole circular space. Reach errors were not clustered around specific directions but showed continuous distributions in both monkeys when target uncertainty was high (data not shown), suggesting that the monkeys did not reach to overtrained target locations. When testing feedback uncertainty, monkey Z also had 16 possible targets, while monkey Y had eight possible targets (cardinal and oblique, spaced 45°). Following target disappearance, a variable memory period of 400-1200 ms started, in which monkeys had to hold the hand and eye position within the fixation point. Having a delay period in which the target was not visible allowed us to remove influences of immediate processing of the visual stimulus on neural activity. After this, both fixation points disappeared and a go cue sound was played, signaling the animal to initiate the movement. The monkeys had 2000 ms to reach to the target and had to hold it for 200 ms. Upon success, they received a liquid reward and a reward sound was played. If they failed at any stage of the trial, an error tone was played and a new trial started after a timeout of 1000 ms.

Two types of visual uncertainty were modulated on separate sessions: target and feedback uncertainty. For each of these types, two levels of uncertainty (low and high) were tested within a session by interleaving them pseudo-randomly from trial to trial in order to get approximately equal number of trials for each target and uncertainty condition.

Target uncertainty was varied by either presenting the true target consisting of the 20mm arc described above (low uncertainty), or showing an array of five bars (white, each 2 mm arc) distributed randomly along the ring (high uncertainty), similar to (Amann et al., 2024; Dekleva et al., 2016). The position along the ring of each bar was drawn from a 1D Gaussian distribution with a standard deviation of 25° centered on the true target direction. In this manner, target uncertainty was only visually present during the target cue epoch. Hand movements in the target uncertainty task were represented by a cursor consisting of a small single dot (yellow, 1.5 mm radius), keeping feedback uncertainty negligibly small.

Feedback uncertainty of the hand position was experimentally varied by having monkeys control the same cursor as in the target uncertainty task (low uncertainty) or a cloud of five individually moving dots (high uncertainty) (Casasnovas et al., 2024). The cursor and cloud dots had the same dimensions (yellow, 1.5 mm radius). The initial position of each cloud dot was drawn from a 2D Gaussian distribution with a standard deviation of 20 mm centered at the true hand position, which the monkeys controlled. Additionally, each dot was assigned a random velocity direction (fixed speed of 30 mm/s) and had a limited lifetime of 300 ms, after which it reappeared at another location drawn from the 2D distribution. Feedback uncertainty was present throughout the trial, as the cursor or cloud was set at the start of

each trial. In feedback uncertainty sessions, while only one target position was cued in each trial, the array of all potential target positions within the ring was continuously shown as reference to minimize target uncertainty. Otherwise, the target in the feedback uncertainty task was the same as the low-uncertainty target in the target uncertainty task.

Brain control (BC)

To avoid reliance on proprioceptive feedback for estimating hand position, particularly during trials with high visual feedback uncertainty, we also conducted a version of the center-out reach task in which animals controlled the cursor/cloud not manually, but via a brain-computer interface (BCI). Monkeys followed an equivalent trial structure in the BC and MC tasks. The initial hold period was set to 500 ms, the variable memory period to 400-1000 ms, and the monkey had 3000 ms to reach the target area. This target area was a circle (15 mm radius) centered on the visual target. The target ring was slightly larger than in MC (110 mm inner radius, 130 mm outer radius), and there were eight potential target directions (cardinal and oblique, spaced 45°) for both monkeys. The visual feedback was clamped at the fixation point until the go cue, upon which the monkey started to control it. The trial was rewarded as successful and finished as soon as the cursor or cloud center entered the target area. The arm contralateral to the implantation hemisphere was additionally lightly restrained for monkey Z, while monkey Y was required to hold the haptic manipulandum handle without attempting to move it. To ensure this, the haptic manipulandum position was fixed, which allowed us to measure any isometric forces applied to the handle. As soon as these forces exceeded a threshold (force at the start of the trial ± 0.4N), the trial was aborted.

Spike counts from M1 and PMd (monkey Y) or only PMd (monkey Z) were used as input to the BCI decoder (for details see below). For better neural yield, we did not treat areas PMd and M1 separately in monkey Y. At the start of each session, we performed online manual PCA-based spike sorting (Blackrock Central Software Suite, Blackrock Microsystems LLC) to detect multi- and single-units. All identified units were used as input to the decoder, ranging from 40-60 units for monkey Y and 46-54 units for monkey Z across sessions. Time-continuous decoding (50 ms update interval) for BC was achieved with a velocity-based Kalman filter calibrated using the recalibrated feedback-intention (ReFIT) protocol (Gilja et al., 2012). To mimic sensorimotor transduction delays, a 50 ms time lag between the input neural activity and the output cursor velocity was introduced. At the start of each session, a new decoder was calibrated using a two-step procedure. First, monkeys passively observed "cursor reaches" for 80 trials (ten trials per target direction), with which an initial decoder was calibrated. In these trials, the cursor was moved at a constant speed of 120 mm/s following a straight trajectory from the center of the fixation point to the target. Second, monkeys performed closed-loop brain-controlled reaches in which they had to move the cursor via the decoder with increasing levels of control. "Control" refers to the fraction of the velocity vector that comes from the neural activity with respect to an ideal velocity vector that would

direct the cursor towards the target. The level of control was manually increased throughout a block of 80 trials and the decoder was recalibrated before each increase, including the newly performed trials. As final step of the calibration procedure, the monkey performed 40 trials with 100% control and the decoder was calibrated one more time.

Since the motivation for testing BC was to increase the monkey's reliance on visual feedback, we only tested the feedback uncertainty type. The properties of the low and high feedback uncertainty stimuli remained the same as in MC. Different to MC, in BC we employed a block design in which the uncertainty level was switched every 48 trials (six trials per target) to reduce task difficulty.

Neural recordings and preprocessing

We recorded neural activity using 32-channel digital CerePlex M Blackrock head stages (Blackrock Microsystems LLC, Salt Lake City, USA) with a sampling rate of 30 kHz per channel. The digitalized signal was sent to the Cerebus Neural Processor (Blackrock Microsystems LLC, Salt Lake City, USA). We recorded the raw and high-pass filtered signals (250 Hz Butterworth filter 4th order) with a threshold of -4.5 x RMS. After the experiments, stored spike waveforms were manually sorted offline (Offline Sorter v4, Plexon Inc.) to identify putative neurons for analysis. We considered single- and multi-unit activity. We excluded a unit if its trial-averaged firing rate was lower than 2 Hz for all target directions. This offline sorting procedure was more conservative than the one used for online sorting during the BC sessions, leading to slightly different unit counts for the analyses. Considering all sessions, the range of identified units was 24-51 (M1 monkey Y), 10-32 (PMd monkey Y), and 32-54 (PMd monkey Z). Given the low amount of units detected in PMd of monkey Y, we combined units from PMd and M1 for this monkey. As preprocessing, we computed smoothed spike densities by convolving the spike counts with a Gaussian kernel with 50 ms standard deviation. Spike densities were resampled to 200 Hz, which we used for subsequent neural analyses.

Data inclusion criteria

Behavioral analyses were done in MATLAB R2021b (Mathworks Inc.). The same applied to neural data preprocessing and analyses, except within-level decoding, which was performed in Python (version 3.7.7). All plots were generated using GRAMM visualization toolbox for MATLAB (Morel, 2018). In total, we analyzed eight sessions per monkey testing MC target uncertainty, and ten sessions per monkey testing feedback uncertainty in each MC and BC. In MC sessions with 16 targets, we only analyzed eight target directions (cardinal and oblique, spaced 45°) to be comparable to BC sessions. Including all 16 directions in our analysis did not change our conclusions (data not shown). Moreover, we only analyzed valid reaches of MC sessions, defined as having crossed the target ring eccentricity, regardless of whether the target was hit. We only analyzed successful trials of BC sessions to make sure the monkey was fully engaged in the task.

Behavioral measures

Success rates for MC sessions were calculated as the percentage of trials in which the monkey hit the target over all valid trials, whereas for BC sessions the percentage was computed over all trials in which the monkey initiated its reach. In the main text we report the average success rate across sessions for each monkey and uncertainty level. Behavioral movement trajectories were aligned to the go cue for across-trial analyses. The early reach error was computed by determining the absolute angular difference between the cued target direction and the vector pointing from the initial hand position to the hand position after reaching 25% of the target eccentricity. Thereby, we ensured that the early reach direction reflected the planned movement direction since visual feedback about the movement could not have been processed, and, therefore, no corrections were made. The late reach error was calculated similarly, but taking the hand position when it reached 75% of the target eccentricity. Reach speed traces in time were aligned to go cue, as was the distance from the center. The distance from the center was scaled by the target eccentricity. Traces were first averaged across trials, regardless of their length, and then across sessions. Therefore, the visualized error measures only capture variability across sessions. Reaction time measures the time from go cue to movement onset and movement time refers to the time from movement onset to target acquisition. Movement onset was defined as the time after go cue when the hand crossed a speed threshold of 0.05 mm/ms in MC, or when the brain-controlled cursor (or cloud) left the fixation point area in BC. We note that in BC, the measured reaction time is an estimate, due to the low sampling rate of behavioral trajectories and potentially different strategies for movement initiation. For example, the monkey could already be trying to move towards the target during the memory period when the cursor is clamped at the fixpoint. To test for behavioral differences between uncertainty levels for each uncertainty type and monkey, we used paired t-tests with a significance threshold of $=0.05$. This means that the average measures from the low and from the high uncertainty levels, respectively, were paired for each session.

Reach direction tuning

We used linear regression to find if the activity of each neuron was significantly modulated by target direction (tuned) for the early planning, late planning and movement initiation epochs. We only considered activity from low uncertainty trials, as they provide the baseline condition for each neuron. First, we time-averaged spike densities from each epoch (early planning: -50–150 ms from target offset; late planning: -150–50 ms from go cue; movement initiation: -50–150 ms from movement onset). Then, we regressed the spike densities to the target position (x and y coordinates), pooling across low uncertainty trials from a session. If any of the target position coefficients were significantly different from zero ('coefTest' function), we considered the unit as tuned. We then computed the percentage of tuned units from the

recorded population of each session. We report the average percentage of tuned units across sessions and uncertainty types for each monkey and time epoch.

SVM decoding

We trained linear support vector machine (SVM) classifiers for decoding reach direction using the 'Scikit-learn' package for Python (version 3.7.7). Spike densities within a moving 100 ms time window (50 ms shift) were used to classify the executed reach direction in each trial, separately for each time window, for time-continuous analysis. Reach direction was computed using the hand position at the ring eccentricity. Moreover, we grouped reach directions into eight 45° bins, each centered around a target direction. Spike densities were z-scored before being used as input to the decoder. Decoders were independently trained and tested for each time window, uncertainty level and session (within-level decoding). We performed 5-fold cross-validation by randomly grouping trials of one session into five groups, matching the number of trials per uncertainty level and reach direction. Each of these groups was then used once as testing set while the remaining four were used to train the decoder. The number of trials used for the decoding analyses depended on the minimum number of repetitions per reach direction. On average, across monkeys and task conditions, each fold included 105 ± 6 (mean ± std) training trials and 26 ± 3 testing trials. For each session we then averaged the decoding performance across the five folds. In Fig. 4c-e we plotted the average of these average within-session performances across all sessions, pooling both monkeys, separately for each uncertainty level. To test for significant differences in decoding performance between uncertainty levels over the time course of the trial, we used a cluster-based permutation test with N=1000 (Maris & Oostenveld, 2007) and a significance threshold of =0.05.

Cross-level decoding was performed in MATLAB R2021b (Mathworks Inc.). We trained error-correcting output codes (ECOC) models with eight binary linear SVMs ('fitcecoc' function) on trials with low uncertainty. As training input, we used z-scored spike densities from three 200 ms epochs: early planning: -50–150 ms from target offset; late planning: -150–50 ms from go cue; movement initiation: -50–150 ms from movement onset. We assessed decoding (=classification) performance using 5-fold cross-validation ('crossval' function). We then selected five random test sets of trials with high uncertainty from the same session and used these as input to the classifier to determine the cross-level decoding performance. The performance loss was calculated by subtracting the performance of the classifiers based on low uncertainty trials from the performance achieved when using high uncertainty trials as test sets. To test if these differences were significantly lower than zero, we used one-tailed one-sample t-tests with a significance threshold of =0.05, pooling differences across monkeys for the main results (Fig. 4f-h).

dPCA for task-related dimensions

We used dPCA (Kobak et al., 2016), a dimensionality reduction method, to evaluate the dependency of the neural activity on the uncertainty level. dPCA finds dimensions that best capture variance in neural activity related to chosen behavioral task parameters. We used the openly available dPCA toolbox (https://github.com/machenslab/dPCA) to compute such dimensions for each session. To evaluate how uncertainty-related activity progressed over time, we analyzed concatenated spike densities aligned to target cue onset (-100–600 ms), go cue (-200–600 ms) and movement onset (-200–400 ms). We first soft-normalized spike densities by dividing each unit by its range across all times and trials plus a constant (2 Hz) to prevent division by zero (s/(max(s)-min(s)+2), where s is the spike density). We then centered each unit by subtracting the mean across all trials for each timepoint, removing any common time-related fluctuations across conditions (Elsayed et al., 2016). Finally, we trial-averaged the spike densities for each condition and concatenated them to form a (number of units x time points x target directions x uncertainty levels) input matrix. We set the dimensionality of the dPCA output space to m=20, and included target direction, uncertainty level, and their interaction as task parameters. The high dimensionality of the output space was needed to ensure finding at least one uncertainty dPC.

The variance explained for each task parameter was calculated by the sum of the variances of all components assigned to that parameter, divided by the total variance in the data We report the average variance captured across sessions for each monkey for the uncertainty and interaction parameters in the main text. We projected the spike densities to the first dPC that explained most of the data variance related to uncertainty level (Supplementary Fig. S3b). We time-averaged the projections over shorter epochs (baseline: -200–0 ms from target onset; early planning: -50–150 ms from target offset; late planning: -150–50 ms from go cue; movement initiation: -50–150 ms from movement onset) for Fig. 5b to match the time windows used for the decoding analyses. For statistical testing, we computed the difference between uncertainty levels for each time epoch. We provided this difference as input to a repeated measures ANOVA with time as the main effect. We considered the intercept as measure of a difference between uncertainty levels. The significance threshold was $=0.05$. Similarly, we also projected the spike densities onto the first two dPCs that explained most of the target-related variance and averaged the projections in time for the movement initiation epoch. In Fig 5a, we plotted trial-averaged projections onto the space formed by the two target dPCs and the uncertainty dPC for the movement initiation time epoch for three example sessions of monkey Y. Note that we did not orthogonalize the three axes.

Data availability

Data for reproducing figures and statistics is publicly available at https://doi.org/10.25625/KVGHV2 (GRO.data repository). Additional data is available from the corresponding author

upon reasonable request.

Code availability

Code for reproducing figures and statistics is publicly available at https://doi.org/10.25625/KVGHV2 (GRO.data repository).

References

Aflalo, T., Kellis, S., Klaes, C., Lee, B., Shi, Y., Pejsa, K., Shanfield, K., Hayes-Jackson, S., Aisen, M., Heck, C., Liu, C., & Andersen, R. A. (2015). Decoding motor imagery from the posterior parietal cortex of a tetraplegic human. *Science*, *348*(6237), 906–910.

Ahmed, Z., Agha, N., Trunk, A., Berger, M., & Gail, A. (2022). Universal guide for skull extraction and custom-fitting of implants to continuous and discontinuous skulls. *eNeuro*, *9*(3).

Ajiboye, A. B., Willett, F. R., Young, D. R., Memberg, W. D., Murphy, B. A., Miller, J. P., Walter, B. L., Sweet, J. A., Hoyen, H. A., Keith, M. W., Peckham, P. H., Simeral, J. D., Donoghue, J. P., Hochberg, L. R., & Kirsch, R. F. (2017). Restoration of reaching and grasping movements through brain-controlled muscle stimulation in a person with tetraplegia: A proof-of-concept demonstration. *The Lancet*, *389*(10081), 1821–1830.

Alais, D., & Burr, D. (2004). The ventriloquist effect results from near-optimal bimodal integration. *Current biology: CB*, *14*(3), 257–262.

Amann, L. K., Casasnovas, V., Hainke, J., & Gail, A. (2024). Optimality of multisensory integration while compensating for uncertain visual target information with artificial vibrotactile cues during reach planning. *Journal of NeuroEngineering and Rehabilitation*, *21*(1), 155.

Ames, K. C., Ryu, S. I., & Shenoy, K. V. (2019). Simultaneous motor preparation and execution in a last-moment reach correction task. *Nature Communications*, *10*(1), 2718.

Angelaki, D. E., Gu, Y., & DeAngelis, G. C. (2009). Multisensory integration: Psychophysics, neurophysiology, and computation. *Current Opinion in Neurobiology*, *19*(4), 452–458.

Batista, A. P., Buneo, C. A., Snyder, L. H., & Andersen, R. A. (1999). Reach plans in eye-centered coordinates. *Science*, *285*(5425), 257–260.

Batista, A. P., Santhanam, G., Yu, B. M., Ryu, S. I., Afshar, A., & Shenoy, K. V. (2007). Reference frames for reach planning in macaque dorsal premotor cortex. *Journal of Neurophysiology*, *98*(2), 966–983.

Bayramova, R., Valori, I., McKenna-Plumley, P. E., Callegher, C. Z., & Farroni, T. (2021). The role of vision and proprioception in self-motion encoding: An immersive virtual reality study. *Attention, Perception, & Psychophysics*, *83*(7), 2865–2878.

Bays, P. M., & Wolpert, D. M. (2007). Computational principles of sensorimotor control that minimize uncertainty and variability. *The Journal of Physiology*, *578*(2), 387–396.

Berger, M., Agha, N. S., & Gail, A. (2020). Wireless recording from unrestrained monkeys reveals motor goal encoding beyond immediate reach in frontoparietal cortex (J. I. Gold, B. Pesaran, & S. R. Santacruz, Eds.). *eLife*, *9*, e51322.

Bouton, C. E., Shaikhouni, A., Annetta, N. V., Bockbrader, M. A., Friedenberg, D. A., Nielson, D. M., Sharma, G., Sederberg, P. B., Glenn, B. C., Mysiw, W. J., Morgan, A. G., Deogaonkar, M., & Rezai, A. R. (2016). Restoring cortical control of functional movement in a human with quadriplegia. *Nature*, *533*(7602), 247–250.

Braun, J.-M., Fauth, M., Berger, M., Huang, N.-S., Simeoni, E., Gaeta, E., Rodrigues do Carmo, R., García-Betances, R. I., Arredondo Waldmeyer, M. T., Gail, A., Larsen, J. C., Manoonpong, P., Tetzlaff, C., & Wörgötter, F. (2024). A brain machine interface framework for exploring proactive control of smart environments. *Scientific Reports*, *14*(1), 11054.

Bremner, L. R., & Andersen, R. A. (2012). Coding of the reach vector in parietal area 5d. *Neuron*, *75*(2), 342–351.

Bremner, L. R., & Andersen, R. A. (2014). Temporal analysis of reference frames in parietal cortex area 5d during reach planning. *Journal of Neuroscience*, *34*(15), 5273–5284.

Burge, J., Ernst, M. O., & Banks, M. S. (2008). The statistical determinants of adaptation rate in human reaching. *Journal of Vision*, *8*(4), 20–20.

Caminiti, R., Johnson, P. B., Galli, C., Ferraina, S., & Burnod, Y. (1991). Making arm movements within different parts of space: The premotor and motor cortical representation of a coordinate system for reaching to visual targets. *Journal of Neuroscience*, *11*(5), 1182–1197.

Caminiti, R., Johnson, P. B., & Urbano, A. (1990). Making arm movements within different parts of space: Dynamic aspects in the primate motor cortex. *The Journal of Neuroscience: The Official Journal of the Society for Neuroscience*, *10*(7), 2039–2058.

Casasnovas, V., Amann, L. K., Haas, G. L., & Gail, A. (2024). Task-relevant visual feedback uncertainty attenuates visuomotor adaptation. *Journal of Neurophysiology*, *132*(3), 879–889.

Chase, S. M., Kass, R. E., & Schwartz, A. B. (2012). Behavioral and neural correlates of visuomotor adaptation observed through a brain-computer interface in primary motor cortex. *Journal of Neurophysiology*, *108*(2), 624–644.

Churchland, M. M., Cunningham, J. P., Kaufman, M. T., Ryu, S. I., & Shenoy, K. V. (2010). Cortical preparatory activity: Representation of movement or first cog in a dynamical machine? *Neuron*, *68*(3), 387–400.

Cisek, P. (2007). Cortical mechanisms of action selection: The affordance competition hypothesis. *Philosophical Transactions of the Royal Society B: Biological Sciences*, *362*(1485), 1585–1599.

Cisek, P., & Kalaska, J. F. (2002). Modest gaze-related discharge modulation in monkey dorsal premotor cortex during a reaching task performed with free fixation. *Journal of Neurophysiology*, *88*(2), 1064–1072.

Cisek, P., & Kalaska, J. F. (2005). Neural correlates of reaching decisions in dorsal premotor cortex: Specification of multiple direction choices and final selection of action. *Neuron*, *45*(5), 801–814.

Coallier, Michelet, T., & Kalaska, J. F. (2015). Dorsal premotor cortex: Neural correlates of reach target decisions based on a color-location matching rule and conflicting sensory evidence. *Journal of Neurophysiology*, *113*(10), 3543–3573.

Collinger, J. L., Wodlinger, B., Downey, J. E., Wang, W., Tyler-Kabara, E. C., Weber, D. J., McMorland, A. J., Velliste, M., Boninger, M. L., & Schwartz, A. B. (2013). High-performance neuroprosthetic control by an individual with tetraplegia. *The Lancet*, *381*(9866), 557–564.

Crammond, D. J., & Kalaska, J. F. (2000). Prior information in motor and premotor cortex: Activity during the delay period and effect on pre-movement activity. *Journal of Neurophysiology*, *84*(2), 986–1005.

Crevecoeur, F., Munoz, D. P., & Scott, S. H. (2016). Dynamic multisensory integration: Somatosensory speed trumps visual accuracy during feedback control. *Journal of Neuroscience*, *36*(33), 8598–8611.

Cross, K. P., Cook, D. J., & Scott, S. H. (2024). Rapid online corrections for proprioceptive and visual perturbations recruit similar circuits in primary motor cortex. *eNeuro*, *11*(2).

Dadarlat, M. C., O'Doherty, J. E., & Sabes, P. N. (2015). A learning-based approach to artificial sensory feedback leads to optimal integration. *Nature Neuroscience*, *18*(1), 138–144.

Dekleva, B. M., Ramkumar, P., Wanda, P. A., Kording, K. P., & Miller, L. E. (2016). Uncertainty leads to persistent effects on reach representations in dorsal premotor cortex (M. J. Frank, Ed.). *eLife*, *5*, e14316.

Elsayed, G. F., Lara, A. H., Kaufman, M. T., Churchland, M. M., & Cunningham, J. P. (2016). Reorganization between preparatory and movement population responses in motor cortex. *Nature Communications*, *7*(1), 13239.

Ernst, M. O., & Banks, M. S. (2002). Humans integrate visual and haptic information in a statistically optimal fashion. *Nature*, *415*(6870), 429–433.

Faisal, A. A., Selen, L. P. J., & Wolpert, D. M. (2008). Noise in the nervous system. *Nature Reviews Neuroscience*, *9*(4), 292–303.

Ferrea, E., Franke, J., Morel, P., & Gail, A. (2022a). Statistical determinants of visuomotor adaptation along different dimensions during naturalistic 3d reaches. *Scientific Reports*, *12*(1), 10198.

Ferrea, E., Morel, P., & Gail, A. (2022b). BCImat: A matlab-based framework for intracortical brain-computer interfaces and their simulation with an artificial spiking neural network. *Journal of Open Source Software*, *7*(75), 3956.

Ferrea, E., Morel, P., & Gail, A. (2024). Planning and movement activities co-adapt in a motor-reference frame during 3d BCI-controlled reach adaptation in monkey frontal and parietal cortices (preprint). *bioRxiv*, 621745.

Flesher, S. N., Collinger, J. L., Foldes, S. T., Weiss, J. M., Downey, J. E., Tyler-Kabara, E. C., Bensmaia, S. J., Schwartz, A. B., Boninger, M. L., & Gaunt, R. A. (2016). Intracortical microstimulation of human somatosensory cortex. *Science Translational Medicine*, *8*(361), 361ra141–361ra141.

Flesher, S. N., Downey, J. E., Weiss, J. M., Hughes, C. L., Herrera, A. J., Tyler-Kabara, E. C., Boninger, M. L., Collinger, J. L., & Gaunt, R. A. (2021). A brain-computer interface that evokes tactile sensations improves robotic arm control. *Science*, *372*(6544), 831–836.

Gamberini, M., Dal Bò, G., Breveglieri, R., Briganti, S., Passarelli, L., Fattori, P., & Galletti, C. (2018). Sensory properties of the caudal aspect of the macaque's superior parietal lobule. *Brain Structure and Function*, *223*(4), 1863–1879.

Ganguly, K., & Carmena, J. M. (2009). Emergence of a stable cortical map for neuroprosthetic control. *PLOS Biology*, *7*(7), e1000153.

Gilja, V., Nuyujukian, P., Chestek, C. A., Cunningham, J. P., Yu, B. M., Fan, J. M., Churchland, M. M., Kaufman, M. T., Kao, J. C., Ryu, S. I., & Shenoy, K. V. (2012). A high-performance neural prosthesis enabled by control algorithm design. *Nature Neuroscience*, *15*(12), 1752–1757.

Golub, M. D., Chase, S. M., Batista, A. P., & Yu, B. M. (2016). Brain-computer interfaces for dissecting cognitive processes underlying sensorimotor control. *Current Opinion in Neurobiology*, *37*, 53–58.

Golub, M. D., Sadtler, P. T., Oby, E. R., Quick, K. M., Ryu, S. I., Tyler-Kabara, E. C., Batista, A. P., Chase, S. M., & Yu, B. M. (2018). Learning by neural reassociation. *Nature Neuroscience*, *21*(4), 607–616.

Hatsopoulos, N. G., Xu, Q., & Amit, Y. (2007). Encoding of movement fragments in the motor cortex. *Journal of Neuroscience*, *27*(19), 5105–5114.

Hochberg, L. R., Serruya, M. D., Friehs, G. M., Mukand, J. A., Saleh, M., Caplan, A. H., Branner, A., Chen, D., Penn, R. D., & Donoghue, J. P. (2006). Neuronal ensemble control of prosthetic devices by a human with tetraplegia. *Nature*, *442*(7099), 164–171.

Hoffmann, A. H., & Crevecoeur, F. (2024). Dissociable effects of urgency and evidence accumulation during reaching revealed by dynamic multisensory integration. *eNeuro*, *11*(12).

Hudson, T. E., & Landy, M. S. (2012). Motor learning reveals the existence of multiple codes for movement planning. *Journal of Neurophysiology*, *108*(10), 2708–2716.

Izawa, J., & Shadmehr, R. (2008). On-line processing of uncertain information in visuomotor control. *Journal of Neuroscience*, *28*(44), 11360–11368.

Kasuga, S., Crevecoeur, F., Cross, K. P., Balalaie, P., & Scott, S. H. (2022). Integration of proprioceptive and visual feedback during online control of reaching. *Journal of Neurophysiology*, *127*(2), 354–372.

Kaufman, M. T., Churchland, M. M., Ryu, S. I., & Shenoy, K. V. (2014). Cortical activity in the null space: Permitting preparation without movement. *Nature Neuroscience*, *17*(3), 440–448.

Kim, H. E., Avraham, G., & Ivry, R. B. (2021). The psychology of reaching: Action selection, movement implementation, and sensorimotor learning. *Annual Review of Psychology*, *72*(1), 61–95.

Klaes, C., Shi, Y., Kellis, S., Minxha, J., Revechkis, B., & Andersen, R. A. (2014). A cognitive neuroprosthetic that uses cortical stimulation for somatosensory feedback. *Journal of Neural Engineering*, *11*(5), 056024.

Klaes, C., Westendorff, S., Chakrabarti, S., & Gail, A. (2011). Choosing goals, not rules: Deciding among rule-based action plans. *Neuron*, *70*(3), 536–548.

Kobak, D., Brendel, W., Constantinidis, C., Feierstein, C. E., Kepecs, A., Mainen, Z. F., Qi, X.-L., Romo, R., Uchida, N., & Machens, C. K. (2016). Demixed principal component analysis of neural population data (M. C. van Rossum, Ed.). *eLife*, *5*, e10989.

Körding, K. P., & Wolpert, D. M. (2004). Bayesian integration in sensorimotor learning. *Nature*, *427*(6971), 244–247.

Mante, V., Sussillo, D., Shenoy, K. V., & Newsome, W. T. (2013). Context-dependent computation by recurrent dynamics in prefrontal cortex. *Nature*, *503*(7474), 78–84.

Maris, E., & Oostenveld, R. (2007). Nonparametric statistical testing of EEG- and MEG-data. *Journal of Neuroscience Methods*, *164*(1), 177–190.

McGuire, L. M. M., & Sabes, P. N. (2011). Heterogeneous representations in the superior parietal lobule are common across reaches to visual and proprioceptive targets. *Journal of Neuroscience*, *31*(18), 6661–6673.

Miall, R. C., & Wolpert, D. M. (1996). Forward models for physiological motor control. *Neural Networks*, *9*(8), 1265–1279.

Morel, P. (2018). Gramm: Grammar of graphics plotting in matlab. *Journal of Open Source Software*, *3*(23), 568.

Morel, P., Ulbrich, P., & Gail, A. (2017). What makes a reach movement effortful? physical effort discounting supports common minimization principles in decision making and motor control. *PLOS Biology*, *15*(6), e2001323.

Moscatelli, A., Bianchi, M., Ciotti, S., Bettelani, G. C., Parise, C. V., Lacquaniti, F., & Bicchi, A. (2019). Touch as an auxiliary proprioceptive cue for movement control. *Science Advances*, *5*(6), eaaw3121.

Mulliken, G. H., Musallam, S., & Andersen, R. A. (2008). Forward estimation of movement state in posterior parietal cortex. *Proceedings of the National Academy of Sciences*, *105*(24), 8170–8177.

Pesaran, B., Nelson, M. J., & Andersen, R. A. (2006). Dorsal premotor neurons encode the relative position of the hand, eye, and goal during reach planning. *Neuron*, *51*(1), 125–134.

Pruszynski, J. A., Omrani, M., & Scott, S. H. (2014). Goal-dependent modulation of fast feedback responses in primary motor cortex. *Journal of Neuroscience*, *34*(13), 4608–4617.

Remington, E. D., Narain, D., Hosseini, E. A., & Jazayeri, M. (2018). Flexible sensorimotor computations through rapid reconfiguration of cortical dynamics. *Neuron*, *98*(5), 1005–1019.e5.

Riehle, A., & Requin, J. (1989). Monkey primary motor and premotor cortex: Single-cell activity related to prior information about direction and extent of an intended movement. *Journal of Neurophysiology*, *61*(3), 534–549.

Risso, G., Valle, G., Iberite, F., Strauss, I., Stieglitz, T., Controzzi, M., Clemente, F., Granata, G., Rossini, P. M., Micera, S., & Baud-Bovy, G. (2019). Optimal integration of intraneural somatosensory feedback with visual information: A single-case study. *Scientific Reports*, *9*(1), 7916.

Sabatini, D. A., & Kaufman, M. T. (2024). Reach-dependent reorientation of rotational dynamics in motor cortex. *Nature Communications*, *15*(1), 7007.

Saunders, J. A., & Knill, D. C. (2004). Visual feedback control of hand movements. *Journal of Neuroscience*, *24*(13), 3223–3234.

Shadmehr, R., Smith, M. A., & Krakauer, J. W. (2010). Error correction, sensory prediction, and adaptation in motor control. *Annual Review of Neuroscience*, *33*(1), 89–108.

Smoulder, A. L., Marino, P. J., Oby, E. R., Snyder, S. E., Miyata, H., Pavlovsky, N. P., Bishop, W. E., Yu, B. M., Chase, S. M., & Batista, A. P. (2024). A neural basis of choking under pressure. *Neuron*, S0896627324006081.

Sober, S. J., & Sabes, P. N. (2003). Multisensory integration during motor planning. *Journal of Neuroscience*, *23*(18), 6982–6992.

Stavisky, S. D., Kao, J. C., Ryu, S. I., & Shenoy, K. V. (2017). Motor cortical visuomotor feedback activity is initially isolated from downstream targets in output-null neural state space dimensions. *Neuron*, *95*(1), 195–208.e9.

Suminski, A. J., Tkach, D. C., Fagg, A. H., & Hatsopoulos, N. G. (2010). Incorporating feedback from multiple sensory modalities enhances brain-machine interface control. *Journal of Neuroscience*, *30*(50), 16777–16787.

Sun, X., O'Shea, D. J., Golub, M. D., Trautmann, E. M., Vyas, S., Ryu, S. I., & Shenoy, K. V. (2022). Cortical preparatory activity indexes learned motor memories. *Nature*, *602*(7896), 274–279.

Suriya-Arunroj, L., & Gail, A. (2019). Complementary encoding of priors in monkey frontoparietal network supports a dual process of decision-making (E. Vaadia & R. B. Ivry, Eds.). *eLife*, *8*, e47581.

Suway, S. B., & Schwartz, A. B. (2019). Activity in primary motor cortex related to visual feedback. *Cell Reports*, *29*(12), 3872–3884.e4.

Taghizadeh, B., Fortmann, O., & Gail, A. (2024). Position- and scale-invariant object-centered spatial localization in monkey frontoparietal cortex dynamically adapts to cognitive demand. *Nature Communications*, *15*(1), 3357.

Thaler, L., & Todd, J. T. (2009). The control parameters used by the CNS to guide the hand depend on the visuo-motor task: Evidence from visually guided pointing. *Neuroscience*, *159*(2), 578–598.

Thura, D., Cabana, J.-F., Feghaly, A., & Cisek, P. (2022). Integrated neural dynamics of sensorimotor decisions and actions. *PLOS Biology*, *20*(12), e3001861.

Thura, D., & Cisek, P. (2014). Deliberation and commitment in the premotor and primary motor cortex during dynamic decision making. *Neuron*, *81*(6), 1401–1416.

Tsay, J. S., Avraham, G., Kim, H. E., Parvin, D. E., Wang, Z., & Ivry, R. B. (2021). The effect of visual uncertainty on implicit motor adaptation. *Journal of Neurophysiology*, *125*(1), 12–22.

van Beers, R. J., Wolpert, D. M., & Haggard, P. (2002). When feeling is more important than seeing in sensorimotor adaptation. *Current Biology*, *12*(10), 834–837.

Velliste, M., Perel, S., Spalding, M. C., Whitford, A. S., & Schwartz, A. B. (2008). Cortical control of a prosthetic arm for self-feeding. *Nature*, *453*(7198), 1098–1101.

Willett, F. R., Avansino, D. T., Hochberg, L. R., Henderson, J. M., & Shenoy, K. V. (2021). High-performance brain-to-text communication via handwriting. *Nature*, *593*(7858), 249–254.

Wolpert, D. M., Ghahramani, Z., & Jordan, M. I. (1995). An internal model for sensorimotor integration. *Science*, *269*(5232), 1880–1882.

Wong, A. L., Haith, A. M., & Krakauer, J. W. (2015). Motor planning. *The Neuroscientist*, *21*(4), 385–398.

Zhang, Z., Wang, H., Zhang, T., Nie, Z., & Wei, K. (2024). Perceptual error based on bayesian cue combination drives implicit motor adaptation. *eLife*, *13*.

Acknowledgments

We thank Enrico Ferrea for his help during early study conceptualization and BCI implementation. The authors also thank Sina Plümer for her support with animal training and handling. Support was provided by the European Commission in the context of the Plan4Act consortium (H2020-FETPROACT-16 732266 WP1), the State of Lower Saxony in the context of the DeMoDiag consortium (ZN3422) and the German Research Foundation in the context of the Collaborative Research Center "Cellular mechanisms of sensory processing" (DFG SFB-889 C4) and “Disease Mechanisms and Functional Restoration of Sensory and Motor Systems” (DFG SFB-1690 B09).

Author contributions

L.K.A., V.C., and A.G. conceptualized and designed the study. L.K.A. and V.C. performed experiments and analyzed the data. L.K.A., V.C., and A.G. interpreted the data. L.K.A. and V.C. drafted the manuscript. L.K.A., V.C., and A.G. edited and revised the manuscript.

Competing interests

The authors declare that they have no competing interests concerning the research, authorship, and/or publication of this article.

Additional information

Correspondence and requests for materials should be addressed to Alexander Gail.

Supplementary material

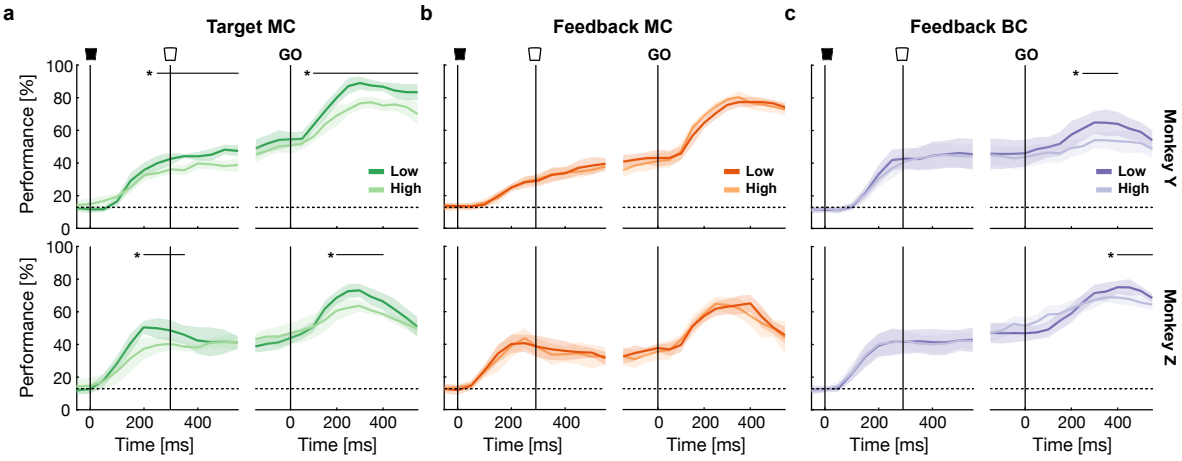

FIGURE S1: **Time-continuous within-level decoding of reach direction for both monkeys separately. a.** Decoding performance of decoders trained on spike densities of 100 ms time intervals shifted by 50 ms for target MC. Performance was estimated for each session and uncertainty level independently using 5-fold cross-validation. Shaded areas depict 95% CIs for the averaged performance across sessions. Dotted lines indicate chance level at 12.5%. Lightness indicates uncertainty level (low: light, high: dark). Upper row shows results for monkey Y, lower row for monkey Z. Filled black arc: Target cue onset, empty arc: target cue offset, and GO: go cue. Horizontal bars indicate time windows in which accuracies were significantly different for SVMs trained on different uncertainty levels (*$p<0.05$, permutation test). **b.** Same as in (**a**) but for feedback MC. **c.** Same as in (**a**) and (**b**) but for feedback BC.

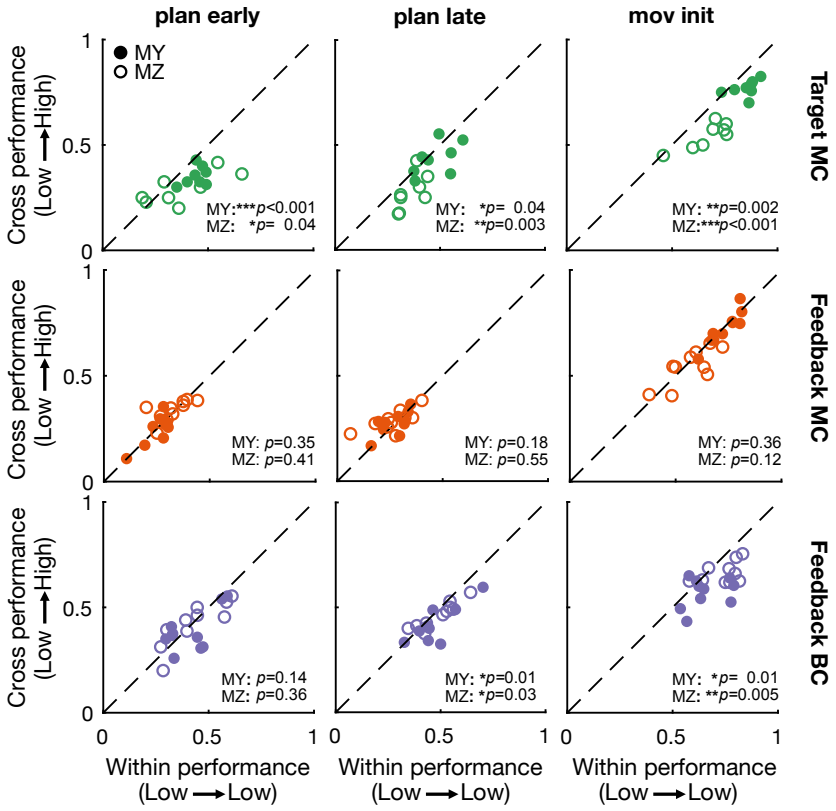

FIGURE S2: **Cross-conditional decoding for individual sessions.** Decoding performance of decoders trained and tested on low uncertainty trials (Low/Low) plotted against performance of decoders trained on low and tested on high uncertainty trials (Low/High). Results from monkey Y in filled circles and monkey Z in open circles. Performance was evaluated for three 200 ms time windows spanning early planning to movement initiation. Target MC in green, feedback MC in orange, and feedback BC in purple. *p<0.05, **p<0.01, and ***p<0.001 correspond to one-tailed one-sample t-tests on the performance difference between within and cross decoding.

FIGURE S3: dPCA results. a. Average explained variance of each dPC task parameter for each monkey for target MC (green, left), feedback MC (orange, middle) and feedback BC (purple, right). Lightness indicates task parameter: target (dark), uncertainty (medium), target and uncertainty interaction (light). Error bars indicate CIs across sessions. b-d. Projection of trial-averaged neural activity onto first uncertainty dPC over time for monkey Y (upper row) and Z (lower row). Projection aligned to visual target onset and go cue. Same colors as in a). Lightness indicates uncertainty level (high: light and low: dark). Shaded areas correspond to 95% CIs across sessions and reach directions.

FIGURE S4: Distribution of neural states in direction dPC space. a. Projections onto the first two directional dPCs for the same session of Monkey Y as shown in Figure 5a at movement initiation under conditions of low (lower row) and high (upper row) target uncertainty. Large points represent trial- and time-averaged projections for each reach direction, indicated by different colors. Small points correspond to time-averaged projections of individual trials. Ellipses denote 95% confidence intervals around the mean projections. b. Same as in (a) but for corresponding session of feedback MC.c. Same as in (a) and (b) but for corresponding session of feedback BC.

TABLE S1: Summary of experimental sessions.

Session	Monkey	Task condition	Trials Low	Trials High	Units
1	MY	Target MC	167	165	50
2	MY	Target MC	188	184	50
3	MY	Target MC	161	158	51
4	MY	Target MC	128	128	55
5	MY	Target MC	175	164	59
6	MY	Target MC	232	218	52
7	MY	Target MC	176	168	60
8	MY	Target MC	290	281	55
9	MZ	Target MC	136	151	48
10	MZ	Target MC	105	121	49
11	MZ	Target MC	85	126	46
12	MZ	Target MC	125	132	47
13	MZ	Target MC	158	150	48
14	MZ	Target MC	147	166	49
15	MZ	Target MC	305	243	36
16	MZ	Target MC	211	163	35
1	MY	Feedback MC	132	115	83
2	MY	Feedback MC	180	153	54
3	MY	Feedback MC	167	147	53
4	MY	Feedback MC	164	162	46
5	MY	Feedback MC	191	174	50
6	MY	Feedback MC	159	145	44
7	MY	Feedback MC	201	182	44
8	MY	Feedback MC	162	145	41
9	MY	Feedback MC	189	164	45
10	MY	Feedback MC	134	118	47
11	MZ	Feedback MC	161	152	44
12	MZ	Feedback MC	233	217	34
13	MZ	Feedback MC	202	189	45
14	MZ	Feedback MC	188	162	54
15	MZ	Feedback MC	96	82	36
16	MZ	Feedback MC	106	106	37
17	MZ	Feedback MC	150	136	34
18	MZ	Feedback MC	159	154	35
19	MZ	Feedback MC	161	159	33
20	MZ	Feedback MC	130	128	32
1	MY	Feedback BC	145	148	43

2	MY	Feedback BC	259	289	43
3	MY	Feedback BC	96	119	44
4	MY	Feedback BC	240	255	39
5	MY	Feedback BC	132	142	52
6	MY	Feedback BC	98	96	44
7	MY	Feedback BC	97	96	38
8	MY	Feedback BC	97	96	35
9	MY	Feedback BC	184	144	41
10	MY	Feedback BC	181	144	49
11	MZ	Feedback BC	143	113	35
12	MZ	Feedback BC	226	192	32
13	MZ	Feedback BC	183	144	35
14	MZ	Feedback BC	262	240	45
15	MZ	Feedback BC	327	288	43
16	MZ	Feedback BC	281	288	41
17	MZ	Feedback BC	239	238	50
18	MZ	Feedback BC	119	142	41
19	MZ	Feedback BC	192	194	43
20	MZ	Feedback BC	144	180	33

TABLE S2: Post-hoc results for repeated-measures ANOVA on the difference in rst uncertainty dPC between high and low uncertainty levels. Difference between values of epoch 1 and epoch 2. StdError indicates standard error. Lower (2.5%) and upper (97.5%) con dence levels (CL) of the difference.

Epoch 1	Epoch 2	Difference	StdError	p-value	Lower CL	Upper CL
MC target uncertainty						
plan early	plan late	0.053	8.54e-03	8.22e-05	0.029	0.078
plan early	mov init	0.058	6.03e-03	4.99e-07	0.040	0.075
plan early	baseline	0.077	9.30e-03	2.88e-06	0.10	0.051
plan late	mov init	-4.23e-03	4.89e-03	0.82	-0.018	-9.87e-03
plan late	baseline	0.034	3.38e-03	1.95e-05	0.014	0.034
mov init	baseline	0.020	4.58e-03	0.003	6.60e-03	0.033
MC Feedback uncertainty						
plan early	plan late	-2.52e-03	3.14e-03	0.85	-0.011	6.31e-03
plan early	mov init	-3.83e-03	5.10e-03	0.87	-0.011	0.018
plan early	baseline	-2.74e-03	3.92e.03	0.90	-8.83e-03	0.014
plan late	mov init	-6.35e-03	3.88e-03	0.38	-4.55e-03	0.017
plan late	baseline	-5.23e-03	3.99e-03	0.56	-5.95e-03	0.016
mov init	baseline	-1.08e-03	4.96e-03	0.99	-0.015	0.013
BC Feedback uncertainty						
plan early	plan late	-0.020	5.95e-03	0.02	-0.037	-3.05e-03
plan early	mov init	-0.024	4.53e-03	1.8e-04	-0.037	-0.018
plan early	baseline	6.35e-03	4.16e-03	0.44	-5.35e-03	0.018
plan late	mov init	4.61e-03	5.26e-03	0.81	-0.010	0.019
plan late	baseline	0.013	4.36e-03	0.03	1.18e-03	0.026
mov init	baseline	0.018	5.32-e03	0.01	3.09e-03	0.033

3.1 Supplementary analyses

In the previous manuscript we evaluated how visual feedback uncertainty affects planning activity in motor cortex, mostly focusing on how target direction information is represented. Our main finding is that feedback uncertainty only affects neural representations of the motor goal or target when it is behaviorally relevant, namely around movement initiation in the case of BCI reaches. In the following supplementary section, I will present additional analyses that broaden our understanding of the effect of feedback uncertainty. First, I will confirm that behavior is particularly affected during the late stages of the reach. Then, I will present neural activity analyses, first looking into potential changes in single-neuron tuning with uncertainty. I will also present population activity results regarding the transition into execution, and the execution stage in the case of BCI reaches. Each section will present and discuss the corresponding results, and shortly describe any new methods employed. The findings from the supplementary analyses support the conclusions from the manuscript: feedback uncertainty is mainly present when it is relevant for adequate control.

Behavior is impaired by feedback uncertainty towards late stage of reach

In the main manuscript, we showed that movement times were higher for high visual feedback uncertainty in both manual-control (MC) and brain-control (BC). However, we wanted to see from what part of the reach the differences in movement times stemmed from. Since visual feedback is mostly used at the late part of the reach to home-in the target, we hypothesized that the differences in movement time would come from this late stage, and not an overall reduction in speed throughout the reach. We thus split the overall movement time into the time taken for the first and second half of the reach. The division point was when the trajectory crossed half of the target eccentricity. Results showed that only the second half movement times were consistently higher for high compared to low visual feedback uncertainty for the two monkeys, applying to both MC (Figure 3.1a; first half: monkey Y: $p=0.51$, monkey Z: $p<0.001$; second half: monkey Y: $p<0.001$, monkey Z: $p<0.001$) and BC (Figure 3.1b: first half: monkey Y: $p=0.001$, monkey Z: $p=0.17$; second half: monkey Y: $p<0.001$, monkey Z: $p<0.001$) reaches. While we did also find significant differences between uncertainty levels for the first half movement times in a single monkey, the magnitude of these differences was smaller than those of the second half. Therefore, we conclude that behavior was especially impaired by feedback uncertainty when potential corrective movements were needed to enter the target area, in line with previous behavioral findings (Heath, 2005; Meyer et al., 1988; Sarlegna et al., 2003).

Methods

The total reach movement time was divided into two segments based on the distance traveled from the center of the workspace. Movement times during the first half of the reach were computed by finding the time between movement onset and the time upon which half

the target eccentricity was crossed. Then, movement times during the second half of the reach were calculated as the time between the half target eccentricity crossing and when the monkey entered the target area. We averaged these times across trials from each target direction and session. To test if there were signi cant differences between uncertainty level, we performed paired Wilcoxon signed-rank tests (=0.05).

FIGURE 3.1: Movement times during rst and second half of the reach. a. Average movement times calculated during the rst and second half of the reach trajectory for both monkeys (MY and MZ) in manual-control (MC) reaches. Lightness indicates uncertainty level (dark: low, light: high). b. Same as (a) but for brain-control (BC) reaches. Error bars indicate CI across target directions and sessions. **p<0.01, ***p<0.001 for Wilcoxon signed-rank tests.

Minor single-neuron tuning changes between uncertainty levels

We assessed whether reach direction tuning of single neurons differed between visual feedback uncertainty levels (Figure 3.2a). In this regard, a previous study tested M1 single-neuron activity when monkeys had to make reaches with and without visual feedback of their hand (Suway & Schwartz, 2019). They evaluated tuning changes between visibility conditions at different stages of the reach and found that only activity at the nal stage of the reach was affected. In particular, a percentage of neurons showed a decrease in modulation depth when reaching without compared to with visual feedback. Here, we shifted the focus to the planning period, evaluating tuning computed from early and late planning, and around movement initiation. Moreover, we expanded the set of compared parameters, including the neurons baseline or offset ring rate and modulation depth.

Across MC sessions and time epochs, an average of 39% (44%) of neurons were tuned to reach direction under both low and high visual feedback uncertainty for monkey Y (Z). Similarly, in BC sessions, an average of 50% (58%) of neurons were tuned under both feedback uncertainty levels for monkey Y (Z). In general, we found minor to no changes in the single-neuron tuning parameters for either MC (Figure 3.2b) or BC (Figure 3.2c) reaches in the different time epochs. Moreover, signi cant changes in a given epoch hardly applied to both monkeys, and in the only case in which they did (BC, offset change, early planning: monkey Z: p=0.002, monkey Y: p=0.002), changes were opposite in sign between monkeys.

In the case of a signi cant change in modulation depth (MC: monkey Y, late planning: p=0.002, monkey Z, movement initiation: p=0.02; BC: monkey Z, late planning: p=0.002), we found that this was higher for high compared to low visual feedback uncertainty, which contrasts the aforementioned study (Suway & Schwartz, 2019). However, it is important to note the epoch being analysed. In their study, the decrease in modulation depth was only notable during the late stage of reach. This decrease could be due to the lack of feedback-based corrective movements to home-in the target, as monkeys had no salient feedback on their hand location. Supporting this idea, they also found a mild reduction EMG activity in the late stage of the reach when no visual feedback was provided. On the contrary, we evaluated tuning changes during the planning phase. In this phase, and in the case of high feedback uncertainty, monkeys could have been more engaged to try to compensate for the potential dif culty in the upcoming reach, resulting in increases in modulation depth.

Overall, the effects on single-neuron tuning we found were small and non-consistent between monkeys. Therefore, our main conclusion is that visual feedback uncertainty did not have a prominent effect on single-neuron tuning in motor cortex during the planning and early movement phase.

FIGURE 3.2: Single-neuron tuning changes between feedback uncertainty levels. a. Firing rates for each neuron were modeled as a cosine function with respect to target direction. The offset, modulation depth (MD) and preferred direction (PD) tuning parameters were obtained. Changes in offset and modulation depth parameters for neurons that were tuned to target direction for high and low feedback uncertainty were assessed. b. Average change in offset (left) and MD (right) between high and low feedback uncertainty for monkey Y (MY) and Z (MZ) for manual-control (MC) reaches (orange color). Color lightness indicates the different epochs tested (dark: early planning, neutral: late planning, light: movement initiation). c. Same as (b) but for brain-control (BC) reaches (purple color). *p<0.05, **p<0.01 for Wilcoxon signed-rank tests.

Methods

For each recorded neuron, we time-averaged the spike densities for the early planning (-50 to 150 ms from target offset), late planning (-150 to 50 ms from go cue) and movement initiation (-50 to 150 ms from movement onset) epochs, performing the tuning analysis for each epoch independently. We assumed that the activity of a neuron changed with respect to the target direction following a cosine curve (Figure 3.2a). To nd the tuning parameters, we rst linearly regressed each neuron's ring rate to the x- and y-coordinates of the target position, pooling across trials from a single session. We did this separately for trials from each uncertainty level. We obtained three parameters from the linear regression: an offset and two weights corresponding to the x and y target position. Next, we computed the modulation depth as the norm of the target position weights, and the preferred direction as their angle in the polar space. Motivated by previous related research (Bosco et al., 2010; Suway & Schwartz, 2019), we focused on changes in the offset and modulation depth measures between uncertainty levels. We only measured these changes in neurons that were classi ed as tuned for both uncertainty levels. Our conclusions do not change if we considered neurons that were tuned based only on low uncertainty trials. Whether a neuron was considered to be tuned was determined by the regression model, namely if it had a signi cant slope ($p<0.05$). We computed the change in each tuning parameter by subtracting its value from the low uncertainty level to that of the high uncertainty level. Finally, we averaged the change in each parameter across all selected neurons from that session. To evaluate whether this average change was signi cantly different from zero across sessions, we performed Wilcoxon signed-rank tests (=0.05).

High visual feedback uncertainty affected the transition from planning to movement

The transition from planning to movement in motor cortex is presumably mediated by an input trigger-like signal (Kaufman et al., 2016). This input signal is characterized for being condition-independent, mostly re ecting the timing but not the type of movement. Given that we found a delay in reaction time with high feedback uncertainty, we hypothesized that the dynamics of this condition-independent signal (CIS) differed between uncertainty levels.

For each uncertainty level, we applied dPCA on the time-resolved spike densities independently, to nd both the condition-independent and the target direction components. We then projected the spike densities onto the condition-independent component that explained the most data variance, which we call the CIS (Figure 3.3b,d). We found that the CIS differed in two ways across uncertainty levels. First, the onset of the signal was delayed for high compared to low feedback uncertainty in MC (Figure 3.3c left; monkey Y: $p<0.001$, monkey Z: $p<0.001$) and BC (Figure 3.3e, left; monkey Y: $p<0.001$, monkey Z: $p<0.001$). Second, the rise of the signal was slower under high feedback uncertainty in BC (Figure 3.3e right; monkey Y: $p<0.001$, monkey Z: $p<0.001$), and also in MC for monkey Y (Figure 3.3c right;

FIGURE 3.3: Condition-independent signal (CIS). a. CI components of neural activity were found through dPCA, applied separately for both uncertainty levels. dPCA also estimated target direction components. b. Average spike density projection onto the first CI dPC (considered here the CIS) in time for MC reaches (orange color). Lightness indicates uncertainty level (dark: low, light: high). Inset shows average explained data variance by the first CI dPC across sessions. c. Average latency (left) and slope (right) of the CIS for each uncertainty level and monkey for MC reaches. d, e. Same as (b) and (c) but for BC reaches (purple color). Shaded areas and error bars represents CI across target direction and sessions. ***p<0.001 for Wilcoxon ranksum tests. f. Histograms of reaction time and CIS latency correlations pooling across target directions and sessions for MC reaches. Triangles indicate distribution means. g. Same as (f) but for BC reaches. *p<0.05, ***p<0.001 for Wilcoxon signed-rank tests.

monkey Y: p<0.001, monkey Z: p=0.4). Furthermore, to confirm that the computed CIS had a behavioral effect on the timing of movement initiation, we correlated the measured CIS latency to the reaction time on a single-trial basis. Indeed, we found positive correlations

for manual reaches (Figure 3.3f; low uncertainty: monkey Y: $p<0.001$, monkey Z: $p<0.001$; high uncertainty: monkey Y: $p<0.001$, monkey Z: $p<0.001$). For BCI-controlled reaches, we also found a positive correlation for monkey Y (Figure 3.3g; low uncertainty: $p<0.001$; high uncertainty: $p=0.049$), but not for monkey Z (low uncertainty: $p=0.09$; high uncertainty: $p=0.22$). However, we note the reaction time computed for BC reaches is of limited interpretation due to low sampling times and potentially different strategies for movement initiation. For instance, instead of withholding movement during the planning epoch as in MC, monkeys could have already been actively trying to move the feedback towards the target, but as the feedback was clamped at the center, there was no net movement produced.

Finding that the CIS was both delayed and slower for high feedback uncertainty could indicate that the transition from planning to movement is impaired in this condition. Liking this finding to the within-level decoding results, one reason for the decrease in performance for high feedback uncertainty in BC around movement onset could be the delayed and slower ramping up of activity after the go cue. Along this line, not finding differences in decoding performance in MC could be because CIS impairments are comparably less marked than in BC, especially in monkey Z. While we cannot discard that the CIS delay is caused by increased distraction of the stimulus used in the high uncertainty level, this would not explain the difference in speed observed. Thus, feedback uncertainty had an effect on movement initiation dynamics, more apparent under BCI control.

Methods

We performed dPCA in a similar manner to the manuscript. However, there are a few key differences. First, as pre-processing of the spike densities, we did not apply the time-normalization procedure, but only subtracted the mean firing activity for each unit, and later scaled the activity as described in the manuscript. Second, we computed dPCA with data from each uncertainty level separately to be able to capture differences across uncertainty levels in the condition-independent components and not in the interaction ones. Thus, we only included time (condition-independent component), target direction, and their interaction as task parameters.

After finding the corresponding dPCs, we focused our analysis on the dPC that explained most of the condition-independent or common timing related variance. We trial-averaged the spike densities (-200 to 600 ms from go cue) for each target and session, and projected them onto this first condition-independent dPC, rendering the CIS. We then computed the latency of the CIS as the time point at which half of the signal was crossed. This half magnitude was the average between the maximum magnitude and the average magnitude in a small time window after the go cue (0 to 100 ms). The slope of the CIS was computed as the slope in a 100 ms time window centered on the half-magnitude point. Finally, we computed the correlation between the reaction times and projection latencies on a single-trial basis for each target direction and session, which we used to build the histograms. For this,

we removed trials with reaction times below 200 ms and above 600 ms. To test for signi - cant differences in CIS latency and slope between uncertainty conditions, we used unpaired Wilcoxon rank sum tests (=0.05). Moreover, we tested whether the reaction time and CIS latency correlations were signi cant with Wilcoxon signed-rank tests (=0.05).

Neural control through the BCI was worse with high visual feedback uncertainty

One of the bene ts of using a BCI is that neural activity can be directly related to the behavioral output. Hence, it is possible to quantify how neural activity contributed to achieving the task goal. In this nal supplementary analysis, we focused on movement execution activity from BCI sessions. In our experiments, neural activity from motor cortex was translated into the velocity vector of the visual feedback, which was updated at each time step (Figure 3.4a). This velocity vector can be formalized as the addition of two vectors: one derived from the transition dynamics and another resulting from the neural activity. Thus, for of ine analysis, we can focus on the component of the velocity vector resulting from the neural activity alone. At each time step, we projected this neural velocity vector onto an ideal vector that pointed from the controlled position to the target (Figure 3.4b). This projection is known as neural progress, and it quanti es how much the neural activity "pushes" the feedback into the ideal direction to reach the target (Losey et al., 2024; Oby et al., 2019; Stavisky et al., 2017). Here, we hypothesized that the neural progress would be higher in the case of low uncertainty feedback, given that the controlled position, and as a result, the ideal direction in which to move it, is easier to determine.

When plotting the neural progress in time, we found that it rapidly increased after the go cue (Figure 3.4c), as expected in order to initiate the reach. We observed slightly different trends in the progress time course between uncertainty levels for each monkey. In the time close after the go cue, including the reaction time, monkey Y did not show differences in progress between uncertainty levels (Figure 3.4d, left; $p=0.53$), while monkey Z showed increased progress with high feedback uncertainty ($p<0.001$). This potentially indicates a difference in strategy during the late planning phase taken by each monkey. In particular, monkey Z might have been trying to compensate for the upcoming dif culty in the reach under high feedback uncertainty during late planning, while monkey Y did not. Close after movement initiation, progress was higher under low feedback uncertainty for both monkeys (Figure 3.4d, right; monkey Y: $p<0.001$, monkey Z: $p=0.007$). Therefore, as movement control approached, neural activity was more strongly contributing to move the feedback into the target direction under low compared to high feedback uncertainty.

As movement trajectories were highly variable, we wanted to parse neural progress from more or less accurate reaches. For this aim, we binned the neural progress in time and reach trajectory error angle. This error angle measured how deviated the reach trajectory was to a straight line connecting the workspace center and the target. We then computed the average difference in neural progress between uncertainty levels for each bin, constructing a heat-map

(Figure 3.4e). These heat-maps revealed that progress was relatively constant with trajectory error angle, and mainly changed in time, mirroring the progress time-course for each monkey. In this manner, even if the trajectory was deviated, progress was not particularly higher for low feedback uncertainty.

Finally, we assessed neural progress throughout the entire reach. We first classified reaches based on whether a single straight movement was sufficient to acquire the target (direct) or not (non-direct). Thus, the latter would have likely required movement corrections, which we expected to be impaired by high feedback uncertainty. Then, for each reach type, we averaged the progress from movement onset to movement offset or until 1500 ms after go cue, to avoid particularly poorly performed reaches that resulted in long movement times. Neural progress was not different between uncertainty levels for direct reaches (Figure 3.4f left; monkey Y: p=0.2, monkey Z: p=0.31), as likely there was no substantial online control in these. Nevertheless, neural progress was higher for low feedback uncertainty in the case of non-straight reaches (Figure 3.4f right; monkey Y: p=0.03, monkey Z: p=0.002), indicating greater difficulty in control. Since progress is influenced by both neural vector magnitude and its alignment to the ideal vector, we further quantified the normalized progress, capturing only the alignment contribution. Thus, this measure would specifically capture how well the neural activity was aiming towards the target, important for accurate online control. Again, we found that the normalised progress was higher for low feedback uncertainty (monkey Y: p<0.001, monkey Z: p=0.009), indicating that neural activity was better directed towards the target for this uncertainty level. Altogether, we could confirm neural activity is less effective for BCI movement control under high compared to low visual feedback uncertainty.

Methods

For BCI offline analysis, we decomposed the velocity vector of the feedback into two components. One component resulted from the transition from the previous velocity vector, ensuring smooth dynamics. The other component was the readout from the neural activity. At each time step, we computed the ideal unit vector from the feedback to the target. Then, we projected the neural velocity component onto this ideal vector. The resulting magnitude is known as the neural progress. In general, we computed the trial-averaged neural progress for each target direction, session and monkey. For Figure 3.4d, we averaged the neural progress in time for two epochs, namely from 0 to 200 ms after go cue and movement initiation. To compute the heat-maps from Figure 3.4e, we first computed the difference in binned progress for each target and session, and then averaged across these for each monkey. Finally, for Figure 3.4f we computed the time-averaged progress from movement onset to offset or until 1500 ms for reaches that took longer. We averaged separately for direct and non-direct reaches. Direct reaches were defined as reach trajectories whose arc length with respect to the target direction did not exceed the target area radius. Thus, direct reaches did not include movement corrections as the feedback was always on the correct path to reach the target. The

rest of the reaches were classi ed as non-direct. We used paired Wilcoxon signed-rank tests (=0.05) to test for signi cant differences in neural progress between uncertainty levels for analyses shown in Figure 3.4d,f.

FIGURE 3.4: Neural progress from BCI movement execution. a . In our BCI experiments, the velocity vector of the visual feedback was decoded from motor cortex activity at each time step. This velocity vector can split into a component coming from the velocity transition dynamics and a component from the neural activity. b. Neural progress was computed by projecting the neural only velocity vector onto the ideal vector pointing from the visual feedback to the target at each time step. c. Average neural progress in time, aligned to go cue for low (red) and high (blue) uncertainty levels. Shaded areas indicate SEM across target directions and sessions. d. Average neural progress binned in two 200 ms time windows: starting from go cue (left) and movement initiation (right). e. Heat-maps of the average difference in neural progress between uncertainty levels at each time and trajectory error angle bin. Positive values (red) indicates progress was higher for low uncertainty and negative values (blue) that is was higher for high uncertainty. f. Average neural progress over execution for direct (left) and non-direct (right) reaches. Error bars for point plots indicate CI across target directions and sessions. Small dots indicate individual averages for each target direction and session. *p<0.05, **p<0.01, ***p<0.001 for Wilcoxon sign-rank tests.

Chapter 4

General discussion

Our motor system continuously integrates sensory feedback for the control of movement, which comes from the visual and somatosensory domains. In the case of visual feedback, this information is essential to assess where our limbs are in relation to external objects that we might want to interact with, that is, our motor goals. However, sensory feedback has two inherent limitations, namely that it is delayed and uncertain. To overcome this, it has been proposed that movement control is not only based on sensory feedback, but sensorimotor predictions from internal models are also used (McNamee & Wolpert, 2019; Wolpert et al., 1995). Visual feedback uncertainty is considered at the state estimation process, when internal predictions and sensory feedback are combined (Körding & Wolpert, 2004). Nevertheless, relying on internal predictions may not be an option when movement corrections, which call for close tracking of sensory feedback, are needed. Therefore, conditions of visual feedback uncertainty pose a challenge to properly make these corrections in order to ultimately achieve our motor goals.

The main aim of this thesis was to evaluate the behavioral and neural consequences of movement under uncertain visual feedback of the hand. Given that sensory feedback is critical when perturbations affect our movements, this thesis focused on the impact of visual feedback uncertainty during motor adaptation. This was speci cally evaluated in Chapter 2, where behavioral results from human participants showed that visuomotor adaptation is attenuated under high visual feedback uncertainty. As a rst step to explore the neural counterpart, Chapter 3 evaluated motor cortex activity of rhesus monkeys when reaching with uncertain visual hand feedback, which was also tested using a BCI to preclude the reliance on somatosensory information. Uncertainty affected behavior of both hand-controlled and brain-controlled reaches, though we could only observe a neural effect in terms of target representations for the latter. Altogether, we conclude that visual feedback uncertainty is re ected at the behavioral and neural level when it becomes critical to achieve our motor goals.

Motor adaptation to large errors is attenuated by visual feedback uncertainty

Our first study showed that visuomotor adaptation in humans is attenuated when using uncertain visual feedback of the hand. Our results add to previous work indicating that sensory uncertainty influences motor adaptation (Burge et al., 2008; Ferrea et al., 2022; Körding & Wolpert, 2004; Tsay et al., 2021; van Beers et al., 2002; Wei & Körding, 2010; Zhang et al., 2024). To interpret our findings, we have to consider that motor adaptation is a greatly multifaceted process (Morehead & Orban de Xivry, 2021). To start, motor adaptation is composed by unconscious implicit changes in our internal sensorimotor mappings and explicit cognitive compensation strategies. Focusing on implicit adaptation, this process is modulated by the specific properties of the experienced movement errors. These properties could be categorized into size, origin and modality. Following, I will evaluate how errors defined by each property could be affected by visual feedback uncertainty.

Attending to the size of error, implicit adaptation aims to correct for small errors likely caused by our motor system (Wei & Körding, 2009). Conversely, large errors are more likely to stem from external factors and should be discounted. In this sense, it is observed that the size of trial-to-trial corrections gets smaller as error sizes get bigger (Hutter & Taylor, 2018; Kim et al., 2018; Marko et al., 2012). While a different assignment of relevance could be the cause of the differential adaptation to small compared to large errors (Wei & Körding, 2009), an alternative explanation is that our motor system cannot rapidly change due to plasticity constraints (Tsay et al., 2021). Therefore, implicit adaptation is a gradual process, which entails that corrections from one trial to another are small. Conceivably, small errors will be more notably affected by uncertainty, as their detection is hindered. Indeed, a number of studies have confirmed this (Burge et al., 2008; Körding & Wolpert, 2004; Tsay et al., 2021; Wei & Körding, 2010). However, as we have shown, also large errors can be impacted by uncertainty. Thus, reduced adaptation does not solely result from a detection or mislocalisation deficit. Uncertainty possibly reduces the relevance or integration weight assigned to errors across the size range.

Another way to define errors is by their origin, namely if they relate to internal or external measures. Implicit adaptation corrects primarily for sensory-prediction errors (SPEs), the discrepancy between internally predicted and received feedback, as they indicate that our motor system holds faulty internal models. However, implicit adaptation also appears to be sensitive to task performance metrics, such as target errors, the difference between task goal and received feedback (Al-Fawakhiri et al., 2023; Albert et al., 2022; Leow et al., 2018). Since SPEs and target errors are computed relative to the received feedback, both should be affected by visual feedback uncertainty.

Our movement-contingent visuomotor rotation (VMR) results in SPEs and target errors, as visual feedback is task-relevant. This is in contrast to the error-clamp method, which makes visual feedback task-irrelevant by instructing participants to ignore target errors, and only results in SPEs (Morehead et al., 2017). The use of method, and resulting errors, appears to

be critical for observing an effect of visual feedback uncertainty on implicit adaptation. While a number of studies employing the error-clamp method did not find a reduction in adaptation to large errors (Tsay et al., 2021; Tsay et al., 2023), this was found in our study using a movement-contingent perturbation. We note that with a movement-contingent perturbation, we cannot disentangle the contribution of SPE and target errors to adaptation. Therefore, we cannot specifically know if the uncertainty in SPEs, target errors, or both, caused the attenuation in adaptation. Another possibility is that SPEs computed from task-relevant feedback have a different contribution to adaptation than SPEs computed from task-irrelevant feedback, which might be less sensitive to visual feedback uncertainty. Nevertheless, we think that having task-relevant visual feedback and target errors is important to see the effects of feedback uncertainty on adaptation to large errors.

Finally, adaptation is not only guided by errors in the visual sensory modality, but hand proprioceptive information also has a role in this process (Tsay et al., 2022; Zhang et al., 2024). Visual feedback uncertainty is considered when visual and proprioceptive feedback are combined to form a single hand estimate, previously shown to follow Bayesian principles (Ernst & Banks, 2002; van Beers et al., 2002). Along this line, a recent model has put forth that implicit adaptation could be based on Bayesian combination of visual feedback, proprioceptive hand estimates, and sensory predictions (Zhang et al., 2024). Therefore, when visual feedback is uncertain, the other two signals dominate and implicit adaptation to visual errors is reduced.

Explicit adaptation encompasses the cognitive processes involved in motor adaptation (Tsay et al., 2024). Despite its contribution, explicit adaptation has not been as explored as its implicit counterpart. In our study, we have added to the characterization of explicit processing by quantifying how it is affected by visual feedback uncertainty. While our explicit adaptation measures were overall small, consistent with previous studies applying our perturbation size (Bond & Taylor, 2015; Modchalingam et al., 2019), we found differences between uncertainty conditions. In particular, explicit adaptation was reduced when visual feedback was uncertain, indicating that visual feedback uncertainty also impairs the cognitive strategies involved in adaptation. Thus, future research could aim to more precisely evaluate these effects, exploring the link between cognitive and adaptation processes.

Motor cortex is affected by behaviorally-relevant visual feedback uncertainty

Hand reaching behavior under visual feedback uncertainty in monkeys was impaired in the final stages of movement, when corrective movements were potentially needed to enter the target area. When making reaches through a BCI, monkeys showed poorer movement control even earlier, after the middle stage of the reach. This indicates that, for manual reaches, the initial part of the reach is likely performed based on internal predictions and the more reliable somatosensory feedback of the limb (Heath, 2005). Hence, the behavioral effect of uncertain visual feedback was only visible at the end of the reach. However, for BCI reaches, since

there was no behaviorally-relevant somatosensory feedback, monkeys could not rely on this source of input to compensate for the uncertain visual one.

Our behavioral findings showcase the negative impact of visual feedback uncertainty on movement control. To uncover the neural underpinnings of this impact, we evaluated activity from motor cortex, including dorsal premotor cortex (PMd) and primary motor cortex (M1). We found that feedback uncertainty did not affect neural representations of the upcoming reach direction during planning. While both feedback and target information should be needed to compute a movement plan (Shadmehr & Wise, 2004; Sober & Sabes, 2003), it is possible that feedback uncertainty does not affect this initial process in the evaluated areas. As the movement was initiated, neural target representations were still unaffected by uncertainty when making reaches in manual-control (MC). In contrast, when reaches were made in BCI-control (BC) and the only source of relevant feedback was in the visual domain, neural target representations were poorer under visual feedback uncertainty around movement initiation.

Our findings in the MC condition are in agreement with previous work showing that M1 activity was not affected by withdrawing visual feedback in the initiation and early stages of movement (Suway & Schwartz, 2019). Instead, changes in M1 activity were observed during the late stage of the reach, when feedback-based corrections to enter the target would be needed. This aligns with our BC results in the sense that control should be feedback-based throughout the movement. Thus, uncertainty affected neural target representations when it began to be behaviorally relevant, that is, when movement started. Furthermore, we found that neural activity was less suited to move the feedback towards the target throughout movement execution in BC.

In addition, we found that visual feedback uncertainty was represented in motor cortex activity, independent of its effect on target direction representations. Thus, neural activity patterns were different between uncertainty levels for both MC and BC reaches, and this difference applied to all target directions. The uncertainty-related difference was observed even before the target was cued, likely starting when the visual feedback stimulus was set at the beginning of the trial. Moreover, we found that in BC this difference increased as movement initiation approached, which parallels the increase in behavioral relevance of the feedback. The found population activity difference could indicate that uncertainty is represented as a higher-level variable, potentially reflecting the context in which the upcoming reach will be made. Related to this, studies have shown that motor cortex activity can be similarly modulated by the reach context in terms of kinetic (Sun et al., 2022) or kinematic requirements (Saxena et al., 2022), as well as reward contingencies (Smoulder et al., 2024). Therefore, the knowledge of whether the upcoming reach would be under low or high feedback uncertainty could have been reflected in the neural activity without necessarily interacting with target encoding. Alternatively, there might have been a change in the monkeys attention or arousal between uncertainty levels, causing the observed modulation in motor cortex activity (Hennig et al.,

2021). A potential way to test if the uncertainty-related separation is due to reach context, indicating its behavioral relevance, or changes in the monkeys internal state, could be to provide both the low and high uncertainty visual feedback stimuli. This would render the high uncertainty stimulus behaviorally irrelevant while still presenting this visual input. Thus, when both stimuli are presented, we do not expect to find the uncertainty-related difference in population activity if this is due to reach context representation.

Within the optimal feedback control framework (OFC), motor cortex, in particular M1, is considered to act as a controller, using the motor system's state to generate motor commands (Scott, 2004). Accordingly, motor cortex is thought to receive processed feedback information from upstream areas. One key region for the integration of movement-derived sensory feedback is the posterior parietal cortex (PPC) (Andersen et al., 1997). Given that PPC receives somatosensory and visual feedback, as well as motor command information, this region has been related to state estimation in movement control (Archambault et al., 2009; Battaglia-Mayer et al., 2016; Battaglia-Mayer et al., 2013; Desmurget et al., 1999; Mulliken et al., 2008; Takei et al., 2021; Wolpert et al., 1998). Therefore, areas within the PPC would be candidate regions to represent visual feedback uncertainty. In this regard, neurons in area V6A, located in the caudal superior parietal lobule, have been shown to be modulated by reaching in light or dark visual conditions, thus, with or without visual feedback of the limb (Bosco et al., 2010). This study could find visual-related neurons, which only were active when visual feedback was present, movement-related neurons, which were more active without visual feedback, and visuo-movement neurons, which showed varied modulation when reaching with visual feedback with respect to without. Since V6A projects to other areas of the PPC, as well as to PMd (Caminiti et al., 1999), this area could form an early stage of visual feedback processing where uncertainty is continuously encoded. More generally, PPC is interconnected with motor cortex (Wise et al., 1997), potentially relaying state estimates that would have been computed integrating feedback uncertainty.

The next question derived from this thesis would be how does visual feedback uncertainty influence motor cortex activity during motor adaptation. Along this line, two related studies evaluated motor cortex activity during force-field adaptation showing visual feedback continuously throughout the reach or only at reach endpoint (Arce et al., 2010a; Arce et al., 2010b). They found that with continuous visual feedback, more neurons whose preferred direction countered the imposed force-field were recruited, compared to when only reach endpoint visual feedback was shown. Thus, the amount of presented visual feedback influenced the extent of neural adaptation. We hypothesize that a similar effect would be found in the case of visuomotor adaptation under visual feedback uncertainty. Since the aforementioned studies primarily compared neural activity before and after adaptation, it would be compelling to assess how this activity evolves throughout adaptation. In terms of neural population states, these would potentially change more slowly towards the final adapted state under visual feedback uncertainty, resulting in an expected slower behavioral adaptation rate

in line with our human participant study. Furthermore, adaptation could be tested under BCI control, allowing to more precisely determine whether neural changes are effective or not for behavioral improvements. Since we already observed that movement execution was impaired under feedback uncertainty in BC, we expect further dif culties when compensating for perturbations during the reach. Similarly, impairments in adaptation could be due to neural changes having a higher output-null component when visual feedback is uncertain compared to when it is not, and thus, not appropriately contributing to behavioral improvements.

An important observation for clinical applications is that visual feedback uncertainty primarily affected motor cortex activity when making reaches through a BCI. Consequently, BCI users that only receive visual feedback would be at risk of impaired movement control under conditions of uncertainty. Major research efforts are aimed at incorporating additional feedback sources to BCI users (Bensmaia & Miller, 2014; Dadarlat et al., 2023). These sources include somatosensory feedback provided in a non-invasive manner (Deo et al., 2021) or directly activating somatosensory cortex through electrical stimulation (Flesher et al., 2016; Flesher et al., 2021). In general, clinical studies show that BCI performance is improved when incorporating such supplementary somatosensory information (Deo et al., 2021; Flesher et al., 2016; Flesher et al., 2021; Klaes et al., 2014). Thus, this would be a potential option to make BCIs more robust to conditions of visual feedback uncertainty.

4.1 Conclusion

This thesis investigated movement control under visual feedback uncertainty. Visuomotor adaptation of human participants to large errors was reduced when provided with uncertain visual feedback of their hand. When dissociating between implicit and explicit contributions, we found an attenuation in both. Our results add to previous work that tested small errors, suggesting that errors are integrated depending on their uncertainty. As well, large errors have to be relevant to achieve the task goal in order for visual feedback uncertainty to affect adaptation. Prior to testing how visual feedback uncertainty impacts monkey motor cortex activity during motor adaptation, we studied its effect during center-out reaches that were made manually or via a BCI. Focusing on the planning process, neural representations of the motor goal were not affected by visual feedback uncertainty during manual reaching. In contrast, these representations were impaired around movement initiation for BCI reaching. This suggests that visual feedback uncertainty affects motor goal encoding as it becomes critical for movement control. Nevertheless, we found that, irrespective of its effect on motor goal representations, visual feedback uncertainty was represented in motor cortex activity for both manual and BCI reaches. Finally, our study highlights the liability that conditions of visual feedback uncertainty can pose to BCI users, showcasing the need for additional sources of feedback for movement control.

Appendix A

Optimality of multisensory integration while compensating for uncertain visual target information with arti cial vibrotactile cues during reach planning

Lukas K. Amann, Virginia Casasnovas, Jannis Hainke, and Alexander Gail

Published in Journal of NeuroEngineering and Rehabilitation (Amann et al., 2024)

Author contributions:

LKA, VC, and AG conceived and designed the study.

JH collected the data.

LKA analyzed the data.

LKA, VC, JH, and AG interpreted results.

LKA prepared gures and drafted the manuscript.

LKA, VC, and AG edited and revised the manuscript.

LKA, VC, JH, and AG read and approved the nal version of the manuscript.

Bibliography

Afshar, A., Santhanam, G., Yu, B. M., Ryu, S. I., Sahani, M., & Shenoy, K. V. (2011). Single-trial neural correlates of arm movement preparation. Neuron, 71(3), 555–564.

Al-Fawakhiri, N., Ma, A., Taylor, J. A., & Kim, O. A. (2023). Exploring the role of task success in implicit motor adaptation. Journal of Neurophysiology, 130(2), 332–344.

Albert, S. T., Jang, J., Modchalingam, S., 't Hart, B. M., Henriques, D., Lerner, G., Della-Maggiore, V., Haith, A. M., Krakauer, J. W., & Shadmehr, R. (2022). Competition between parallel sensorimotor learning systems. eLife, 11, e65361.

Albert, S. T., Jang, J., Sheahan, H. R., Teunissen, L., Vandevoorde, K., Herzfeld, D. J., & Shadmehr, R. (2021). An implicit memory of errors limits human sensorimotor adaptation. Nature Human Behaviour, 5(7), 920–934.

Ali, Y. H., Bodkin, K., Rigotti-Thompson, M., Patel, K., Card, N. S., Bhaduri, B., Nason-Tomaszewski, S. R., Mifsud, D. M., Hou, X., Nicolas, C., Allcroft, S., Hochberg, L. R., Yong, N. A., Stavisky, S. D., Miller, L. E., Brandman, D. M., & Pandarinath, C. (2024). BRAND: A platform for closed-loop experiments with deep network models. Journal of Neural Engineering, 21(2), 026046.

Altan, E., Ma, X., Miller, L. E., Perreault, E. J., & Solla, S. A. (2023). Low-dimensional neural manifolds for the control of constrained and unconstrained movements (preprint). bioRxiv, New Results, 542264.

Ames, K. C., Ryu, S. I., & Shenoy, K. V. (2019). Simultaneous motor preparation and execution in a last-moment reach correction task. Nature Communications, 10(1), 2718.

Andersen, R. A., A alo, T., Bashford, L., Bjånes, D., & Kellis, S. (2022). Exploring cognition with brain–machine interfaces. Annual Review of Psychology, 73(1), 131–158.

Andersen, R. A., Snyder, L. H., Bradley, D. C., & Xing, J. (1997). MULTIMODAL REPRESENTATION OF SPACE IN THE POSTERIOR PARIETAL CORTEX AND ITS USE IN PLANNING MOVEMENTS. Annual Review of Neuroscience, 20(1), 303–330.

Anguera, J. A., Reuter-Lorenz, P. A., Willingham, D. T., & Seidler, R. D. (2010). Contributions of spatial working memory to visuomotor learning. Journal of Cognitive Neuroscience, 22(9), 1917–1930.

Arce, F., Novick, I., Mandelblat-Cerf, Y., Israel, Z., Ghez, C., & Vaadia, E. (2010a). Combined adaptiveness of speci c motor cortical ensembles underlies learning. Journal of Neuroscience, 30(15), 5415–5425.

Arce, F., Novick, I., Mandelblat-Cerf, Y., & Vaadia, E. (2010b). Neuronal correlates of memory formation in motor cortex after adaptation to force field. Journal of Neuroscience, 30(27), 9189–9198.

Archambault, P. S., Caminiti, R., & Battaglia-Mayer, A. (2009). Cortical mechanisms for online control of hand movement trajectory: The role of the posterior parietal cortex. Cerebral Cortex, 19(12), 2848–2864.

Athalye, V. R., Ganguly, K., Costa, R. M., & Carmena, J. M. (2017). Emergence of coordinated neural dynamics underlies neuroprosthetic learning and skillful control. Neuron, 93(4), 955–970.e5.

Battaglia-Mayer, A., Babicola, L., & Satta, E. (2016). Parieto-frontal gradients and domains underlying eye and hand operations in the action space. Neuroscience, 334, 76–92.

Battaglia-Mayer, A., Ferrari-Toniolo, S., Visco-Comandini, F., Archambault, P. S., Saberi-Moghadam, S., & Caminiti, R. (2013). Impairment of online control of hand and eye movements in a monkey model of optic ataxia. Cerebral Cortex, 23(11), 2644–2656.

Bensmaia, S. J., & Miller, L. E. (2014). Restoring sensorimotor function through intracortical interfaces: Progress and looming challenges. Nature Reviews Neuroscience, 15(5), 313–325.

Benson, B. L., Anguera, J. A., & Seidler, R. D. (2011). A spatial explicit strategy reduces error but interferes with sensorimotor adaptation. Journal of Neurophysiology, 105(6), 2843–2851.

Blakemore, S.-J., Wolpert, D., & Frith, C. (2000). Why can't you tickle yourself? NeuroReport, 11(11), R11–R16.

Bond, K. M., & Taylor, J. A. (2015). Flexible explicit but rigid implicit learning in a visuomotor adaptation task. Journal of Neurophysiology, 113(10), 3836–3849.

Bosco, A., Breveglieri, R., Chinellato, E., Galletti, C., & Fattori, P. (2010). Reaching activity in the medial posterior parietal cortex of monkeys is modulated by visual feedback. Journal of Neuroscience, 30(44), 14773–14785.

Burge, J., Ernst, M. O., & Banks, M. S. (2008). The statistical determinants of adaptation rate in human reaching. Journal of Vision, 8(4), 20–20.

Caminiti, R., Johnson, P. B., Galli, C., Ferraina, S., & Burnod, Y. (1991). Making arm movements within different parts of space: The premotor and motor cortical representation of a coordinate system for reaching to visual targets. Journal of Neuroscience, 11(5), 1182–1197.

Caminiti, R., Genovesio, A., Marconi, B., Mayer, A. B., Onorati, P., Ferraina, S., Mitsuda, T., Giannetti, S., Squatrito, S., Maioli, M. G., & Molinari, M. (1999). Early coding of reaching: Frontal and parietal association connections of parieto-occipital cortex. European Journal of Neuroscience, 11(9), 3339–3345.

Caminiti, R., Zeger, S., Johnson, P. B., Urbano, A., & Georgopoulos, A. P. (1985). Corticocortical efferent systems in the monkey: A quantitative spatial analysis of the tangential distribution of cells of origin. Journal of Comparative Neurology, 241(4), 405–419.

Chase, S. M., Kass, R. E., & Schwartz, A. B. (2012). Behavioral and neural correlates of visuomotor adaptation observed through a brain-computer interface in primary motor cortex. Journal of Neurophysiology, 108(2), 624–644.

Cheney, P. D., & Fetz, E. E. (1980). Functional classes of primate corticomotoneuronal cells and their relation to active force. Journal of Neurophysiology, 44(4), 773–791.

Cherian, A., Fernandes, H. L., & Miller, L. E. (2013). Primary motor cortical discharge during force field adaptation reflects muscle-like dynamics. Journal of Neurophysiology, 110(3), 768–783.

Churchland, M. M. (2006). Neural variability in premotor cortex provides a signature of motor preparation. Journal of Neuroscience, 26(14), 3697–3712.

Churchland, M. M., Afshar, A., & Shenoy, K. V. (2006a). A central source of movement variability. Neuron, 52(6), 1085–1096.

Churchland, M. M., Cunningham, J. P., Kaufman, M. T., Foster, J. D., Nuyujukian, P., Ryu, S. I., & Shenoy, K. V. (2012). Neural population dynamics during reaching. Nature, 487(7405), 51–56.

Churchland, M. M., Cunningham, J. P., Kaufman, M. T., Ryu, S. I., & Shenoy, K. V. (2010). Cortical preparatory activity: Representation of movement or first cog in a dynamical machine? Neuron, 68(3), 387–400.

Churchland, M. M., Santhanam, G., & Shenoy, K. V. (2006b). Preparatory activity in premotor and motor cortex reflects the speed of the upcoming reach. Journal of Neurophysiology, 96(6), 3130–3146.

Churchland, M. M., & Shenoy, K. V. (2024). Preparatory activity and the expansive null-space. Nature Reviews Neuroscience, 1–24.

Churchland, M. M., & Shenoy, K. V. (2007). Temporal complexity and heterogeneity of single-neuron activity in premotor and motor cortex. Journal of Neurophysiology, 97(6), 4235–4257.

Cisek, P., & Kalaska, J. F. (2005). Neural correlates of reaching decisions in dorsal premotor cortex: Specification of multiple direction choices and final selection of action. Neuron, 45(5), 801–814.

Crammond, D. J., & Kalaska, J. F. (2000). Prior information in motor and premotor cortex: Activity during the delay period and effect on pre-movement activity. Journal of Neurophysiology, 84(2), 986–1005.

Cross, K. P., Cook, D. J., & Scott, S. H. (2024). Rapid online corrections for proprioceptive and visual perturbations recruit similar circuits in primary motor cortex. eNeuro, 11(2).

Dadarlat, M. C., Canfield, R. A., & Orsborn, A. L. (2023). Neural plasticity in sensorimotor brain-machine interfaces. Annual Review of Biomedical Engineering, 25, 51–76.

Dadarlat, M. C., O'Doherty, J. E., & Sabes, P. N. (2015). A learning-based approach to artificial sensory feedback leads to optimal integration. Nature Neuroscience, 18(1), 138–144.

Dayan, P., & Daw, N. D. (2008). Decision theory, reinforcement learning, and the brain. Cognitive, Affective, & Behavioral Neuroscience, 8(4), 429–453.

Dekleva, B. M., Ramkumar, P., Wanda, P. A., Kording, K. P., & Miller, L. E. (2016). Uncertainty leads to persistent effects on reach representations in dorsal premotor cortex (M. J. Frank, Ed.). eLife, 5, e14316.

Deo, D. R., Rezaii, P., Hochberg, L. R., Okamura, A. M., Shenoy, K. V., & Henderson, J. M. (2021). Effects of peripheral haptic feedback on intracortical brain-computer interface control and associated sensory responses in motor cortex. IEEE Transactions on Haptics, 14(4), 762–775.

Desmurget, M., Epstein, C. M., Turner, R. S., Prablanc, C., Alexander, G. E., & Grafton, S. T. (1999). Role of the posterior parietal cortex in updating reaching movements to a visual target. Nature Neuroscience, 2(6), 563–567.

Desmurget, M., & Grafton, S. (2000). Forward modeling allows feedback control for fast reaching movements. Trends in Cognitive Sciences, 4(11), 423–431.

Diedrichsen, J., Shadmehr, R., & Ivry, R. B. (2010). The coordination of movement: Optimal feedback control and beyond. Trends in Cognitive Sciences, 14(1), 31–39.

Downey, J. E., Schwed, N., Chase, S. M., Schwartz, A. B., & Collinger, J. L. (2018). Intracortical recording stability in human brain–computer interface users. Journal of Neural Engineering, 15(4), 046016.

Dum, R. P., & Strick, P. L. (1991). The origin of corticospinal projections from the premotor areas in the frontal lobe. The Journal of Neuroscience: The Of cial Journal of the Society for Neuroscience, 11(3), 667–689.

Dum, R. P., & Strick, P. L. (2002). Motor areas in the frontal lobe of the primate. Physiology & Behavior, 77(4), 677–682.

Elsayed, G. F., Lara, A. H., Kaufman, M. T., Churchland, M. M., & Cunningham, J. P. (2016). Reorganization between preparatory and movement population responses in motor cortex. Nature Communications, 7(1), 13239.

Ernst, M. O., & Banks, M. S. (2002). Humans integrate visual and haptic information in a statistically optimal fashion. Nature, 415(6870), 429–433.

Evarts, E. V. (1968). Relation of pyramidal tract activity to force exerted during voluntary movement. Journal of Neurophysiology, 31(1), 14–27.

Evarts, E. V., Fromm, C., Kroller, J., & Jennings, V. A. (1983). Motor cortex control of nely graded forces. Journal of Neurophysiology, 49(5), 1199–1215.

Even-Chen, N., Sheffer, B., Vyas, S., Ryu, S. I., & Shenoy, K. V. (2019). Structure and variability of delay activity in premotor cortex (A. M. Haith, Ed.). PLOS Computational Biology, 15(2), e1006808.

Faisal, A. A., Selen, L. P. J., & Wolpert, D. M. (2008). Noise in the nervous system. Nature Reviews Neuroscience, 9(4), 292–303.

Fernandez-Ruiz, J., Wong, W., Armstrong, I. T., & Flanagan, J. R. (2011). Relation between reaction time and reach errors during visuomotor adaptation. Behavioural Brain Research, 219(1), 8–14.

Ferrea, E., Franke, J., Morel, P., & Gail, A. (2022). Statistical determinants of visuomotor adaptation along different dimensions during naturalistic 3d reaches. Scientific Reports, 12(1), 10198.

Fetz, E. E. (1992). Are movement parameters recognizably coded in the activity of single neurons? Behavioral and Brain Sciences, 15(4), 679–690.

Feulner, B., & Clopath, C. (2021). Neural manifold under plasticity in a goal driven learning behaviour. PLOS Computational Biology, 17(2), e1008621.

Feulner, B., Perich, M. G., Chowdhury, R. H., Miller, L. E., Gallego, J. A., & Clopath, C. (2022). Small, correlated changes in synaptic connectivity may facilitate rapid motor learning. Nature Communications, 13(1), 5163.

Flanagan, J. R., & Wing, A. M. (1997). The role of internal models in motion planning and control: Evidence from grip force adjustments during movements of hand-held loads. Journal of Neuroscience, 17(4), 1519–1528.

Flesher, S. N., Collinger, J. L., Foldes, S. T., Weiss, J. M., Downey, J. E., Tyler-Kabara, E. C., Bensmaia, S. J., Schwartz, A. B., Boninger, M. L., & Gaunt, R. A. (2016). Intracortical microstimulation of human somatosensory cortex. Science Translational Medicine, 8(361), 361ra141–361ra141.

Flesher, S. N., Downey, J. E., Weiss, J. M., Hughes, C. L., Herrera, A. J., Tyler-Kabara, E. C., Boninger, M. L., Collinger, J. L., & Gaunt, R. A. (2021). A brain-computer interface that evokes tactile sensations improves robotic arm control. Science, 372(6544), 831–836.

Gallego, J. A., Perich, M. G., Chowdhury, R. H., Solla, S. A., & Miller, L. E. (2020). Long-term stability of cortical population dynamics underlying consistent behavior. Nature Neuroscience, 23(2), 260–270.

Gallego, J. A., Perich, M. G., Miller, L. E., & Solla, S. A. (2017). Neural manifolds for the control of movement. Neuron, 94(5), 978–984.

Gallego, J. A., Perich, M. G., Naufel, S. N., Ethier, C., Solla, S. A., & Miller, L. E. (2018). Cortical population activity within a preserved neural manifold underlies multiple motor behaviors. Nature Communications, 9(1), 4233.

Gandolfo, F., Li, C.-S. R., Benda, B. J., Schioppa, C. P., & Bizzi, E. (2000). Cortical correlates of learning in monkeys adapting to a new dynamical environment. Proceedings of the National Academy of Sciences, 97(5), 2259–2263.

Ganguly, K., & Carmena, J. M. (2009). Emergence of a stable cortical map for neuroprosthetic control. PLOS Biology, 7(7), e1000153.

Ganguly, K., Dimitrov, D. F., Wallis, J. D., & Carmena, J. M. (2011). Reversible large-scale modification of cortical networks during neuroprosthetic control. Nature Neuroscience, 14(5), 662–667.

Georgopoulos, A., Kalaska, J., Caminiti, R, & Massey, J. (1982). On the relations between the direction of two-dimensional arm movements and cell discharge in primate motor cortex. The Journal of Neuroscience, 2(11), 1527–1537.

Georgopoulos, A. P., Schwartz, A. B., & Kettner, R. E. (1986). Neuronal population coding of movement direction. Science, 233(4771), 1416–1419.

Ghosh, S., & Gattera, R. (1995). A comparison of the ipsilateral cortical projections to the dorsal and ventral subdivisions of the macaque premotor cortex. Somatosensory & Motor Research, 12(3), 359–378.

Gilja, V., Nuyujukian, P., Chestek, C. A., Cunningham, J. P., Yu, B. M., Fan, J. M., Churchland, M. M., Kaufman, M. T., Kao, J. C., Ryu, S. I., & Shenoy, K. V. (2012). A high-performance neural prosthesis enabled by control algorithm design. Nature Neuroscience, 15(12), 1752–1757.

Glaser, J. I., Perich, M. G., Ramkumar, P., Miller, L. E., & Kording, K. P. (2018). Population coding of conditional probability distributions in dorsal premotor cortex. Nature Communications, 9(1), 1788.

Godschalk, M., Lemon, R. N., Nijs, H. G. T., & Kuypers, H. G. J. M. (1981). Behaviour of neurons in monkey peri-arcuate and precentral cortex before and during visually guided arm and hand movements. Experimental Brain Research, 44(1), 113–116.

Godschalk, M., Mitz, A. R., Duin, B. v., & Burga, H. v. d. (1995). Somatotopy of monkey premotor cortex examined with microstimulation. Neuroscience Research, 23(3), 269–279.

Golub, M. D., Chase, S. M., Batista, A. P., & Yu, B. M. (2016). Brain-computer interfaces for dissecting cognitive processes underlying sensorimotor control. Current Opinion in Neurobiology, 37, 53–58.

Golub, M. D., Sadtler, P. T., Oby, E. R., Quick, K. M., Ryu, S. I., Tyler-Kabara, E. C., Batista, A. P., Chase, S. M., & Yu, B. M. (2018). Learning by neural reassociation. Nature Neuroscience, 21(4), 607–616.

Haith, A. M., Huberdeau, D. M., & Krakauer, J. W. (2015). The in uence of movement preparation time on the expression of visuomotor learning and savings. Journal of Neuroscience, 35(13), 5109–5117.

Hatsopoulos, N. G., Xu, Q., & Amit, Y. (2007). Encoding of movement fragments in the motor cortex. Journal of Neuroscience, 27(19), 5105–5114.

Hatsopoulos, N., & Suminski, A. (2011). Sensing with the motor cortex. Neuron, 72(3), 477–487.

Heath, M. (2005). Role of limb and target vision in the online control of memory-guided reaches. Motor Control, 9(3), 281–309.

Helmholtz, H. v. (1867). Handbuch der physiologischen Optik (Vol. 9). Voss.

Hennig, J. A., Oby, E. R., Golub, M. D., Bahureksa, L. A., Sadtler, P. T., Quick, K. M., Ryu, S. I., Tyler-Kabara, E. C., Batista, A. P., Chase, S. M., & Yu, B. M. (2021). Learning is shaped by abrupt changes in neural engagement. Nature Neuroscience, 24(5), 727–736.

Homer, M. L., Nurmikko, A. V., Donoghue, J. P., & Hochberg, L. R. (2013). Implants and decoding for intracortical brain computer interfaces. Annual review of biomedical engineering, 15, 383–405.

Huang, V. S., Haith, A., Mazzoni, P., & Krakauer, J. W. (2011). Rethinking motor learning and savings in adaptation paradigms: Model-free memory for successful actions combines with internal models. Neuron, 70(4), 787–801.

Hutter, S. A., & Taylor, J. A. (2018). Relative sensitivity of explicit reaiming and implicit motor adaptation. Journal of Neurophysiology, 120(5), 2640–2648.

Jarosiewicz, B., Chase, S. M., Fraser, G. W., Velliste, M., Kass, R. E., & Schwartz, A. B. (2008). Functional network reorganization during learning in a brain-computer interface paradigm. Proceedings of the National Academy of Sciences, 105(49), 19486–19491.

Johnson, P. B., Ferraina, S., Bianchi, L., & Caminiti, R. (1996). Cortical networks for visual reaching: Physiological and anatomical organization of frontal and parietal lobe arm regions. Cerebral Cortex, 6(2), 102–119.

Jordan, M. I. Chapter 2 - computational aspects of motor control and motor learning (H. Heuer & S. W. Keele, Eds.). In: Handbook of perception and action (H. Heuer & S. W. Keele, Eds.). Ed. by Heuer, H., & Keele, S. W. Vol. 2. Motor skills. Academic Press, 1996, January 1, pp. 71–120.

Jordan, M. I., & Rumelhart, D. E. (1992). Forward models: Supervised learning with a distal teacher. Cognitive Science, 16(3), 307–354.

Kakei, S., Hoffman, D. S., & Strick, P. L. (1999). Muscle and movement representations in the primary motor cortex. Science, 285(5436), 2136–2139.

Kalaska, J. F., Cohen, D. A., Hyde, M. L., & Prud'homme, M. (1989). A comparison of movement direction-related versus load direction- related activity in primate motor cortex, using a two-dimensional reaching task. Journal of Neuroscience, 9(6), 2080–2102.

Kandel, E. R., Koester, J. D., Mack, S. H., & Siegelbaum, S. A. (2021, April 5). Principles of neural science, sixth edition. McGraw Hill Professional.

Kaufman, M. T., Churchland, M. M., Ryu, S. I., & Shenoy, K. V. (2014). Cortical activity in the null space: Permitting preparation without movement. Nature Neuroscience, 17(3), 440–448.

Kaufman, M. T., Seely, J. S., Sussillo, D., Ryu, S. I., Shenoy, K. V., & Churchland, M. M. (2016). The largest response component in the motor cortex re ects movement timing but not movement type. eNeuro, 3(4).

Kim, H. E., Morehead, J. R., Parvin, D. E., Moazzezi, R., & Ivry, R. B. (2018). Invariant errors reveal limitations in motor correction rather than constraints on error sensitivity. Communications Biology, 1(1), 19.

Klaes, C., Shi, Y., Kellis, S., Minxha, J., Revechkis, B., & Andersen, R. A. (2014). A cognitive neuroprosthetic that uses cortical stimulation for somatosensory feedback. Journal of Neural Engineering, 11(5), 056024.

Kriegeskorte, N., & Diedrichsen, J. (2019). Peeling the onion of brain representations. Annual Review of Neuroscience, 42, 407–432.

Kurata, K. (1991). Corticocortical inputs to the dorsal and ventral aspects of the premotor cortex of macaque monkeys. Neuroscience Research, 12(1), 263–280.

Körding, K. P., & Wolpert, D. M. (2006). Bayesian decision theory in sensorimotor control. Trends in Cognitive Sciences, 10(7), 319–326.

Körding, K. P., & Wolpert, D. M. (2004). Bayesian integration in sensorimotor learning. Nature, 427(6971), 244–247.

Latash, M. L., Scholz, J. P., & Schöner, G. (2002). Motor control strategies revealed in the structure of motor variability. Exercise and Sport Sciences Reviews, 30(1), 26.

Lebedev, M. A., & Nicolelis, M. A. L. (2017). Brain-machine interfaces: From basic science to neuroprostheses and neurorehabilitation. Physiological Reviews, 97(2), 767–837.

Lee, W.-H., Karpowicz, B. M., Pandarinath, C., & Rouse, A. G. (2024). Identifying distinct neural features between the initial and corrective phases of precise reaching using AutoLFADS. Journal of Neuroscience, e44(20).

Lemon, R. N. (2008). Descending pathways in motor control. Annual Review of Neuroscience, 31, 195–218.

Leow, L.-A., Marinovic, W., de Rugy, A., & Carroll, T. J. (2018). Task errors contribute to implicit aftereffects in sensorimotor adaptation. European Journal of Neuroscience, 48(11), 3397–3409.

Leow, L.-A., Marinovic, W., Rugy, A. d., & Carroll, T. J. (2020). Task errors drive memories that improve sensorimotor adaptation. Journal of Neuroscience, e40(15), 3075–3088.

Li, C.-S. R., Padoa-Schioppa, C., & Bizzi, E. (2001). Neuronal correlates of motor performance and motor learning in the primary motor cortex of monkeys adapting to an external force field. Neuron, 30(2), 593–607.

Liu, M. F., Gaunt, R. A., Collinger, J. L., Downey, J. E., Batista, A. P., Boninger, M. L., & Weber, D. J. (2024). Volitional control of movement interacts with proprioceptive feedback in motor cortex during brain-computer interface control in humans (preprint). medRxiv, New Results, 24303289.

Losey, D. M., Hennig, J. A., Oby, E. R., Golub, M. D., Sadtler, P. T., Quick, K. M., Ryu, S., Tyler-Kabara, E. C., Batista, A. P., Yu, B. M., & Chase, S. M. (2024). Learning leaves a memory trace in motor cortex. Current Biology.

Malik, W. Q., Truccolo, W., Brown, E. N., & Hochberg, L. R. (2011). Efficient decoding with steady-state kalman filter in neural interface systems. IEEE transactions on neural systems and rehabilitation engineering, 19(1), 25–34.

Malonis, P. J., Hatsopoulos, N. G., MacLean, J. N., & Kaufman, M. T. (2021). M1 dynamics share similar inputs for initiating and correcting movement (preprint). bioRxiv, New Results, 464704.

Maresch, J., Mudrik, L., & Donchin, O. (2021a). Measures of explicit and implicit in motor learning: What we know and what we don't. Neuroscience & Biobehavioral Reviews, 128, 558–568.

Maresch, J., Werner, S., & Donchin, O. (2021b). Methods matter: Your measures of explicit and implicit processes in visuomotor adaptation affect your results. European Journal of Neuroscience, 53(2), 504–518.

Marko, M. K., Haith, A. M., Harran, M. D., & Shadmehr, R. (2012). Sensitivity to prediction error in reach adaptation. Journal of Neurophysiology, 108(6), 1752–1763.

Mazzoni, P., & Krakauer, J. W. (2006). An implicit plan overrides an explicit strategy during visuomotor adaptation. Journal of Neuroscience, 26(14), 3642–3645.

McDougle, S. D., & Taylor, J. A. (2019). Dissociable cognitive strategies for sensorimotor learning. Nature Communications, 10(1), 40.

McNamee, D., & Wolpert, D. M. (2019). Internal models in biological control. Annual Review of Control, Robotics, and Autonomous Systems, 2, 339–364.

Messier, J., & Kalaska, J. F. (2000). Covariation of primate dorsal premotor cell activity with direction and amplitude during a memorized-delay reaching task. Journal of Neurophysiology, 84(1), 152–165.

Meyer, D. E., Abrams, R. A., Kornblum, S., Wright, C. E., & Keith Smith, J. E. (1988). Optimality in human motor performance: Ideal control of rapid aimed movements. Psychological Review, 95(3), 340–370.

Miall, R. C., & Wolpert, D. M. (1996). Forward models for physiological motor control. Neural Networks, 9(8), 1265–1279.

Michaels, J. A., Dann, B., Intveld, R. W., & Scherberger, H. (2015). Predicting reaction time from the neural state space of the premotor and parietal grasping network. Journal of Neuroscience, 35(32), 11415–11432.

Miyamoto, Y. R., Wang, S., & Smith, M. A. (2020). Implicit adaptation compensates for erratic explicit strategy in human motor learning. Nature Neuroscience, 23(3), 443–455.

Modchalingam, S., Ciccone, M., D'Amario, S., 't Hart, B. M., & Henriques, D. Y. P. (2023). Adapting to visuomotor rotations in stepped increments increases implicit motor learning. Scientific Reports, 13(1), 5022.

Modchalingam, S., Vachon, C. M., 't Hart, B. M., & Henriques, D. Y. P. (2019). The effects of awareness of the perturbation during motor adaptation on hand localization. PLOS ONE, 14(8), e0220884.

Moran, D. W., & Schwartz, A. B. (1999). Motor cortical representation of speed and direction during reaching. Journal of Neurophysiology, 82(5), 2676–2692.

Morehead, J. R., & Orban de Xivry, J.-J. (2021). A synthesis of the many errors and learning processes of visuomotor adaptation (preprint). bioRxiv, New Results, 435278.

Morehead, J. R., Taylor, J. A., Parvin, D. E., & Ivry, R. B. (2017). Characteristics of implicit sensorimotor adaptation revealed by task-irrelevant clamped feedback. Journal of Cognitive Neuroscience, 29(6), 1061–1074.

Mulliken, G. H., Musallam, S., & Andersen, R. A. (2008). Forward estimation of movement state in posterior parietal cortex. Proceedings of the National Academy of Sciences, 105(24), 8170–8177.

Neville, K.-M., & Cressman, E. K. (2018). The influence of awareness on explicit and implicit contributions to visuomotor adaptation over time. Experimental Brain Research, 236(7), 2047–2059.

Oby, E. R., Golub, M. D., Hennig, J. A., Degenhart, A. D., Tyler-Kabara, E. C., Yu, B. M., Chase, S. M., & Batista, A. P. (2019). New neural activity patterns emerge with long-term learning. Proceedings of the National Academy of Sciences, 116(30), 15210–15215.

Omrani, M., Murnaghan, C. D., Pruszynski, J. A., & Scott, S. H. (2016). Distributed task-specific processing of somatosensory feedback for voluntary motor control (R. M. Costa, Ed.). eLife, 5, e13141.

Omrani, M., Pruszynski, J. A., Murnaghan, C. D., & Scott, S. H. (2014). Perturbation-evoked responses in primary motor cortex are modulated by behavioral context. Journal of Neurophysiology, 112(11), 2985–3000.

Orsborn, A. L., Dangi, S., Moorman, H. G., & Carmena, J. M. (2012). Closed-loop decoder adaptation on intermediate time-scales facilitates rapid BMI performance improvements independent of decoder initialization conditions. IEEE Transactions on Neural Systems and Rehabilitation Engineering, 20(4), 468–477.

Orsborn, A. L., Moorman, H. G., Overduin, S. A., Shanechi, M. M., Dimitrov, D. F., & Carmena, J. M. (2014). Closed-loop decoder adaptation shapes neural plasticity for skillful neuroprosthetic control. Neuron, 82(6), 1380–1393.

Paz, R., Boraud, T., Natan, C., Bergman, H., & Vaadia, E. (2003). Preparatory activity in motor cortex reflects learning of local visuomotor skills. Nature Neuroscience, 6(8), 882–890.

Perich, M. G., Gallego, J. A., & Miller, L. E. (2018). A neural population mechanism for rapid learning. Neuron, 100(4), 964–976.e7.

Perich, M. G., & Miller, L. E. (2017). Altered tuning in primary motor cortex does not account for behavioral adaptation during force field learning. Experimental Brain Research, 235(9), 2689–2704.

Pruszynski, J. A., Omrani, M., & Scott, S. H. (2014). Goal-dependent modulation of fast feedback responses in primary motor cortex. Journal of Neuroscience, 34(13), 4608–4617.

Rajeswaran, P., Payeur, A., Lajoie, G., & Orsborn, A. L. (2024, March 20). Assistive sensory-motor perturbations influence learned neural representations.

Rathelot, J.-A., & Strick, P. L. (2009). Subdivisions of primary motor cortex based on cortico-motoneuronal cells. Proceedings of the National Academy of Sciences of the United States of America, 106(3), 918–923.

Redding, G. M., & Wallace, B. (1978). Sources of “overadditivity” in prism adaptation. Perception & Psychophysics, 24(1), 58–62.

Riehle, A., & Requin, J. (1989). Monkey primary motor and premotor cortex: Single-cell activity related to prior information about direction and extent of an intended movement. Journal of Neurophysiology, 61(3), 534–549.

Russo, A. A., Bittner, S. R., Perkins, S. M., Seely, J. S., London, B. M., Lara, A. H., Miri, A., Marshall, N. J., Kohn, A., Jessell, T. M., Abbott, L. F., Cunningham, J. P., & Churchland, M. M. (2018). Motor cortex embeds muscle-like commands in an untangled population response. *Neuron*, *97*(4), 953–966.e8.

Sabatini, D. A., & Kaufman, M. T. (2024). Reach-dependent reorientation of rotational dynamics in motor cortex. *Nature Communications*, *15*(1), 7007.

Sadtler, P. T., Quick, K. M., Golub, M. D., Chase, S. M., Ryu, S. I., Tyler-Kabara, E. C., Yu, B. M., & Batista, A. P. (2014). Neural constraints on learning. *Nature*, *512*(7515), 423–426.

Safaie, M., Chang, J. C., Park, J., Miller, L. E., Dudman, J. T., Perich, M. G., & Gallego, J. A. (2023). Preserved neural dynamics across animals performing similar behaviour. *Nature*, 1–7.

Sarlegna, F., Blouin, J., Bresciani, J.-P., Bourdin, C., Vercher, J.-L., & Gauthier, G. M. (2003). Target and hand position information in the online control of goal-directed arm movements. *Experimental Brain Research*, *151*(4), 524–535.

Saxena, S., Russo, A. A., Cunningham, J., & Churchland, M. M. (2022). Motor cortex activity across movement speeds is predicted by network-level strategies for generating muscle activity (J. A. Pruszynski & J. I. Gold, Eds.). *eLife*, *11*, e67620.

Schwartze, K. C., Lee, W.-H., & Rouse, A. G. (2024). Initial and corrective submovement encoding differences within primary motor cortex during precision reaching. *Journal of Neurophysiology*, *132*(2), 433–445.

Scott, S. H. (2016). A functional taxonomy of bottom-up sensory feedback processing for motor actions. *Trends in Neurosciences*, *39*(8), 512–526.

Scott, S. H. (2004). Optimal feedback control and the neural basis of volitional motor control. *Nature Reviews Neuroscience*, *5*(7), 532–545.

Sergio, L. E., Hamel-Pâquet, C., & Kalaska, J. F. (2005). Motor cortex neural correlates of output kinematics and kinetics during isometric-force and arm-reaching tasks. *Journal of Neurophysiology*, *94*(4), 2353–2378.

Shadmehr, R., & Mussa-Ivaldi, F. A. (1994). Adaptive representation of dynamics during learning of a motor task. *Journal of Neuroscience*, *14*(5), 3208–3224.

Shadmehr, R., Smith, M. A., & Krakauer, J. W. (2010). Error correction, sensory prediction, and adaptation in motor control. *Annual Review of Neuroscience*, *33*(1), 89–108.

Shadmehr, R., & Wise, S. P. (2004, October 28). *The computational neurobiology of reaching and pointing: A foundation for motor learning*. MIT Press.

Sheahan, H. R., Franklin, D. W., & Wolpert, D. M. (2016). Motor planning, not execution, separates motor memories. *Neuron*, *92*(4), 773–779.

Shenoy, K. V., & Carmena, J. M. (2014). Combining decoder design and neural adaptation in brain-machine interfaces. *Neuron*, *84*(4), 665–680.

Shenoy, K. V., Sahani, M., & Churchland, M. M. (2013). Cortical control of arm movements: A dynamical systems perspective. *Annual Review of Neuroscience*, *36*, 337–359.

Shmuelof, L., & Krakauer, J. W. (2011). Are we ready for a natural history of motor learning? *Neuron*, *72*(3), 469–476.

Smoulder, A. L., Marino, P. J., Oby, E. R., Snyder, S. E., Miyata, H., Pavlovsky, N. P., Bishop, W. E., Yu, B. M., Chase, S. M., & Batista, A. P. (2024). A neural basis of choking under pressure. *Neuron*, S0896627324006081.

Sober, S. J., & Sabes, P. N. (2003). Multisensory integration during motor planning. *Journal of Neuroscience*, *23*(18), 6982–6992.

Stavisky, S. D., Kao, J. C., Ryu, S. I., & Shenoy, K. V. (2017). Motor cortical visuomotor feedback activity is initially isolated from downstream targets in output-null neural state space dimensions. *Neuron*, *95*(1), 195–208.e9.

Stepniewska, I., Preuss, T. M., & Kaas, J. H. (1993). Architectionis, somatotopic organization, and ipsilateral cortical connections of the primary motor area (m1) of owl monkeys. *Journal of Comparative Neurology*, *330*(2), 238–271.

Suminski, A. J., Tkach, D. C., Fagg, A. H., & Hatsopoulos, N. G. (2010). Incorporating feedback from multiple sensory modalities enhances brain-machine interface control. *Journal of Neuroscience*, *30*(50), 16777–16787.

Sun, X., O'Shea, D. J., Golub, M. D., Trautmann, E. M., Vyas, S., Ryu, S. I., & Shenoy, K. V. (2022). Cortical preparatory activity indexes learned motor memories. *Nature*, *602*(7896), 274–279.

Suriya-Arunroj, L., & Gail, A. (2019). Complementary encoding of priors in monkey frontoparietal network supports a dual process of decision-making (E. Vaadia & R. B. Ivry, Eds.). *eLife*, *8*, e47581.

Sussillo, D., Stavisky, S. D., Kao, J. C., Ryu, S. I., & Shenoy, K. V. (2016). Making brain–machine interfaces robust to future neural variability. *Nature Communications*, *7*(1), 13749.

Suway, S. B., & Schwartz, A. B. (2019). Activity in primary motor cortex related to visual feedback. *Cell Reports*, *29*(12), 3872–3884.e4.

't Hart, B. M., Taqvi, U., Gastrock, R. Q., Ruttle, J. E., Modchalingam, S., & Henriques, D. Y. P. (2024). Measures of implicit and explicit adaptation do not linearly add. *eNeuro*, *11*(8).

Takei, T., Lomber, S. G., Cook, D. J., & Scott, S. H. (2021). Transient deactivation of dorsal premotor cortex or parietal area 5 impairs feedback control of the limb in macaques. *Current Biology*, S0960982221001147.

Taylor, J. A., & Ivry, R. B. (2011). Flexible cognitive strategies during motor learning. *PLOS Computational Biology*, *7*(3), e1001096.

Todorov, E., & Jordan, M. I. (2002). Optimal feedback control as a theory of motor coordination. *Nature Neuroscience*, *5*(11), 1226–1235.

Tokuno, H., & Tanji, J. (1993). Input organization of distal and proximal forelimb areas in the monkey primary motor cortex: A retrograde double labeling study. *Journal of Comparative Neurology*, *333*(2), 199–209.

Tsay, J. S., Avraham, G., Kim, H. E., Parvin, D. E., Wang, Z., & Ivry, R. B. (2021). The effect of visual uncertainty on implicit motor adaptation. *Journal of Neurophysiology*, *125*(1), 12–22.

Tsay, J. S., Kim, H., Haith, A. M., & Ivry, R. B. (2022). Understanding implicit sensorimotor adaptation as a process of proprioceptive re-alignment (J. A. Pruszynski & T. E. Behrens, Eds.). *eLife*, *11*, e76639.

Tsay, J. S., Kim, H. E., McDougle, S. D., Taylor, J. A., Haith, A., Avraham, G., Krakauer, J. W., Collins, A. G., & Ivry, R. B. (2024). Fundamental processes in sensorimotor learning: Reasoning, refinement, and retrieval (J. A. Pruszynski & K. M. Wassum, Eds.). *eLife*, *13*, e91839.

Tsay, J. S., Tan, S., Chu, M. A., Ivry, R. B., & Cooper, E. A. (2023). Low vision impairs implicit sensorimotor adaptation in response to small errors, but not large errors. *Journal of Cognitive Neuroscience*, *35*(4), 736–748.

Tye, K. M., Miller, E. K., Taschbach, F. H., Benna, M. K., Rigotti, M., & Fusi, S. (2024). Mixed selectivity: Cellular computations for complexity. *Neuron*, *112*(14), 2289–2303.

van Beers, R. J., Wolpert, D. M., & Haggard, P. (2002). When feeling is more important than seeing in sensorimotor adaptation. *Current Biology*, *12*(10), 834–837.

Vyas, S., Even-Chen, N., Stavisky, S. D., Ryu, S. I., Nuyujukian, P., & Shenoy, K. V. (2018). Neural population dynamics underlying motor learning transfer. *Neuron*, *97*(5), 1177–1186.e3.

Vyas, S., Golub, M. D., Sussillo, D., & Shenoy, K. V. (2020a). Computation through neural population dynamics. *Annual Review of Neuroscience*, *43*(1), 249–275.

Vyas, S., O'Shea, D. J., Ryu, S. I., & Shenoy, K. V. (2020b). Causal role of motor preparation during error-driven learning. *Neuron*, *106*(2), 329–339.e4.

Wei, K., & Körding, K. P. (2009). Relevance of error: What drives motor adaptation? *Journal of Neurophysiology*, *101*(2), 655–664.

Wei, K., & Körding, K. P. (2010). Uncertainty of feedback and state estimation determines the speed of motor adaptation. *Frontiers in Computational Neuroscience*, *4*.

Weinrich, M., & Wise, S. P. (1982). The premotor cortex of the monkey. *Journal of Neuroscience*, *2*(9), 1329–1345.

Weinrich, M., Wise, S. P., & Mauritz, K. H. (1984). A neurophysiological study of the premotor cortex in the rhesus monkey. *Brain: A Journal of Neurology*, *107 (Pt 2)*, 385–414.

Welch, R. B. (1974). Research on adaptation to rearranged vision: 1966–1974. *Perception*, *3*(4), 367–392.

Werner, S., Aken, B. C. v., Hulst, T., Frens, M. A., Geest, J. N. v. d., Strüder, H. K., & Donchin, O. (2015). Awareness of sensorimotor adaptation to visual rotations of different size. *PLOS ONE*, *10*(4), e0123321.

Wise, S. P., Di Pellegrino, G., & Boussaoud, D. (1992). Primate premotor cortex: Dissociation of visuomotor from sensory signals. *Journal of Neurophysiology*, *68*(3), 969–972.

Wise, S. P., Moody, S. L., Blomstrom, K. J., & Mitz, A. R. (1998). Changes in motor cortical activity during visuomotor adaptation. *Experimental Brain Research*, *121*(3), 285–299.

Wise, S. P., Boussaoud, D., Johnson, P. B., & Caminiti, R. (1997). PREMOTOR AND PARIETAL CORTEX: Corticocortical connectivity and combinatorial computations1. *Annual Review of Neuroscience*, *20*, 25–42.

Wolpaw, J. R. (1980). Amplitude of responses to perturbation in primate sensorimotor cortex as a function of task. *Journal of Neurophysiology*, *44*(6), 1139–1147.

Wolpaw, J., Birbaumer, N., Heetderks, W., McFarland, D., Peckham, P., Schalk, G., Donchin, E., Quatrano, L., Robinson, C., & Vaughan, T. (2000). Brain-computer interface technology: A review of the first international meeting. *IEEE Transactions on Rehabilitation Engineering*, *8*(2), 164–173.

Wolpert, D. M., Diedrichsen, J., & Flanagan, J. R. (2011). Principles of sensorimotor learning. *Nature Reviews Neuroscience*, *12*(12), 739–751.

Wolpert, D. M., & Flanagan, J. (2001). Motor prediction. *Current Biology*, *11*(18), R729–R732.

Wolpert, D. M., Ghahramani, Z., & Jordan, M. I. (1995). An internal model for sensorimotor integration. *Science*, *269*(5232), 1880–1882.

Wolpert, D. M., Goodbody, S. J., & Husain, M. (1998). Maintaining internal representations: The role of the human superior parietal lobe. *Nature Neuroscience*, *1*(6), 529–533.

Wärnberg, E., & Kumar, A. (2019). Perturbing low dimensional activity manifolds in spiking neuronal networks. *PLOS Computational Biology*, *15*(5), e1007074.

Zhang, Z., Wang, H., Zhang, T., Nie, Z., & Wei, K. (2024). Perceptual error based on bayesian cue combination drives implicit motor adaptation. *eLife*, *13*.

Zhou, X., Tien, R. N., Ravikumar, S., & Chase, S. M. (2019). Distinct types of neural reorganization during long-term learning. *Journal of Neurophysiology*, *121*(4), 1329–1341.

Zimnik, A. J., & Churchland, M. M. (2021). Independent generation of sequence elements by motor cortex. *Nature Neuroscience*, *24*(3), 412–424.

Zippi, E. L., You, A. K., Ganguly, K., & Carmena, J. M. (2022). Selective modulation of cortical population dynamics during neuroprosthetic skill learning. *Scientific Reports*, *12*(1), 15948.